SEDIMENTOLOGICAL AND CYCLOSTRATIGRAPHIC ANALYSIS OF UPPER PART OF THE KARTAL FORMATION (SW OF ANKARA)

A THESIS SUBMITTED TO
THE GRADUATE SCHOOL OF NATURAL AND APPLIED SCIENCES
OF
MIDDLE EAST TECHNICAL UNIVERSITY

BY

RUFAT AGHAYEV

IN PARTIAL FULFILLMENT OF THE REQUIREMENTS
FOR
THE DEGREE OF MASTER OF SCIENCE
IN
GEOLOGICAL ENGINEERING

OCTOBER-2008

Approval of thesis

SEDIMENTOLOGICAL AND CYCLOSTRATIGRAPHIC ANALYSIS OF UPPER PART OF THE KARTAL FORMATION (SW OF ANKARA)

submitted by RUFAT AGHAYEV in partial fulfillment of the requirements for the degree of Master of Science in Geological Engineering Department, Middle East Technical University by,

Prof. Dr. Canan Özgen ____________________
Dean, Graduate School of Natural and Applied Sciences

Prof. Dr. Zeki Çamur ____________________
Head of Department, Geoloical Engineering

Assis. Prof. Dr. İsmail Ömer Yılmaz ____________________
Supervisor, Geological Engineering Dept., METU

Examining Committee Members:

Prof. Dr. Demir Altıner ____________________
Geological Engineering Dept., METU

Prof. Dr. Cemal Göncüoğlu ____________________
Geological Engineering Dept., METU

Assist. Prof. Dr. İsmail Ömer Yılmaz ____________________
Supervisor,Geological Engineering Dept., METU

Assoc. Prof. Dr. Erdoğan Tekin ____________________
Geological Engineering Dept., Ankara Univ.

Dr. Zühtü Batı ____________________
Turkish Petroleum Corporation

Date: 20.10.2008

I hereby declare that all information in this document has been obtained and presented in accordance with academic rules and ethical conduct. I also declare that, as required by these rules and conduct, I have fully cited and referenced all material and results that are not original to this work.

Name, Last name: Rufat Aghayev

Signature:

ABSTRACT

SEDIMENTOLOGICAL AND CYCLOSTRATIGRAPHIC ANALYSIS OF UPPER PART OF THE KARTAL FORMATION (SW OF ANKARA)

Rufat Aghayev

M.Sc., Department of Geological Engineering
Supervisor: Assis. Prof. Dr. İsmail Ömer Yılmaz

October 2008, 113 pages

The Montian Kartal Formation lies in the south-west of Ankara region and overlies the Upper Cretaceous Beyobasi Formation and is overlain by Thanetian Kırkkavak Formation conformably in the studied region (Kayabaşı village, NW of town of Haymana). A 283 m stratigraphic section, which is mainly composed of an alternation siliciclastic and carbonate rocks has been measured in the Kartal Formation within the Haymana-Polatlı basin.

The aim of this study is to carry out the sedimentological and cyclostratigraphical analyses of the upper part of the Kartal Formation within Haymana-Polatlı basin which represents a well developed cyclic pattern. In this study, detailed lithofacies analyses were performed and four different facies were recognized along the measured section: sandstones, limestones, mudrocks and conglomerates.

Sedimentological analyses, such as modal, provenance, palaeocurrent, grain-size and grain parameters were also performed and their relation with the depositional environment and change in depositional conditions were discussed. Interpretations of the depositional environment revealed that the deposition occurred by low sinuosity rivers and waves. Additional environmental interpretations suggested that the sediments were deposited in shallow marine and/or coastal (beach) environments. High resolution cyclostratigraphy studies based on meter scale cyclic and rhytmic occurrences of lithofacies along the measured section were performed. The whole section, which is 283 m thick, was divided into large-scale hierarchy-cycles which comprise smaller-scale fining upward and deepening upward cyclic and rhythmic beds.

Key words: Sedimentology, Cyclostratigraphy, Montian, Kartal Formation, Haymana-Polatlı,

ÖZ

KARTAL FORMASYONU ÜST KISMININ SEDİMANTOLOJİK VE DEVİRSELSTRATİGRAFİK ANALİZİ (ANKARA GB'sı)

Rufat Aghayev

Yüksek Lisans Jeoloji Mühendsliği Bölümü
Tez Danışmanı: Yrd. Doç. İsmail Ömer Yılmaz

Ekim 2008, 113 sayfa

Monsiyen yaşlı Kartal Formasyonu Ankara bölgesinin güneybatısında yer almaktadır. Çalışma alanında (Kayabaşı köyü, Haymana ilçesinin KB kesimi) bu Formasyon Üst Kretase yaşlı Beyobası Formasyonunu üzerlemekte ve Tanesiyen yaşlı Kırkkavak Formasyonu tarafından uyumlu olarak üzerlenmektedir. Genelde silisiklastik ve karbonatlı kayaçlardan oluşan Kartal Formasyonu Haymana-Polatlı havzasında yer almakta olup çalışma alanında ölçülen stratigrafik kalınlığı 283 m olarak ölçülmüştür.

Bu çalışma, iyi gelişmiş devirsellikler sergileyen Haymana-Polatlı havzasının içindeki Kartal Formasyonu'nun üst kesminin devirsel stratigrafik ve sedimantolojik analizlerini amaçlamaktadır. Bu çalışmada detaylı litofasiyes analizleri yapılmış olup ölçülü kesit boyunca dört farklı fasiyes tanımlanmıştır. Bunlar : kumtaşı, kireçtaşı, çamurtaşı ve konglomeradır.

Ayrıca modal, provenans, paleoakıntı, taneboyu ve tane parametreleri gibi sedimantolojik analizler de yapılmış olup çalışmada çökel ortamı ve çökelim koşulları tartışılmıştır. Çökel ortamlarda yapılan tanımlamalara göre, sedimanlar baskın olarak düşük sinüziteli ırmak ve dalgalar tarafından kontrol edilmiştir. Ek olarak, çökelim ortamlarının tanımlanması sedimanların sığ deniz ve/veya kıyı (sahil) koşullarında çökeldiğine işaret etmektedir. Bunlara ek olarak, metre ölçeğinde devirsel ve ritmik litofasiyes oluşumları üzerine bina edilmiş olan yüksek çözünürlüklü devirsel stratigrafi çalışmaları yapılmıştır. 283 metre

kalınlığa sahip çalışılan kısmın tamamı küçük ölçekli yukarı doğru tane boyu küçülen ve yukarı doğru derinleşen devirsel ve ritmik tabakalardan oluşan büyük ölçekli hiyerarşik devirselliklerden oluşmaktadır.

Anahtar sözcükler: Sedimantoloji, Devirsel Stratigrafi, Monsiyen, Kartal Formasyonu, Haymana-Polatlı.

To my family

ACKNOWLEDGMENTS

I would like to express my deepest gratitude to my supervisor, Assis. Prof. Dr. İsmail Ömer Yılmaz, whose expertise, understanding, encouragement and patience, added considerably to my graduate experience. I appreciate his vast knowledge and skill in many areas, and his assistance in writing this thesis.

I would like to express my gratitude to all my teachers from the Geological Department of METU.

I would like to express my gratitude to Dr. Hüriye Demircan for her advises during my thesis work.

Very special thanks go out to all my friends for their friendships, motivations and endless encouragements. Especially, I would like to thank Elnur Amirov, Afgan Huseynov, Aydın Çiçek, Khalid Gozal, Kenneth Hayes, Elnur Binyatov, Zaur Mensimov and Aysel Majidova for their helps in field works and encouragements.

I would like to thank to Mr. Orhan Karaman for the preparation of thin sections and his assistance during field works.

Finally I would like to express my grateful appreciation to my family and especially to my mother and brother for their support and encouragements during my studies.

I would like to express my gratitude to BP Caspian Sea Exploration for providing me with scholarship and financial support. Especially I would like to thank David Day and Elshan Rzayev of BP for this wonderful opportunity given to me.

TABLE OF CONTENTS

LIST OF TABLES

LIST OF FIGURES

CHAPTER 1

INTRODUCTION

1.1 Purpose and Scope

The main objective of this study is to investigate the sedimentology and cyclostratigraphy of the uppper part of the Kartal Formation, where cyclicity is well developed. In order to carry out this objective, several studies were performed based on different disciplines of geology including lithostratigraphy, sedimentology and the cyclostratigraphy.

The Haymana-Polatlı basin is characterized by Upper Cretaceous – Middle Eocene clastic turbidite sediments at its center, passing into platform carbonates and continental red beds towards the margins (Yüksel 1970; Görür 1981; Çiner 1992). During Paleocene time, due to continued convergence of the Sakarya continent and northern branch of Neo-Tethyan ocean, and to the on-going growth of the accretionary wedge and its uplift, margins of the Haymana-Polatlı partly emerged i. e. Kartal Formation (Koçyiğit, 1991; Ünalan *et al.*, 1976). Since the Paleocene events in the Haymana-Polatlı are revealed by the widespread and rapid fluvial sedimentation, a 283 m thick stratigraphic section has been measured in details in the upper part of the formation, where continental and shallow marine facies variations and repetitions throughout the section display a cyclic pattern of depositional package. The measured section represented by the alternation of limestone blocks with continental sediments along the measured section, where the middle part is dominated by sandstone-conglomerate alternations. Within the measured section six large-scale hierarchies were identified on the basis of lithological facies description in the field. Sedimentological analyses based on the laboratory and field works yielded several data on the anatomy, provenance and depositional environment within upper part of the Kartal Formation. Cyclostratigraphic analyses of the measured section in this study helped to investigate the nature of the contact with the overlying Kırkkavak Formation and examine the characteristic properties of the upper part of the Kartal Formation in comparison with its lower part.

1.2 Geographic Setting

The town of Polatlı is located about 75 km SW of Ankara in Central Turkey (Figure 1). The study area is located south of Kayabaşı village on the Kartal hill, approximately 5 km south of Polatlı. The measured section starts at the top of Kartal Formation at coordinates 36444920 ° E - 4379470 ºN, and ends at 36445835 ºE-4378062 ° N.

Figure 1. Geographic location map of the studied section.

1.3 Methods of Study

This study mainly consisted of field and laboratory work. In the field, a stratigraphic section 283 m. in thickness was measured (Figure 2). At the bottom, the succession is mainly composed of red mudrocks and sandstones intercalated with limestones, changing upward into sandstone-conglomerate and sandstone-limestone alternations whereas the uppermost part of the section mainly consists of gray colored limestones. During the field work, lithologic and sedimentary structure descriptions were carried out in the field. 76 samples representing sandstone, limestone, mudrock, and thick conglomeratic successions were collected during the study. Samples were collected from the bottom, middle part and top of the measured section. Detailed petrographical, sedimentological, palaeocurrent, grain size analyses of conglomeratic beds and sandstones were carried out during the field and laboratory works. For this purpose, thin sections were prepared from all samples.

In the laboratory, point counting analyses were carried out in order to classify the sandstone, limestone and mudrock beds, and to understand the response of mineral and rock fragment concentrations in the beds to change in depositional environments. Approximately 1000-1500 points were counted in most of the thin sections by using J. Swift Co., apparatus. In order to obtain skewness, sorting, kurtosis, roundness and sphericity, grain size analyses were performed for 16 sandstone samples, using projection techniques. Predictions for sandstone provenance were carried out from thin section analyses. In three conglomeratic successions in the field, approximately 300 pebbles were collected and measured in 3 dimensions by using Vernier Caliper and detailed grain size, shape determination and sphericity analyses were performed in order to give some information about depositional environment and paleocurrent direction.

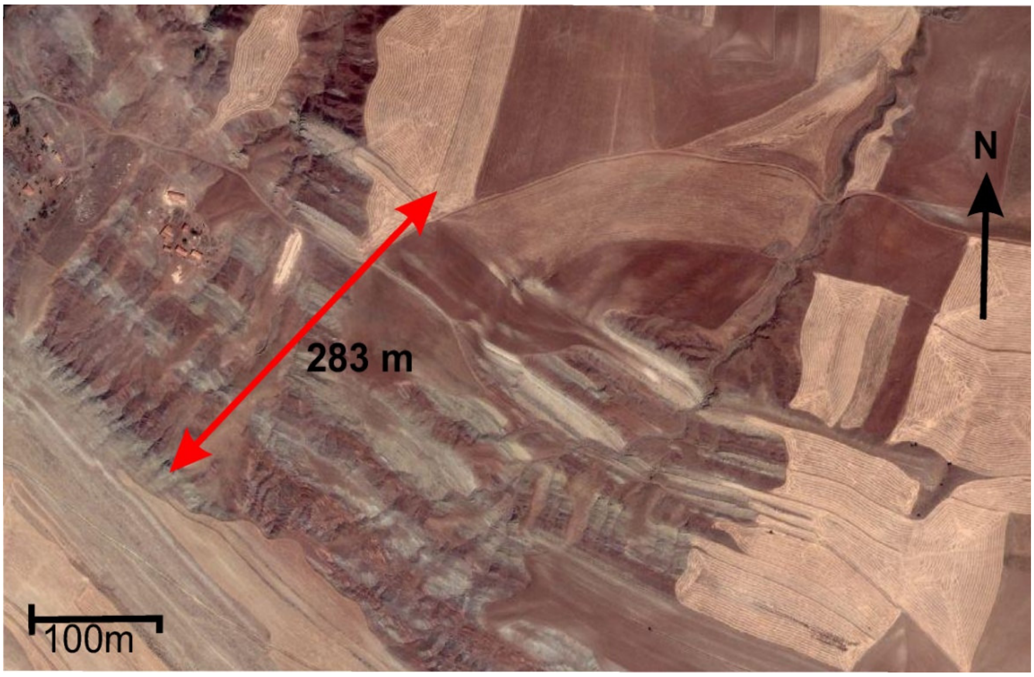

Figure 2. Location of detailed studied section (red line). (snapshot taken from Google Earth, www.earth.google.com).

1.4 Previous works

In the course of the last century, numerous geological studies had been carried on Haymana-Polatı region, for different purposes. Chaput (1936) made one of the earliest studies in the region. His work recognized Cretaceous and Eocene successions in the Haymana region, and from different outcrop studies, he predicted the distribution of flysch sequences in the region. The studies carried out by Erol and Wenidgart (1955), and the Gulf and Mobil companies (1958-1961), were for general geology of the area and economic resources. The studies performed by Rigo de Righi and Cortesini (1959); Reckamp and Özbey (1960), Schimidt (1960), Yüksel (1970), Akarsu (1971) were oriented to petroleum researches and exploration. Sirel (1975) and Ünalan *et al.*, (1976) made detailed studies of the Haymana-Polatlı basin and established the details of the outcrops and Formations in the area.

Sirel (1975) was the first to make detailed paleontological, lithostratigraphic and chronostratigraphic work in the area. Sirel (1975) identified *Rotalia trochidiformis* Lamark, *Missisipina binkhorsti* Reus and *Distichoplax* *biserialis* Dietrich in the upper part of the Kartal Formation and assigned a Montian age (Paleocene) for the whole Formation, composed of red conglomerates and biomicritic limestones. Nummulites from the Paleocene to Eocene in the Haymana-Polatlı basin were also ın the Sirel's (1975) scope of study. Recent biostratigraphic studies of the Haymana-Polatlı area were also carried out by Sirel (1999), Özkan-Altıner and Özcan (1999), Özcan *et al*. (2001 b).

Ünalan *et al*. (1976) studied the stratigraphy and paleogeographical evolution of the Upper Cretaceous-Lower Tertiary sediments in the Polatlı area. Ünalan *et al*. (1976) prepared a geological map in the scale of 1:25000 for an approximately 2800 km^2 area and measured stratigraphic sections comprising Temirözü, Mollaresul, Dereköy, Haymana, Beyobası, Kartal, Çaldag, Yeşilyurt, Kırkkavak, Eskipolatlı, Beldede, Çayraz and Yamak Formations.

Various scientists have investigated the biostratigraphic frame of the Cretaceous to Eocene successions of the Haymana-Polatlı region. Toker (1979), Özcan and Özkan-Altıner, (1997, 1999 a, 2001) studied the Upper Cretaceous units of the basin, based on planktonic and benthonic foraminifers, and calcareous nannoplanktons. Meriç and Görür (1979) carried out detailed paleontological and stratigraphical investigations within limestone blocks of the Çaldağ Formation in the Haymana-Polatlı area.

Şenalp and Gökçen (1978) studied the oil-saturated sandstones of the Haymana region. More recently, Grovel *et al*. (2000) investigated the Haymana Basin for its oil petroleum potential.

Şengör and Yılmaz (1981), Görür *et al*. (1984), Koçyiğit *et al*. (1988), and Koçyığıt (1991) have made valuable contributions to tectonic studies of the area. According to these studies, the Haymana-Polatlı basin developed under a continental collision regime along the northern branch of the Neo–Tethys. Because of the existence of Tertiary calcalkaline volkanism (Galatian volcanics), and the presence of ophiolitic basement in the basin, these authors suggested that Haymana-Polatlı basin had developed on a fore-arc accretionary wedge which was active from the Late Cretaceous to the Late Eocene (Koçyigit, 1991). Arc activity in the Sakarya continent during the Paleocene suggests that subduction was towards the north (Fourquin, 1975; Şengör and Yılmaz, 1981). Recent tectonic studies of the area, which were carried out by Okay and Tüysüz (1998) and Okay *et al*. (2001), proposed that Haymana-Polatlı basin is a composite basin and represents both foreland and forearc basin's features.

Gökçen and Kelling (1983) studied Eocene submarine fan systems of the Haymana-Polatlı basin. Their study was based on investigations of the characteristics and provanence (paleocurrent direction) of the submarine fan systems within the basin.

The most recent study of the area, made by Turgay and Kurtuluş (2000), was based on seismic exploration data. They used the data of Ünalan *et al*. (1976) and seismic data, to discover Haymana-Polatlı area's subsurface characteristics and oil petroleum potential.

The cyclostratigraphic studies have been performed by Çiner *et al*. (1993, 1996), Çiner (1996) in the Haymana-Polatlı basin. Çiner *et al*. (1993) studied the cyclicity in the Middle Eocene Çayraz Formation, which is mainly made up of carbonates and represent the youngest lithologies of the Haymana-Polatlı basin. The aim of their study was to describe coarsening-upward and shallowing-upward nummulite-bearing carbonate cycles of different magnitudes and the sequence of the stratigraphic frame of the study area. Çiner *et al*. (1996) also studied cyclicity of the 1 km thick Lutetian, Yamak Turbidite complex which they found to consist of three depositional sequences. In this study, they described the cyclic sedimentation and depositional environment of the complex. In order to understand its evolution and obtain cyclostratigraphy of the complex, they subdivided it in basic sequences (BS) and basic units (BU), corresponding to 4^{th} and 5^{th} order cycles, respectively.

As our work is directly related to sedimentology and cyclostratigraphy, it is necessary to mention cycle theories studied previously. Milankovitch (1941) proposed an astronomical theory of glaciation, which explained climatic changes as resulting from fluctuations in the seasonal and geographic distribution of insolation (In Schwarzacher, 1993). Brinkman (1932) differentiated between two groups which he called autonomous and induced cycles, depending on time and type of the deposition. Beerbower (1964) introduced the two terms autocycles and allocycles, based on the alluvial fan studies. Ginsburg (1971) prepared cyclic model for carbonate accumulation on a size restricted shelf which undergoes subsidence. Vail *et al*. (1977) made additional, dramatic discoveries in cycle patterns. Using data derived from seismic exploration, they defined the cycles of relative changes of sea level as an interval of time during which a rise and fall of sea level take place. Schwarzacher (1993), Drummond and Wilkinson (1993) suggested cyclic models for different types of depositional environments and applied tectonic approach as well.

Einsele (2000) proposed forearc basin types, their general characteristics and sedimentary successions. He divided forearc basins into accretionary, residual, constructed, and composite basin types and purposed idealized sedimentary successions for residual basins. He also studied the factors controlling cycles in the deep-sea sedimets. According to affromentioned tectonic studies, the Haymana-Polatlı is a composite basin, which represented by forearc and foreland basins (after Okay and Tüysüz, 1998).

1.4 Geological Settings

The Haymana-Polatlı basin, 75 km SW of Ankara, developed on an accretionary wedge (Figure 3). The accretionary complex is made up of a mélange with basalt blocks, radiolarian chert and serpentinite with minor turbidite (Norman, 1984; Göncüoğlu, 1992; Okay *et al*., 2001).

The wedge formed by the convergence and collision of the Sakarya Continent to the north, Tauride-Anatolide block to the south and Kırşehir block to the south-east during the Late Cretaceous to Late Eocene by the closure of the northern branch of Neo-Tethys (Izmir–Ankara suture), (Şengör and Yılmaz, 1981; Görür *et al*., 1984; Koçyiğit *et al*., 1988; Koçyiğit, 1991; Göncüoğlu, 1992) (Figure 4). After the closure of the northern Neo-Thethys Ocean, deformation continued until the Late Pliocene (Koçyiğit, 1991). The shallowing of the basin during the latest Maastrichtian, and evidence for earliest Paleocene continental collision from farther west, indicate that the Haymana-Polatlı basin is a composite basin (Göncüoğlu, 1992; Okay and Tüysüz, 1998). The Campanian-Maastrichtian

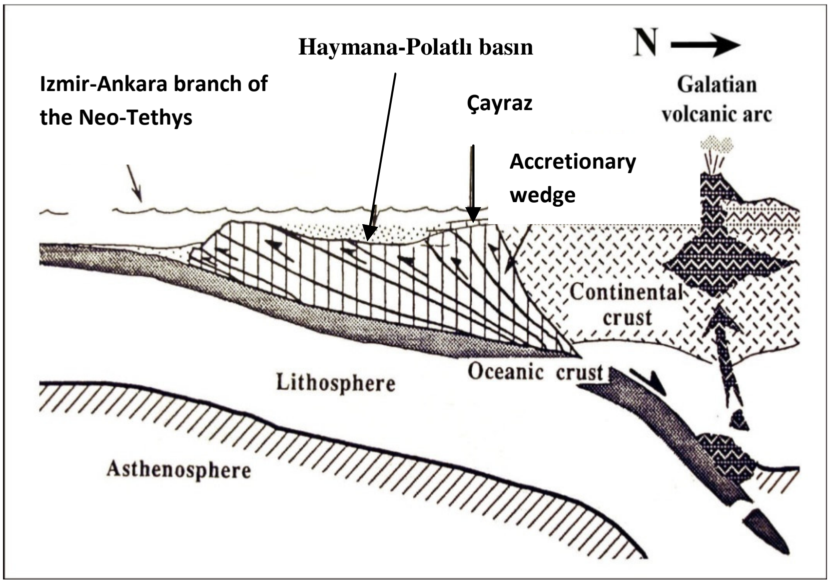

Figure 3. Schematic cross section (not to scale) showing the structural setting of the Haymana Basin during the Campanian to the Maastrichtian time interval (from Koçyiğit, 1991).

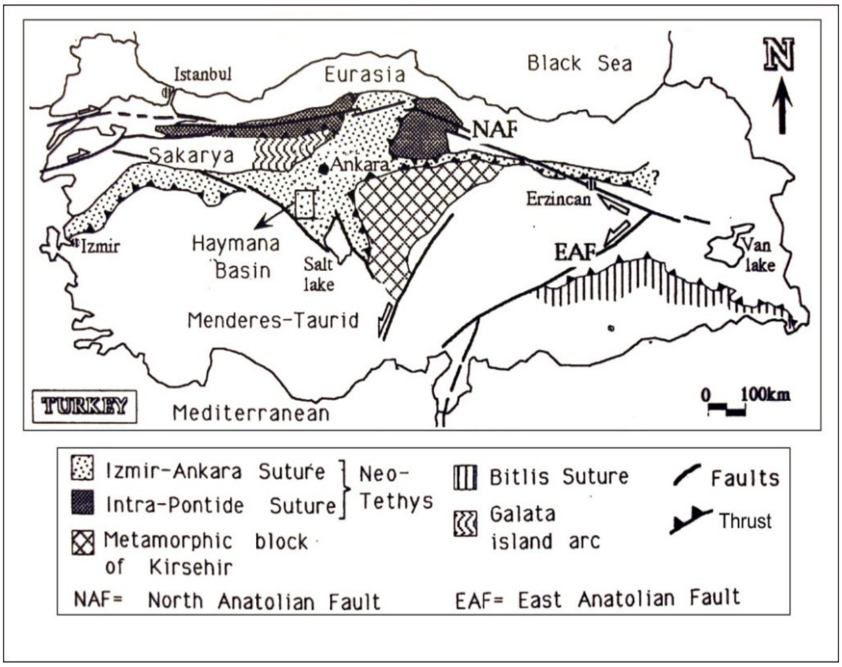

Figure 4. Main structural features of Turkey and location map of Haymana Basin (modified Koçyiğit, 1991).

basin fill represents a fore-arc basin, whereas the overlying Paleocene-Middle Eocene sequence has been deposited in a foreland basin formed during and after the continental collision (Koçyiğit, 1991, Göncüoğlu, 1992; Okay and Tüysüz, 1998). However Cater *et al.* (1991) assigned Campanian-Maastrichtian basin fill of the Haymana-Polatlı to the piggy-back basin.

In the studied area, represented successions are spanning in age from Late Cretaceous to Eocene (Figure 5). The Haymana-Polatlı basin is represented by 5 km thick clastic turbidite sediments at its center and by the alternation of massive carbonates with continental sediments at the margin (Yüksel, 1970; Görür, 1981; Çiner, 1992). The transition from deep sea turbidites to redbeds in the Haymana-Polatlı basin took place during Early Paleocene time (Okay *et al*, 2001).

The basement of the Haymana-Polatlı basin is composed of the Jurassic – Lower Cretaceous carbonate cover of the Tauride-Anatolide Block (Göncüoğlu, 1992), the Karakaya Complex (Şengör and Yılmaz, 1981) and the Ankara Mélange (Norman, 1975; Ünalan *et al*., 1976; Görür and Derman, 1978).

The Haymana–Polatlı basin itself is characterized by highly-deformed sedimentary fill (Koçyiğit, 1991). Different depositional conditions existed toward the NW margin of the basin, where shallow marine clastics, reefal carbonates lacustrine and fluvial deposits occurred (Yüksel, 1970; Ünalan *et al*., 1976; Çiner, 1992). In the Haymana-Polatlı the Upper Cretaceous sequences, represented by marine lımestones and turbidites, lie unconformably over the Upper Jurassic–Lower Cretaceous pelagic carbonates. The overlying Lower Palaeocene sequence shows facies variation and ranges from continental clastics in the northwest through shallow marine limestones to pelagic shales in the southeast. Evidence for earliest Paleocene continental collision and the absence of the Maastrichtian sequence in the western part of the Haymana-Polatlı basin indicate the foreland features. Late Palaeocene (Thanetian) shallow marine limestones and marls characterize second transgressive cycle, which is followed by Eocene turbidites.

During the Early to Middle Eocene time, the Haymana-Polatlı basin was characterized by a shallow transgressive sea in which widespread sandy and nummulite–bearing limestones were deposited on the shelf, but deep marine sedi-

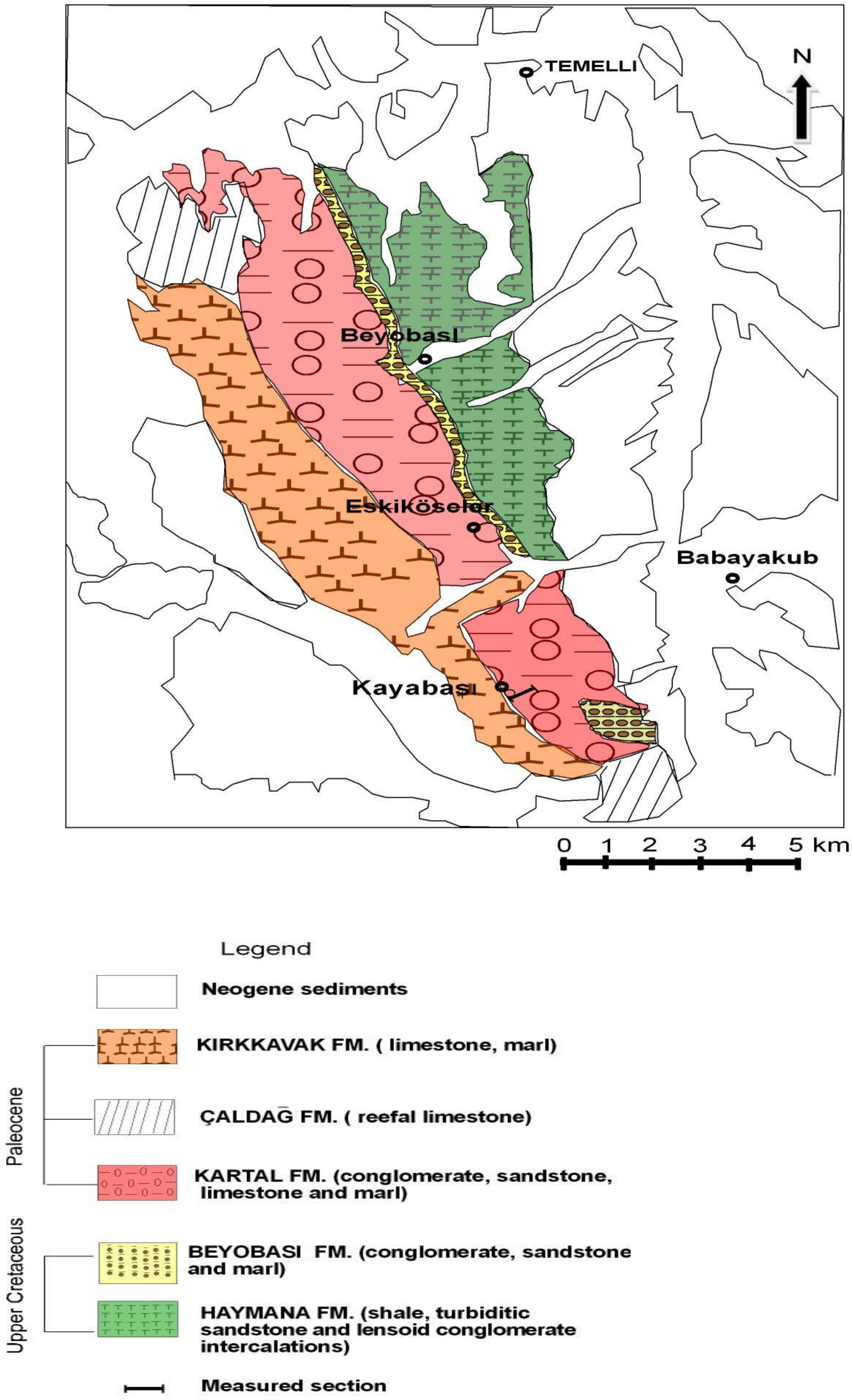

Figure 5. Geological map of the studied area (From Demircan, 1994).

mentation continued to the SE, within the basin interior (Ünalan *et al*., 1976; Koçyiğit and Lünel, 1987; Koçyiğit, 1991). Because of extensive and intensive tectonic deformation, it is not possible to trace the lateral transition from turbiditic strata into shelf and continental facies in the outcrop (Çiner, 1992).

The basal formations here are: Temirözü (Trias-Early Jurassic metagreywackes); Mollaresul (Late Jurrasic limestones); Dereköy (Ophiolitic mélange, consisting on serpentinite, volcanic and limestone blocks) (Ünalan *et al.*, 1976).

Deposition of continental red beds of the Kartal Formation, reefal limestones of the Çaldağ Formation during the Paleocene age characterized the basin edges. The red beds of Paleocene Kartal Formation are characterized by alternation of continental and marine sediments (Görür and Derman, 1978). The relatively deeper water shale-marl with limestone blocks intercalations of the Yeşilyurt Formation were precipitated in the interior part of the basin. The Kırkkavak Formation overlies the Kartal, Çaldağ and Yeşilyurt Formations and represented by algal limestones and marls (Ünalan *et al*, 1976). A semi-circular shelf existed near Haymana, on which the Çaldağ and Çayraz Formations were deposited (Figure 6). The partly-continental units Kartal and Beldede occured behind the shelf, while the flyschoidal units of the Haymana, Polatlı, Yeşilyurt, and Yamak Formations were deposited in front of the shelf (Ünalan *et al*., 1976).

The deposition of thick turbidite successions in the central parts of the basin in Early and Middle Eocene was occupied a larger area than in Paleocene. In Eocene age the depositional areas of the Çaldağ reefal limestones were filled up with turbidites and as a result the shoreline retreated away from the basin centre (Çiner *et al*., 1996).

The turbiditic depositional areas of the Haymana-Polatlı basin began to shrink rapidly from the end of the Middle Eocene. Turbidites graded vertically and laterally into shallow marine nummulitic limestones of the Çayraz Formation and the terrestrial clastic sediments of the Kartal Formation during the Eocene age (Çiner *et al*., 1996). Both the mélange nappe and the units underlying it were later covered unconformably by terrestrial conglomerates, marls, sandstones, evaporates and the tuffs of the Cihanbeyli Formation in Mio-Pliocene age.

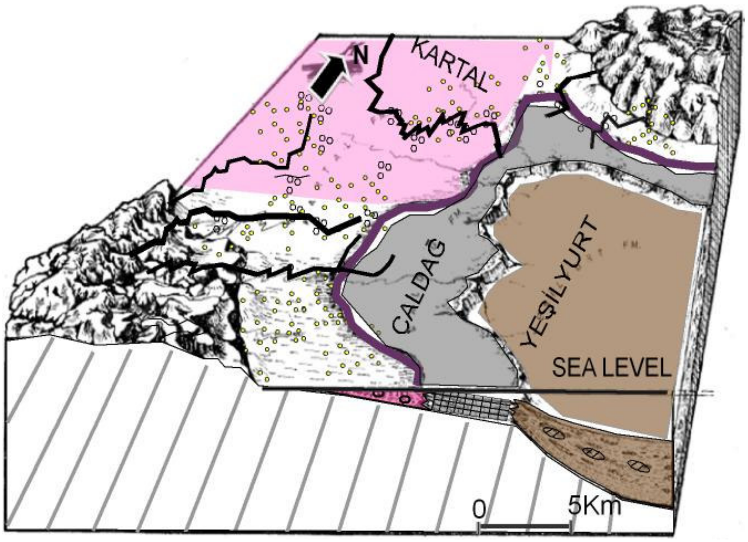

Figure 6. Block diagramm illustrating depositional environment of the Kartal, Çaldağ and Yeşilyurt Formations (modified from Ünalan *et al*, 1976)

CHAPTER 2

LITHOSTRATIGRAPHY

2.1 Regional Lithostratigraphy

Haymana-Polatlı basin deposits are mainly characterized by Upper Cretaceous to Eocene marine and continrntal sequences and the total thickness of these deposits is about 5000 m (Koçyiğit 1991). The lower Paleocene Kartal Formation, which is the subject of this study, mostly represented by continental red beds at the margins of the basin and its total thickness is about 1400 m (Yüksel, 1970; Ünalan *et al.*, 1976; Görür, 1981; Çiner, 1992).

Kartal formation's type locality is well represented near Kayabaşı village on the Kartal hill in the south of Polatlı. This unit also outcrops between Beyobası and Kuşçu villages in the north, around Yenimehmetli village in the west, and between Temirözü and Kavak villages in the south (Sirel 1975, Ünalan *et al* 1976). Sirel (1975) identified *Rotalia trachidiformis* Lamark, *Mississipina binkhorsti* (Reuss) *Distichoplax biserialis Dietrich,* Miliolidae, Gastropoda and Lamellibransh (Ostrea shells), in the upper part of the Kartal Formation. According to these fossil assemblages, Sirel (1975) assigned the Kartal Formation to the Montian age.

Lithostratigraphic units in the studied area the Çaltepe, Seyran, Kocatepe, Haymana, Kartal, Çaldağ, Yeşilyurt, Kırkkavak, Eskipolatlı and Çayraz Formations (Figure 7). According to previous works Kartal Formation comprises 1362 m thick red marl, limestone, lenticular conglomnerate, sandstone, biomicrite and algal limestone successions (Sirel, 1975; Ünalan *et al.*, 1976). Kartal Formation resting at the bottom on the Maastrichtian Beyobası Formation (coral sandstones and conglomerates 125 m thick), bounded at the top with the Thanetian Kırkkavak (limestone and black marls 640 m thick) and laterally wedges out with Yeşilyurt (marls and limestone blocks 342 m thick) and Çaldağ Formations (algal limestones 1187 thick) (Figure 7)

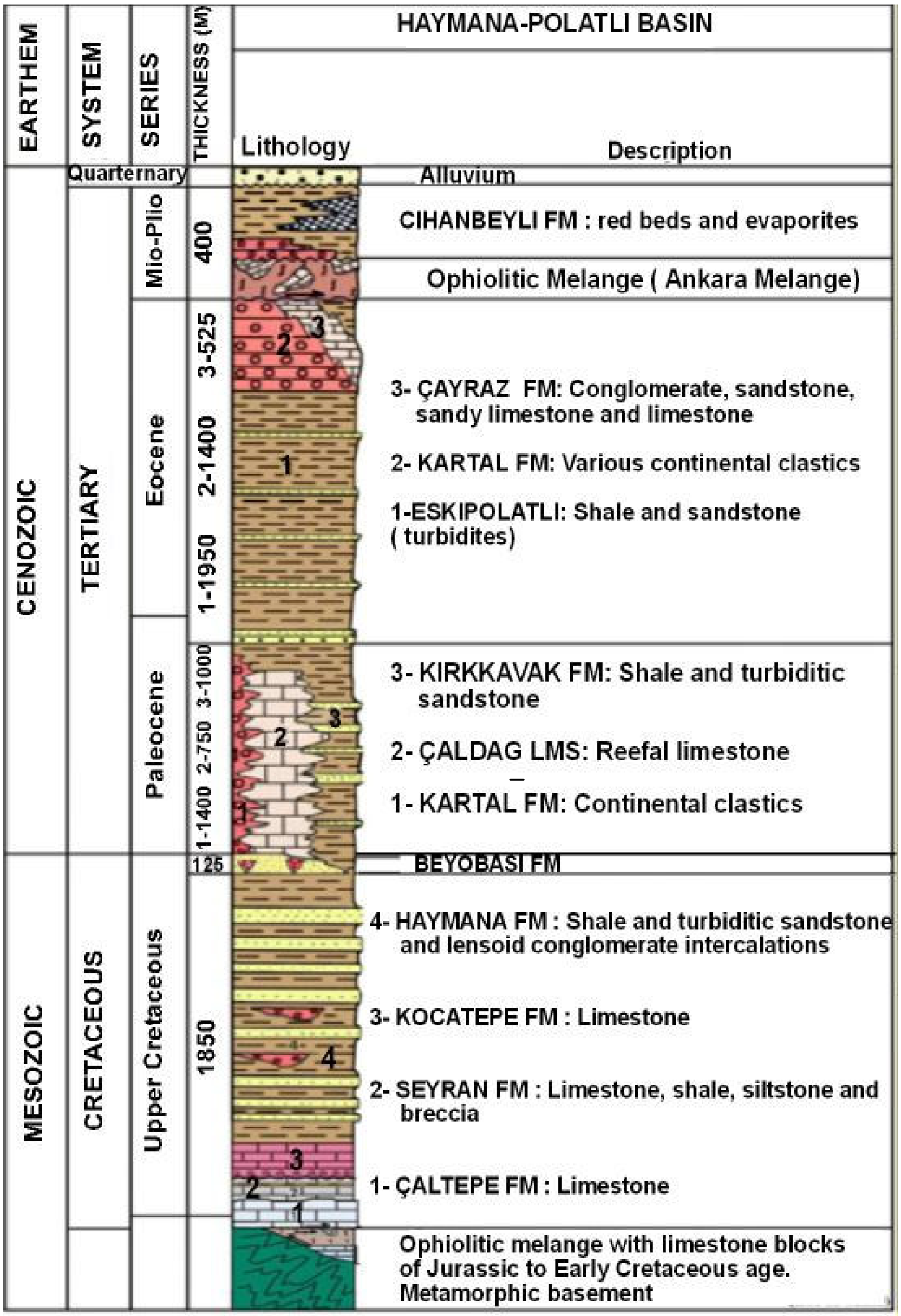

Figure 7. Modified tectonostratigraphic columnar section of the Haymana-Polatlı basin (modified from Yüksel, 1970; Ünalan *et al.,* 1976; based on personal communication with Prof. Dr. Demir Altıner).

2.1 Lithostratigraphy of Upper part of the Kartal Formation

The section studied is located south of Kayabaşı village on the Kartal hill. The measured section starts from the first limestone bed in the upper part of the Kartal Formation and finishes 283 m above at the contact with Thanetian Kırkkavak Formation. Cyclic variations of facies and consistent repetition throughout the section indicate a cyclic pattern of deposition along the measured section.

The lowermost 100 meters of the measured section represented by well developed cyclic alternation of shallow marine carbonates with mudrocks, conglomerates and sandstones, (Samples 65-74) (Figure 8A). The part below measured section, which is out of the scope of study, is completely represented by the alternation of sandstones with mudrocks and conglomerates.

The measured section is enriched with red (or pinkish) to grayish coloured marls and mudrocks from the center to the top of the Kartal Formation. Their percentage is greater than that of other sediments along the whole section. Mudstones along almost all the section contain trace fossils, which according to Demircan (1994) indicate coastal or shallow marine environments of deposition (Figure 8B). Upward to the center the Kartal Formation clearly displays the cyclic repetition of marls and/or mudrocks with cross stratified sandstones and conglomerates (Samples 27-60) (Figure 9A). The sand content increases upward through the mudstone and conglomerate (Figure 12). In general, sandstone facies are composed of lithic greywackes, which are abundant along the entire studied section and litharenites which are mainly observed in the central part of the section. The next upper part is represented by 3 m of gray-colored oolitic limestone succession (samples 21-26) (Figure 9B). Toward the top boundary, continental sediments are dominant (Figure 12). The Kartal Formation consists there of sandstone, conglomerate, sandstone with cross-stratification and mudstone successions (Figure 10A).

Polygenic conglomerate and mudstone alternation grade into pebbly sandstone facies upward through the section (samples 16-20). Grayish to greenish pebbly sandstones here contain some plant fragments, ichnofacies and iron crystal inclusions (Samples 12-15) (Figure 10B). The uppermost most part of the Formation represented by the transition from sandstone into the thick limestone succession indicating transition from continental to marine environment (Figure 11 A).

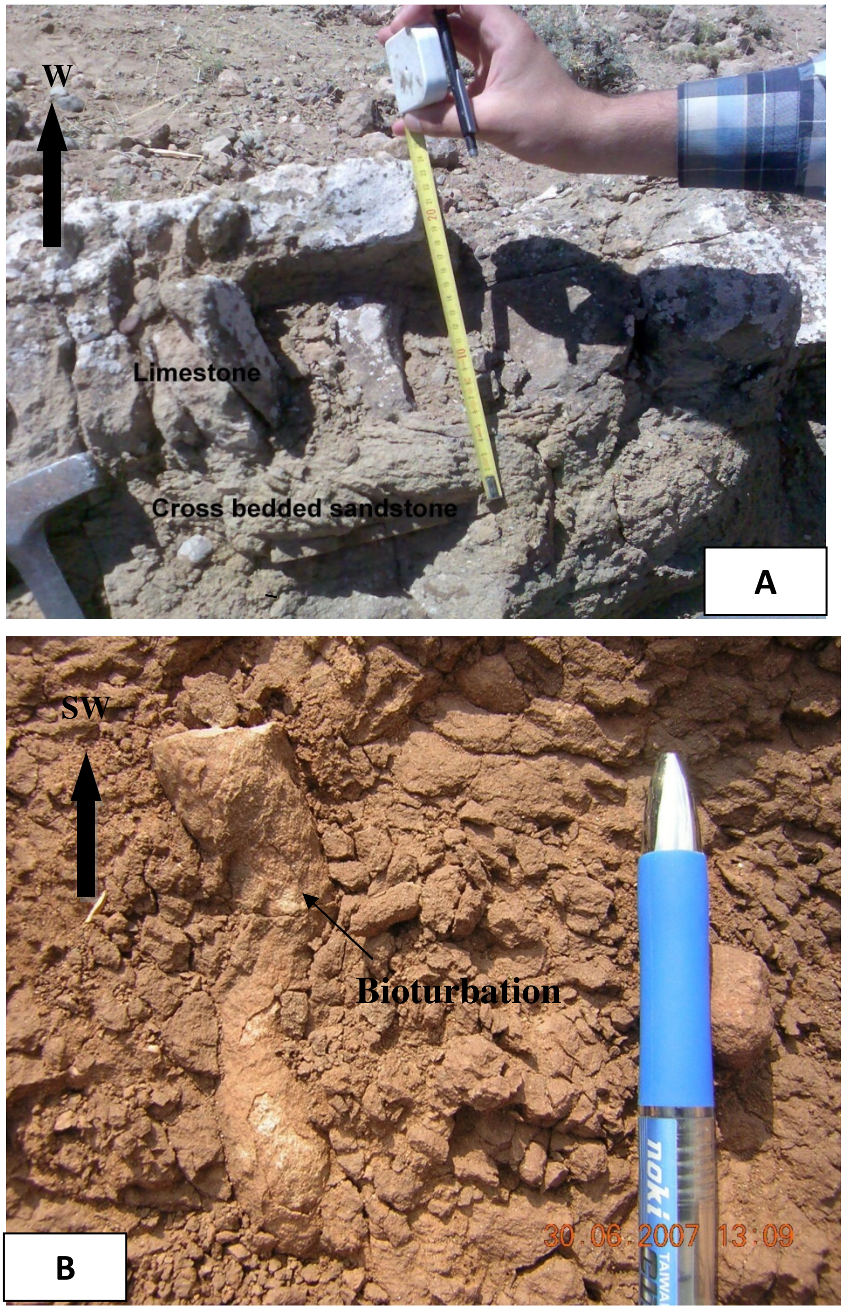

Figure 8. Field photographs of the rock units recognized along the measured section. A- Sandstone-limestone alternation in the lower part of the measured section. B- Bioturbated mudrock (KRF 63).

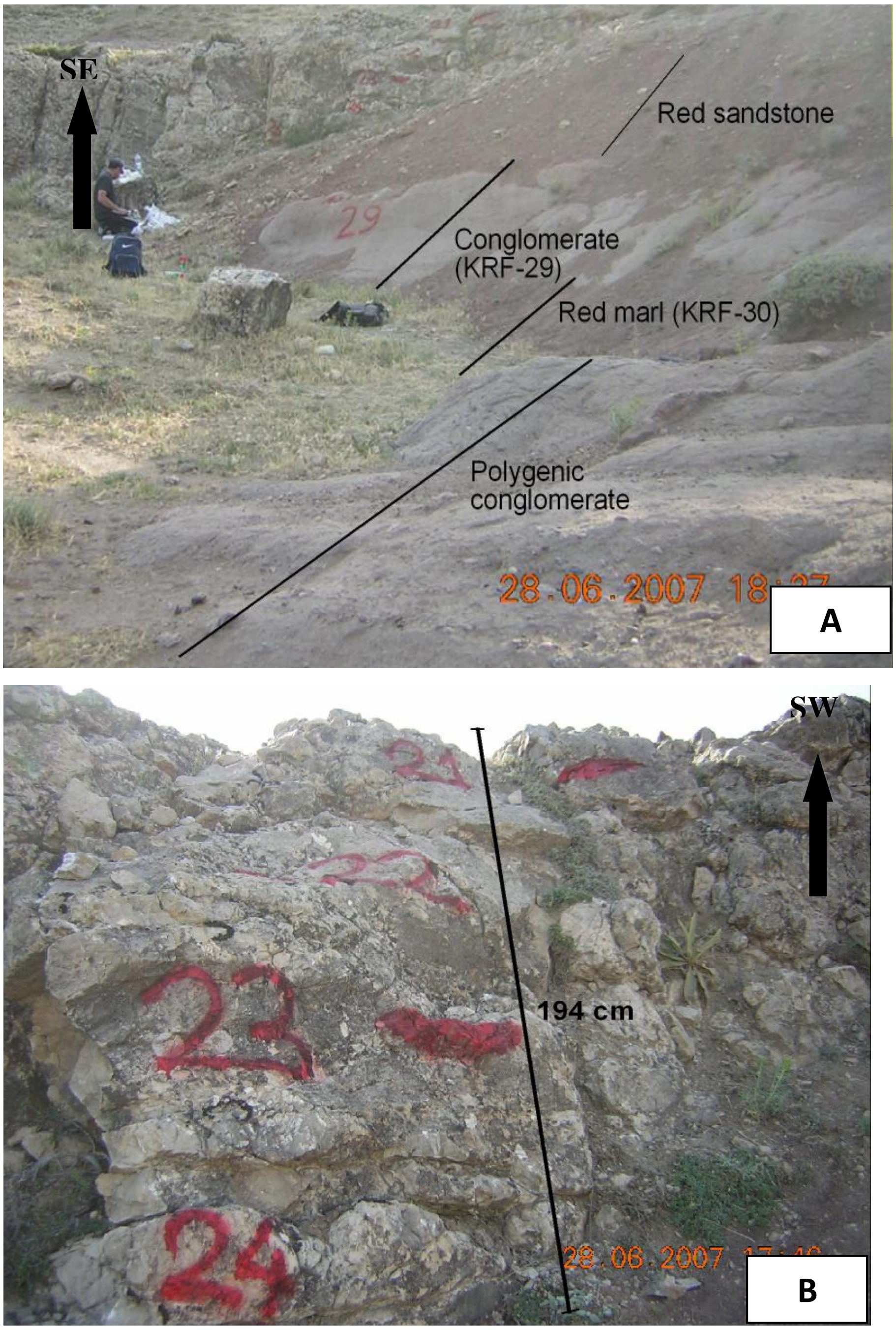

Figure 9. Field photographs of the rock units recognized along the measured section. A- Oolitic limestone succession (KRF 21-26). B- Alternation of conglomerates with red sandstone and marl (KRF: 28-31).

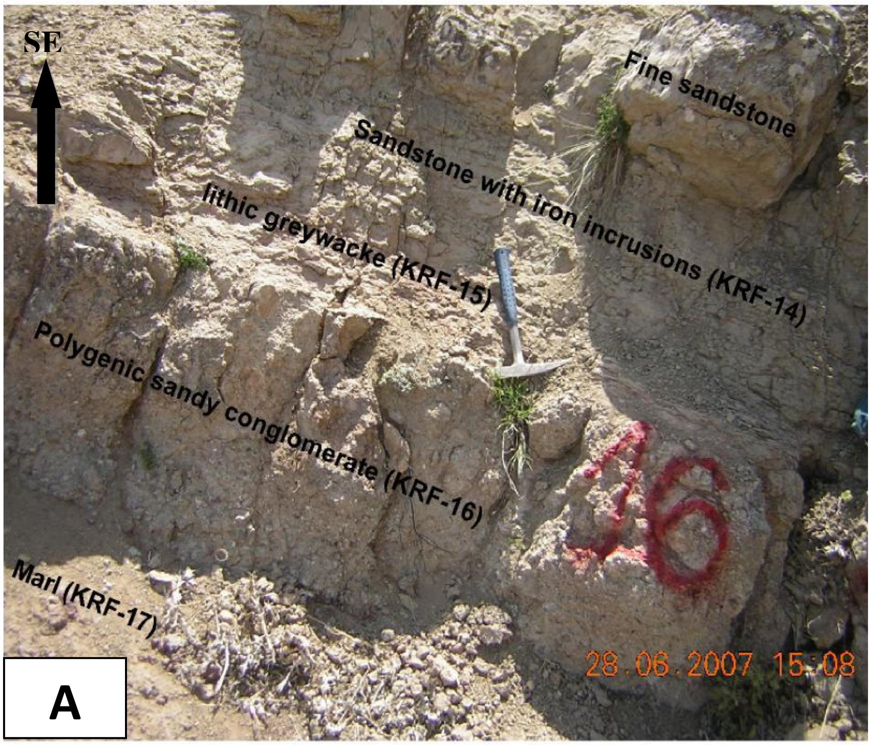

Figure 10. Field photographs of the rock units recognized along the measured section. A-polygenic conglomerate, grading into sandstone (KRF 13-17); B-Transition from continental to marine environment

The presence of ostrea's shells within conglomerates and sandstones is further evidence of a transitional environment (Samples 12, 16) (Figure 11B).

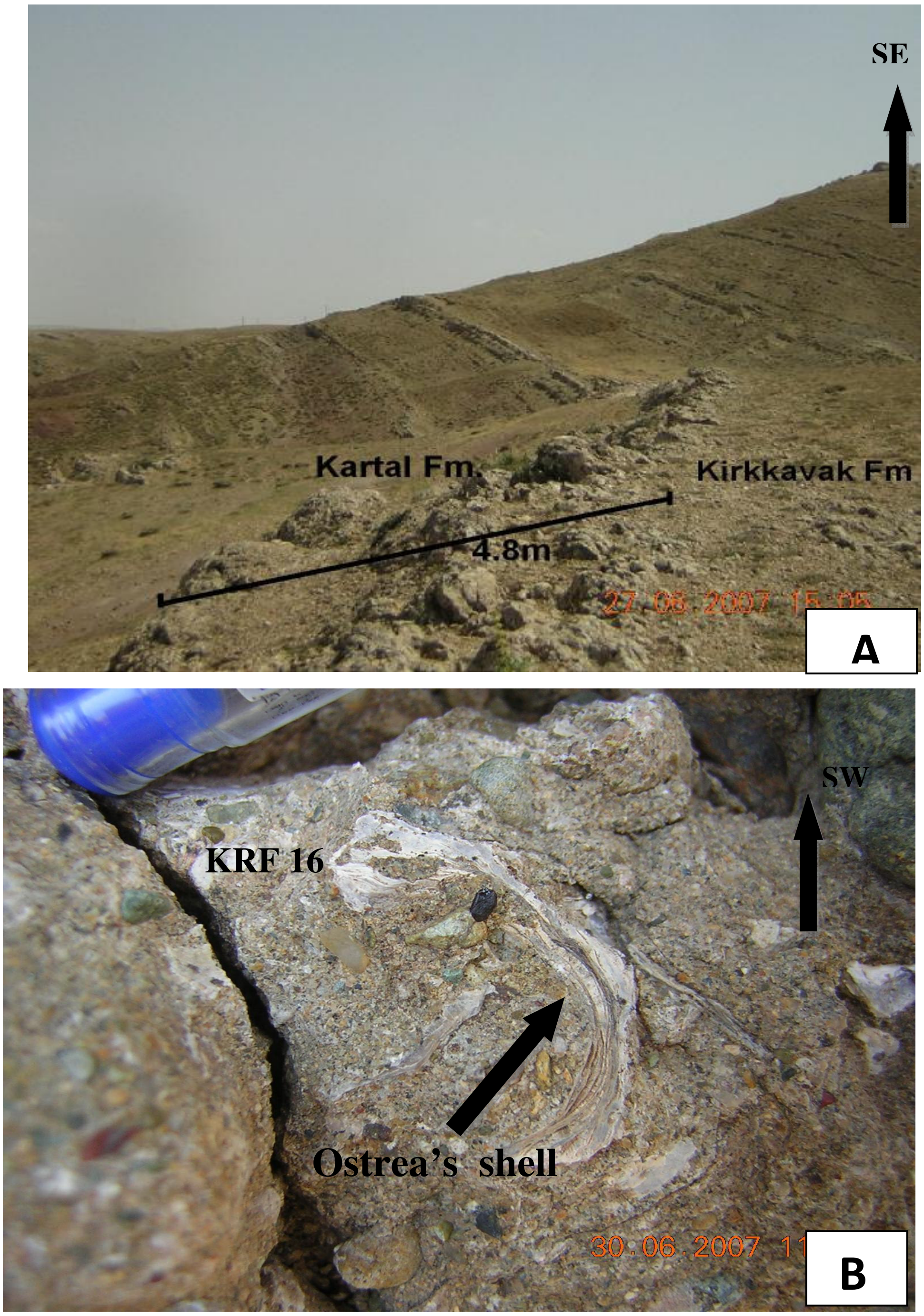

Figure 11. Field photographs of the rock units recognized along the measured section. A- Transition from Kırkkavak to Kartal Formation, represented by 4.8 m; B- Ostrea shell within polygenic conglomerate.

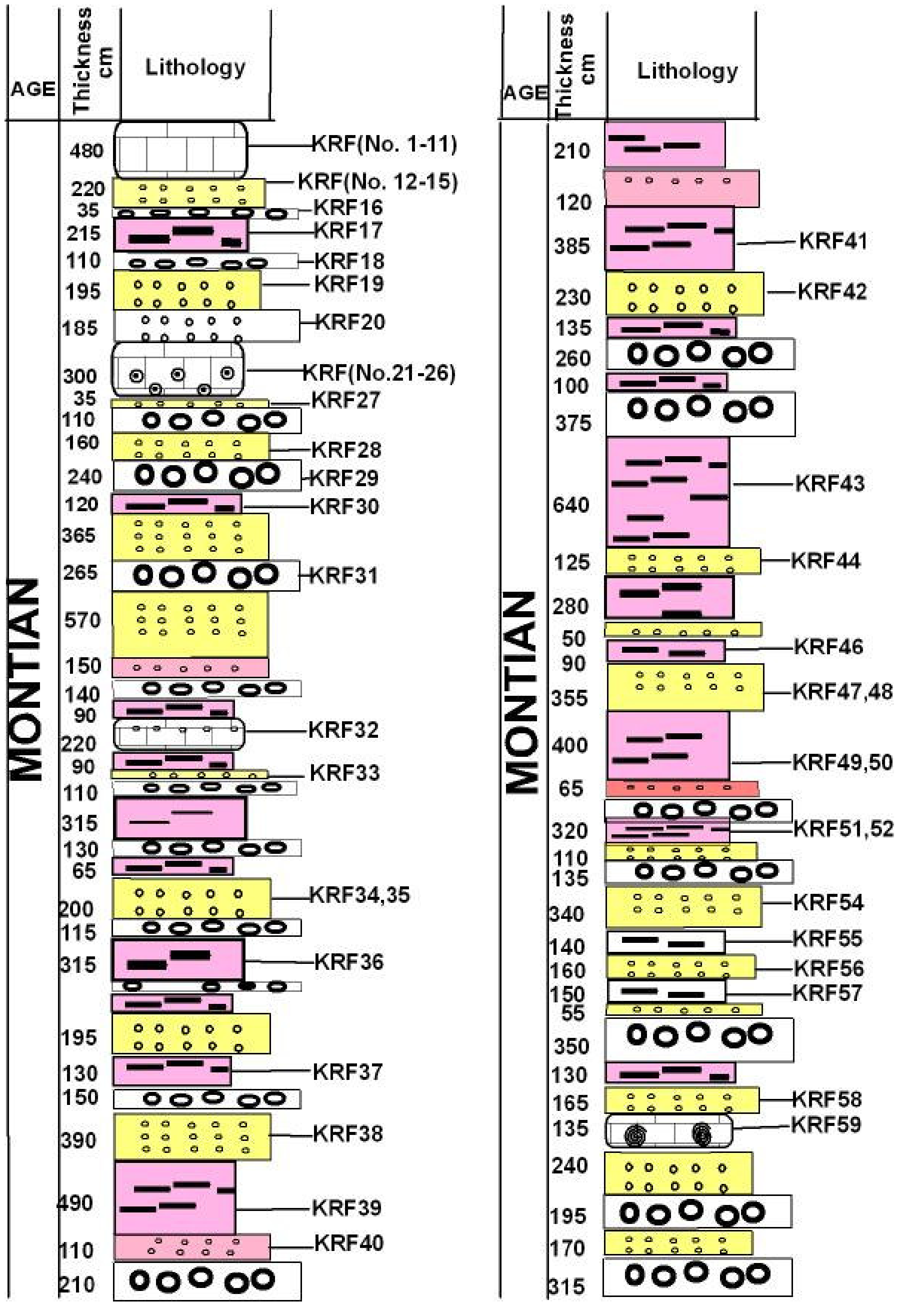

Figure 12. Simplified measured section (for detailed section see appendix A)

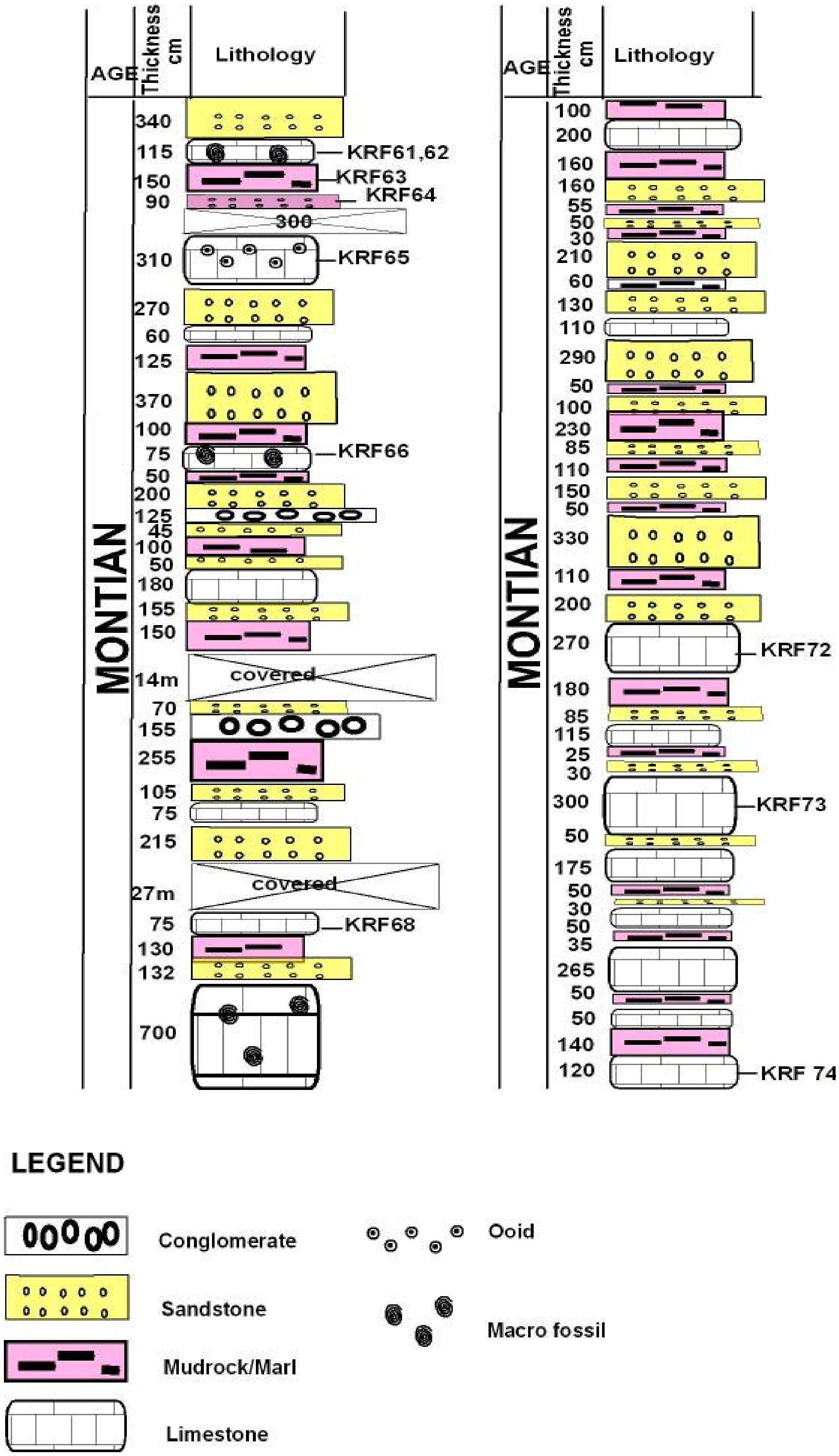

Figure 12. Continued

CHAPTER 3

SEDIMENTOLOGY

Sedimentological study of the upper part of the Kartal Formation comprises petrographical, grain size and grain parameter, provenance, sedimentary structures, paleocurrent analyses. Sedimentary structures were investigated by outcrop studies along the entire measured section. Petrographic analyses were carried out by microscopic examinations. Grain size and grain parameters analyses including roundness, sphericity, sorting, kurtosis and skewness were carried on by the projection of the thin-sections.

3.1 Petrography and Classification of Lithofacies

66 samples were examined under the microscope for microfacies analyses. Using SWIFT point counter machine, a total 750-1000 points were counted within each thin sections in order to obtain accurate percentage of the mineral content. These quantitative data were used to establish the composition and also classify the rock types. According to outcrop and microscope studies, four types of rock were defined in measured section: 1. Sandstones, classified as litharenites, graywackes and sublitharenite; 2. Limestones, which are classified as grainstones, packstones and rudstones; 3. Mudrocks, classified as very fine, fine, coarse mudstones and marls; 4. Conglomerates, classified as polygenic orthoconglomerates (clast-supported).

3.1.1 Sandstones

Sandstone facies are observed throughout the entire measured section of the Kartal Formation. Sandstones were classified as litharenites, lithic greywackes and sublitharenite, according to point counting data (Figure 13). Pettijon *et al*'s classification (1987) - which is based on the percentage of three mineral components: Q=quartz, F=feldspar, L=lithic (rock fragments) - was used to determine sandstones. The term arenite is restricted here to sandstones containing less than 15% of matrix and wacke used for sandstones containing more matrix. Sandstones show current ripples, herringbone cross stratification, planar cross stratification, and channel sedimentary structures along the entire measured section (For details see subchapter.

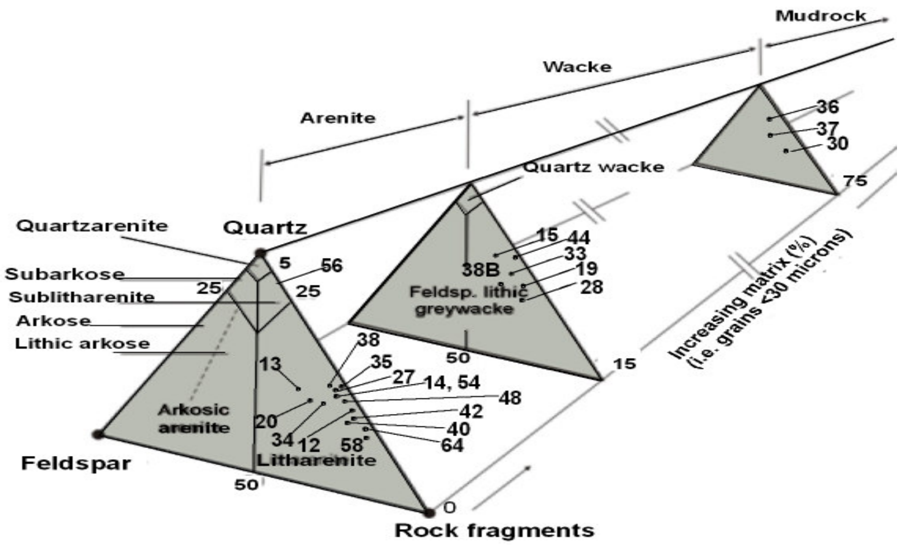

Figure 13. Classification of sandstones. After Pettijohn *et al.* (1987).

3.1.1.1. Litharenites

Litharenite is the prevalent type of sandstone, interpreted in fifteen samples (Sample No: 12, 13, 14, 20, 27, 29, 34, 35, 38, 40, 42, 48, 52, 54, 58, 64) (Appendix B). Minerals or mineral groups identified in the sandstones are: quartz (monocrystalline was prevalent along with minor polycrystalline); feldspar; lithoclast; calcite (mainly as cement); bioclasts; ooids; opaque minerals and micas (Figure 14). Rock fragments are composed of igneous and sedimentary lithoclasts and constituent an average of 33% rock volume. The average content of quartz mineral is 25% within the thin sections, dominated mainly by monocrystaline and some polycrystalline quartz, showing straight extinction. The grains are subangular to subrounded. Minor feldspars are weathered and/or corroded and include plagioclase comprising of the majority of the feldspar component 1.5-4%.

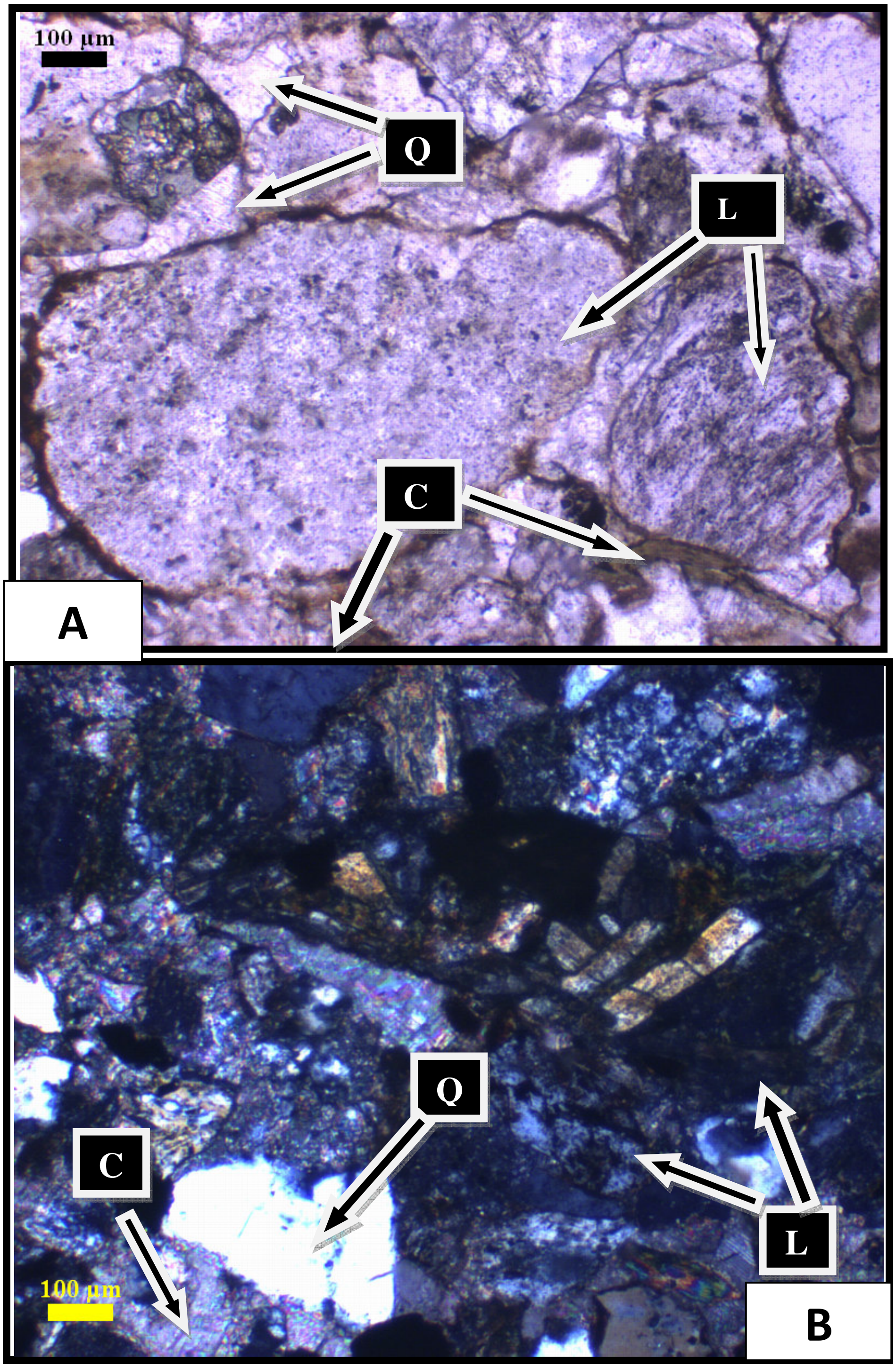

Figure 14. Photomicrographs of the litharenite (Q-quartz, L-rock fragments, C-calcite cement). A: KRF-34, B: KRF-64 (Plane polarized). Barscale below 100 μm

Mica is rarely observed and reached a maximum 1% of total rock volume. Some litharenites contain bioclasts and ooids at an average of 8% throughout the section (Sample No 12, 13, 14, 27). The bioclasts are represented by benthic foraminifers and algae. This factor may be indicative of a shallow marine environment deposition of the aforementioned sandstones (after Flügel, 2004). The cement is calcite, comprising an average 22% of the whole rock volume. Litharenites contain an average 4% of matrix, composed of silt-sized quartz and clay minerals.

3.1.1.2 Lithic greywackes

This type is not prevalent and only observed in five levels (Sample No: 15, 19, 28, 38B, 33, 38, 44) (Appendix B). Quartz, feldspar, calcite and opaque minerals were identified as components in lithic greywacke samples (Figure 15, Appendix B). Quartz represented by 16.5-22% along the succession. These samples are dominated by monocrystaline quartz showing straight extinction. Amount of rock fragments averages 24%. According to visual observation of graywacke samples, grains are subangular to subrounded. Feldspar is ranging between 1.7-3.5%. Opaque minerals are observed in some samples ranging 2.5-7.5% Cement is mainly calcite, and constitutes in average 10-16% of the whole rock volume. Lithic graywackes contain an average 27% of clay matrix stained with iron oxide.

3.1.1.3 Sublitharenites

This type of rock is the least abundant in the measured section and is defined in one level (KRF 56). Quartz (81%), rock fragment (8.8 %), plagioclase (3%) were identified in the sample (Appendix B). Grain size analyses revealed subrounded grains. KRF-56 is moderately well sorted and according to Stewart (1958) and Passega (1964) scattered diagrams, was deposited in the wave dominated environment (for details see subchapter 3.6).

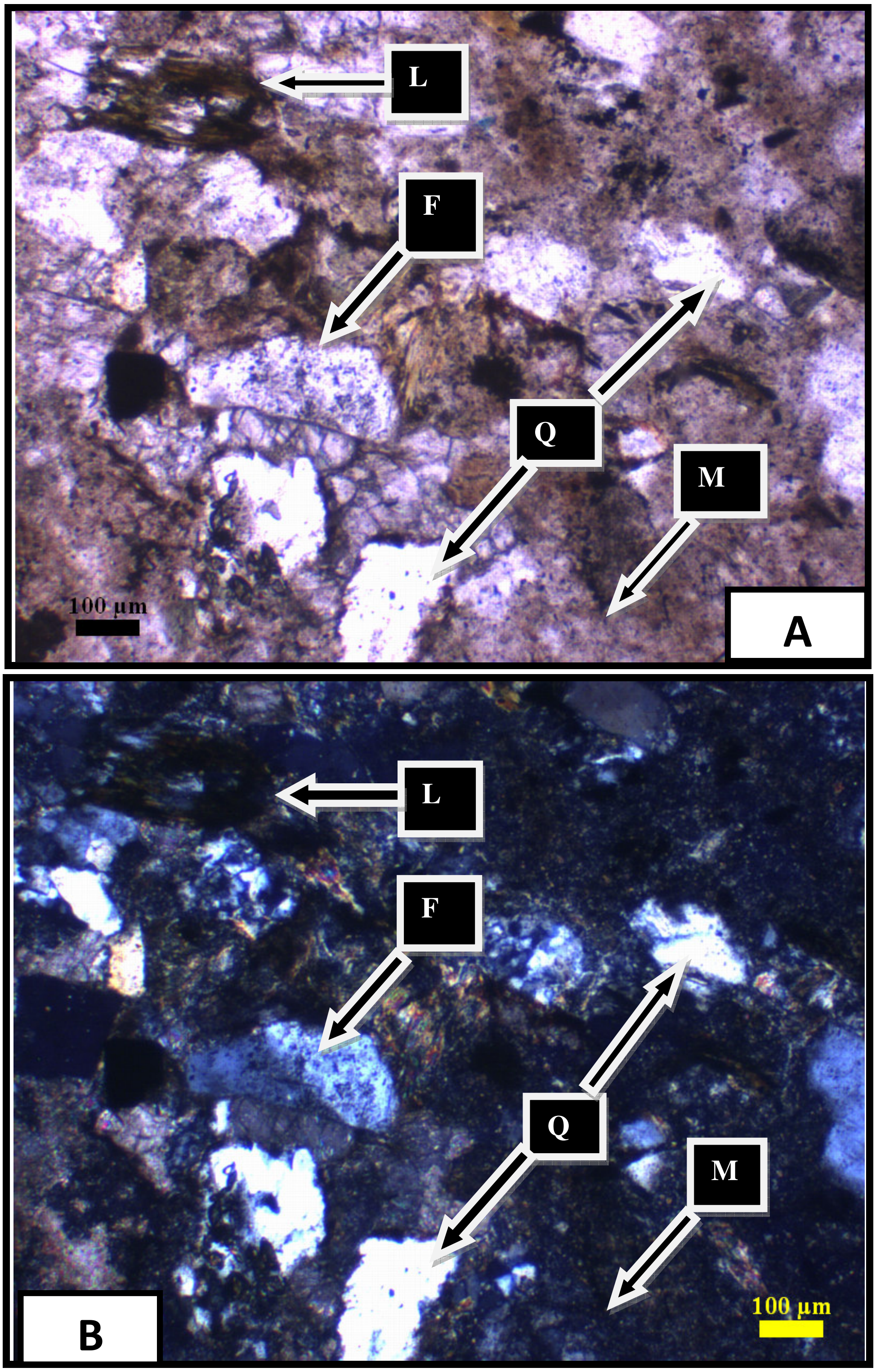

Figure 15. Photomicrographs of lithic greywacke, (Q – quartz, M – clay matrix, F-feldspar, L-rock fragment); A- Transmitted normal, B- Plane polarized. (KRF-19). Barscale below 100 μm

3.1.2 Limestones

Limestones were classified by using Folk (1959) and Dunham (1962) classifications, with additional terms from Embry and Klovan (Figure 16, Figure 19). The classification scheme of Folk is based mainly on composition, and distinguishes three components (Figure 17): 1. Grains (allochems), 2. Matrix (micrite), 3. Cement (drussy sparite). Depending on dominance (bio-skeletal grains, oo-ooids, pel-peloids, intra-intraclasts) abbreviations and prefix to micrite or sparite is used here (Tucker, 2001). Dunham (1962) divides limestone on the basis of the texture. Additional terms of Embry and Klovan in Dunham's (1971) classification give an indication of coarse grains. Six successions of limestones are observed along the measured section from top to bottom: 1. Represented by alternation of oosparites and biosparites (oolitic and bioclastic grainstones respectively) (Sample No 1-11); 2. Represented mostly by oosparites (oolitic grainstones) (Sample No 21-26); 3. Represented by rudstones (biosparites) (Sample No 60-62); 4. Represented by an alternation of oolitic grainstones and rudstones (Sample No 65-66); 5. Represented by bioclastic grainstones (biosparite) (Sample No 68-70); 6. Represented by sandy rudstones (Sample No 72-75). Along the entire measured section, limestones are usually light to dark grey, bluish, beige colored, very well packed, and contain ostrea shells and plant fragments.

3.1.2.1 Oolitic Grainstones (Dunham, 1962), Oosparites (Folk, 1959)

Oolitic grainstone or oosparite is interpreted in twelve levels (Sample No. 1, 6, 7, 8, 9, 10, 11, 21, 22, 23, 24, 25, 65) and contain an average 60% of medium size ooids (1.76-2.06 Φ) cemented by a sparry calcite. A variety of grains serve as nuclei including quartz, rock fragments, bioclasts and skeletal fragments, and especially foraminifers (Figure 18). Samples are moderately-to well-sorted and also include bioclats as benthic foraminifera with an average 15 % of the rock volume. The ooid cortices represented by micritic laminae. Such oolitic grainstone facies are typically deposited under shallow marine environments (Tucker, 2001).

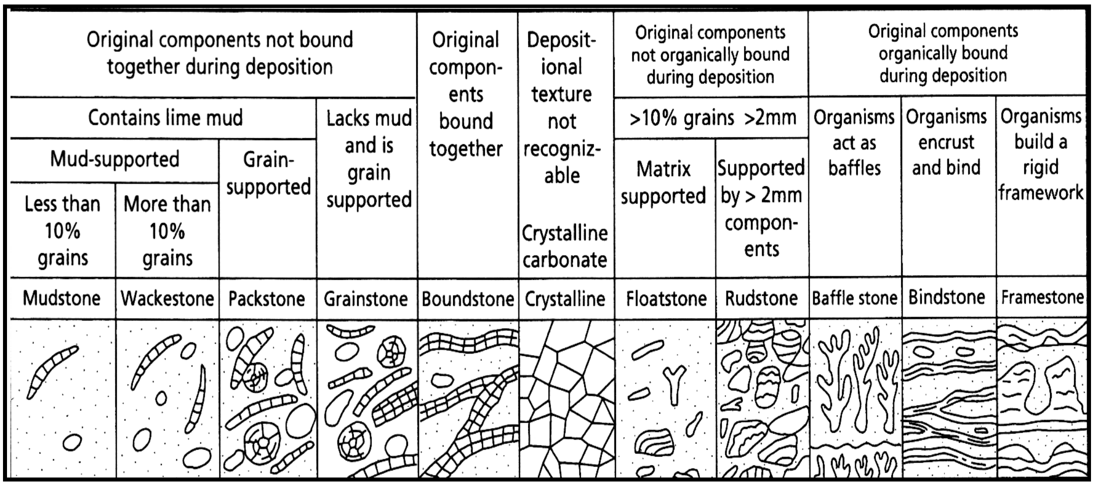

Figure 16. Classification of limestones based on depositional texture, Embry and Klovan, 1971 (after Dunham, 1962).

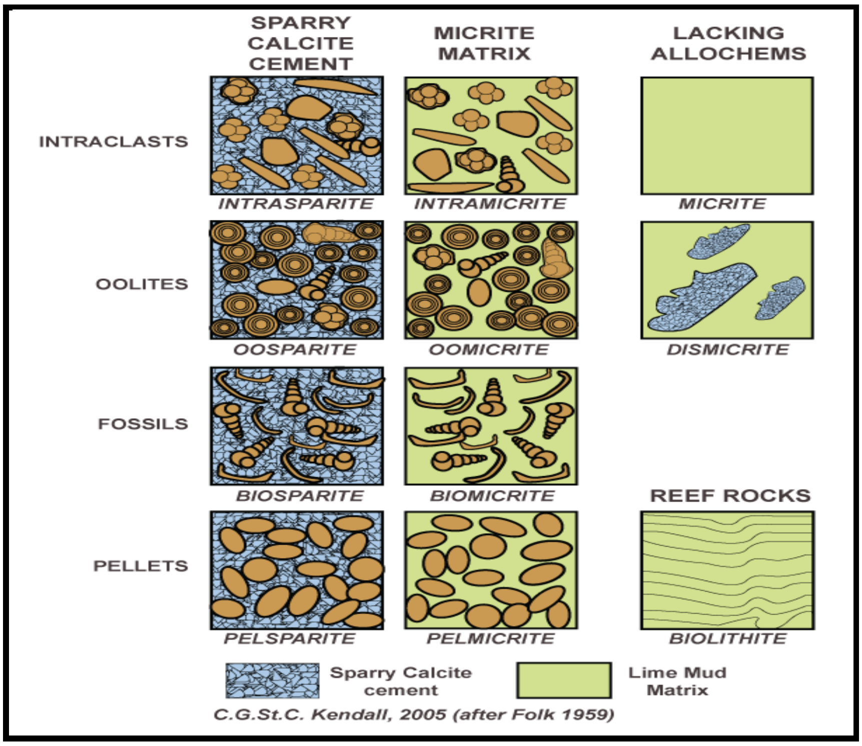

Figure 17. The classification scheme of Folk (1959), based on composition of a limestone.

Samples are characterized by abundant, well-sorted ooids. Two samples (KRF-10, 11) contain an average of 5% quartz and 5 % rock fragments each. Oolitic grainstones contain an average of 20% sparry calcite cement and 5 % micrite matrix. One sample (KRF-22) contains meniscus cement that can be stated as subjected to meteoric-vadose diagenesis (after Tucker and Wright, 2004). The environment of deposition of oolitic grainstones is discussed in detail in the depositional environment subchapter.

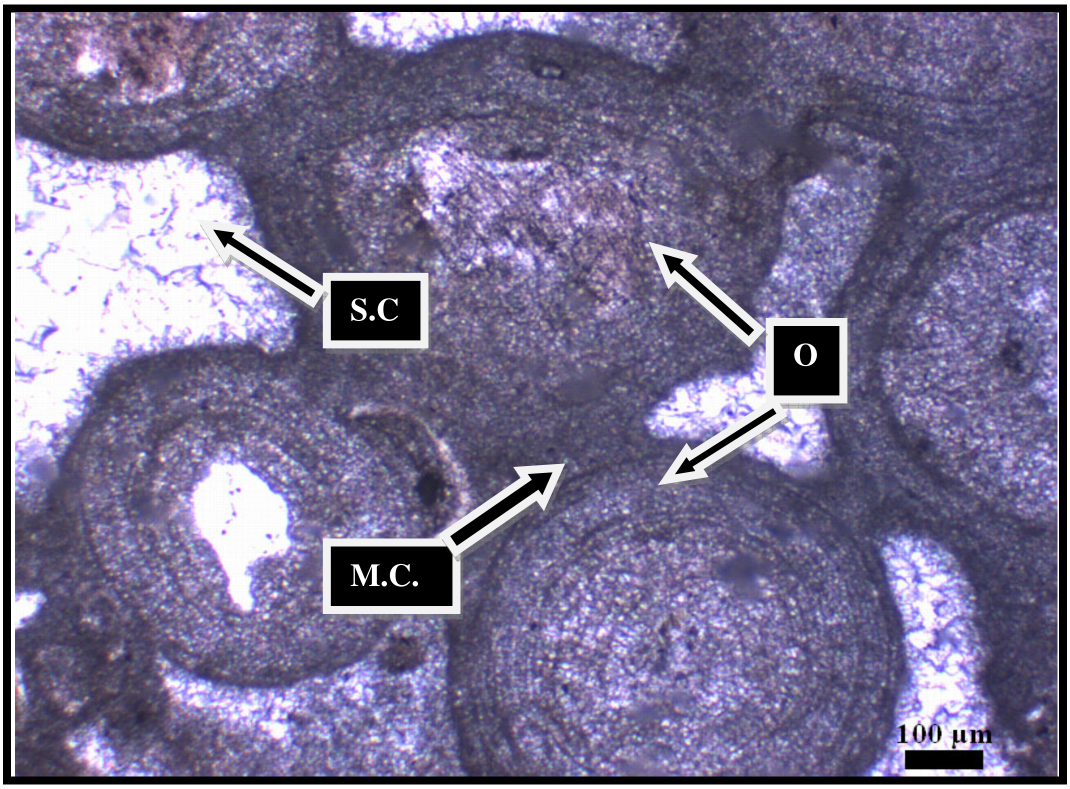

Figure 18. Photomicrograph of oolitic grainstone (O-ooid, M.C. – meniscus cement). Plane polarized (KRF-22). Barscale below 100 μm.

3.1.2.2 Bioclastic Grainstones (Dunham, 1962), Biosparites (Folk, 1959)

This type of limestone is not prevalent and is only observed in seven levels (Sample No: 2, 3, 4, 26, 68, 69, 70). Biosparites mostly take place in the upper (boundary with the overlying Kırkkavak Formation) and lower parts of the measured section. The most common components are benthic foraminifera and some algae; on average, biosparites contain 50.5 % of bioclasts (Figure 19). This limestone type contains some ooids - an average 19.5% of the whole rock. Quartz and sedimentary rock fragment grains serve as nuclei for these ooids. The cement is spary calcite and represents an average 28 % of the whole rock volume. Biosparites contain an average 2% of micrite matrix According to Flügel (2001), this type of limestone constitutes high energy skeletal banks and sheets deposited seaward of ooid shoal, in wave agitated shallow marine settings. These settings mostly represented in the lower and uppermost parts of the measured section (Appendix A).

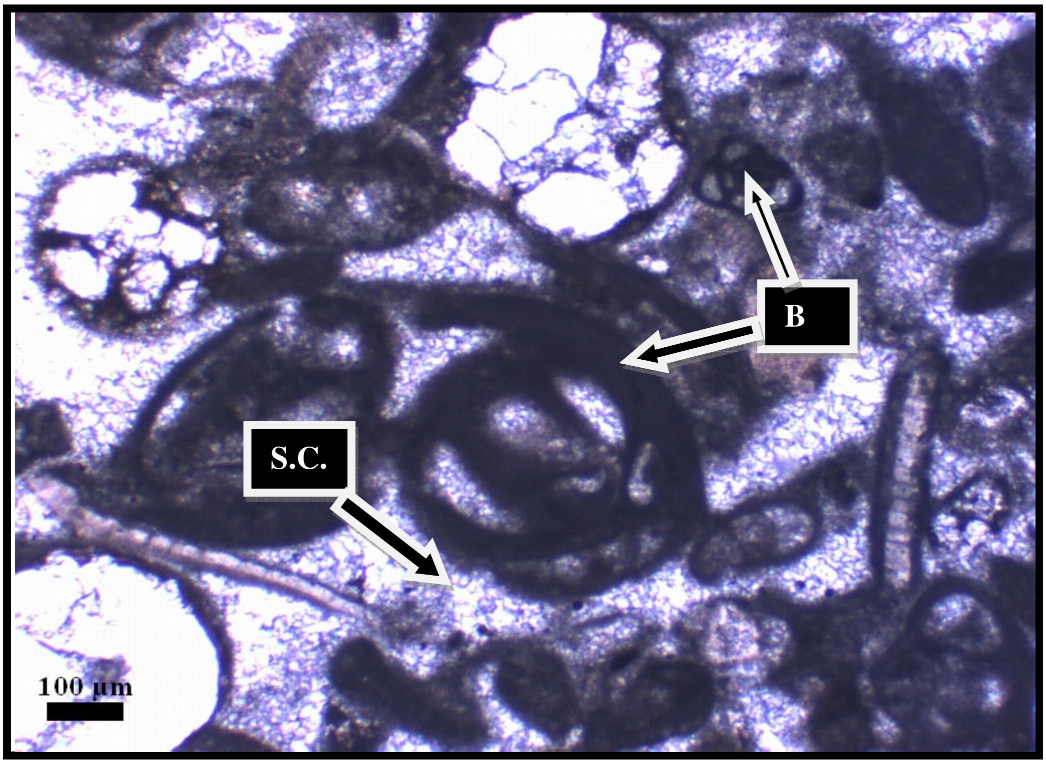

Figure 19. Photomicrographs of bioclastic grainstone (S.C-sparry calcite cement; B- bioclast (foraminifer); Biosparite. Plane polarized (KRF-3). Barscale below 100 μm.

3.1.2.3 Rudstones (Dunham, 1962), Biosparites (Folk, 1959)

This type of limestone is mostly supported by algae fragments more than 2 mm diameter and defined in three levels (Sample No: 60, 61, 62) (Figure 20A). Bioclasts are represented by algae and benthic foraminifers that constitute an average 56% of the rock volume. Ooids constitute 2 % of whole rock volume. Quartz, rock fragments and feldspars are also observed and constitute 9 % of whole rock volume. The cement is spary calcite and represents an average 31 % of the whole rock volume. Rudstones contain minor matrix ranging 2%. One sample

(KRF-60) contains 18% rock fragments, 5.3% quartz and 1.6% feldspar, and can be stated as sandy.

3.1.2.4 Dolomitic Limestone

This type of rock was defined only in 1 level (Sample No: 32) (Figure 20B). This facies takes place in the middle part of studied area, and shows a high level of dolomitization. Dolomitization probably occurred here after during burial diagenesis (Moore, 2001). Calcite cement and bioclastic shells are replaced by idiomorphic dolomite crystals. According to microscope analyses, dolomitic sandy limesone consists of quartz (18.8%), rock fragments (18.3%) and feldspar (2.9%). The rest represents dolomitized calcite cement and shells.

3.1.2.5 Packstones (Dunham, 1962), Biomicrites (Folk, 1959)

This type of rock was interpreted only in one level (Sample No: 5) (Appendix B) and contains 18.5% of matrix. Bioclasts, represented by benthic foraminifera, constitutes 29.4 % of whole rock volume. According to visual observation, this type of limestone is moderately well sorted and includes 22 % of ooids. Packstone is cemented by sparry calcite, which constitutes 21.1 % of the whole rock.

3.1.3 Conglomerates

These beds are composed of clasts of sedimentary, metamorphic and volcanic origin. Visual observations revealed herringbone, planar cross stratifications and finening upward structures in these polygenic conglomerates. All conglomerates were defined as clast-supported (orthoconglomerates) with minor sand matrix according to Boggs's classification (1992). Grains constitute 70-90% of the whole conglomerate volume.

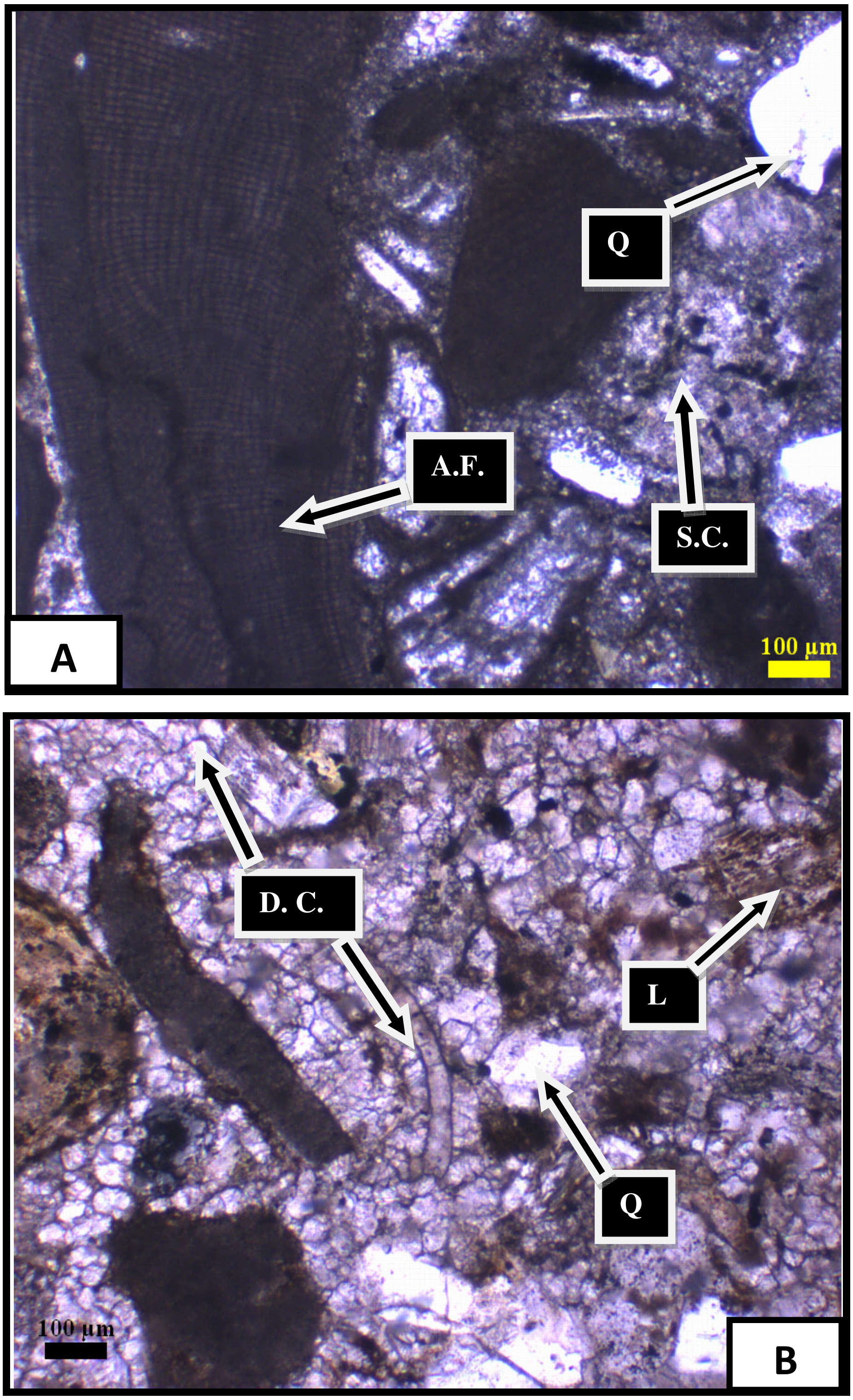

Figure 20. Photomicrographs of limestones (A.F- algae fragment, Q-quartz, S.C- sparry calcite cement, L-rock fragment, D.C.-dolomitic crystals); A-rudstone (KRF-62), B-dolomitic limestone (KRF-32). Plane polarized. Barscale below 100 μm.

3.1.3.1 Clast-supported Conglomerates (Orthoconglomerates)

This type of rock is matrix-poor (80% or more framework grains), and has an intact, stable, grain-supported sandy matrix. These lithofacies were interpreted in 4 levels (Sample No: 16, 18, 29, 31). Among the minerals recognized in the matrix of orthoconglomerates, quartz ranges from 8 to 18%, opaque minerals from 2 to 12% and feldspar from 1.5 to 3. Rock fragments constitute in average of 27% of the whole rock matrix, and most of them are metamorphic. Average content of clay matrix is 2%. Orthoconglomerates contain an average of 25-38% calcite cement by volume. One sample (KRF-16) contains 32% of bioclasts, represented by benthic foraminifera (Figure 21). Marine environment of deposition may be suggested for this bed. The grains are subrounded to rounded.

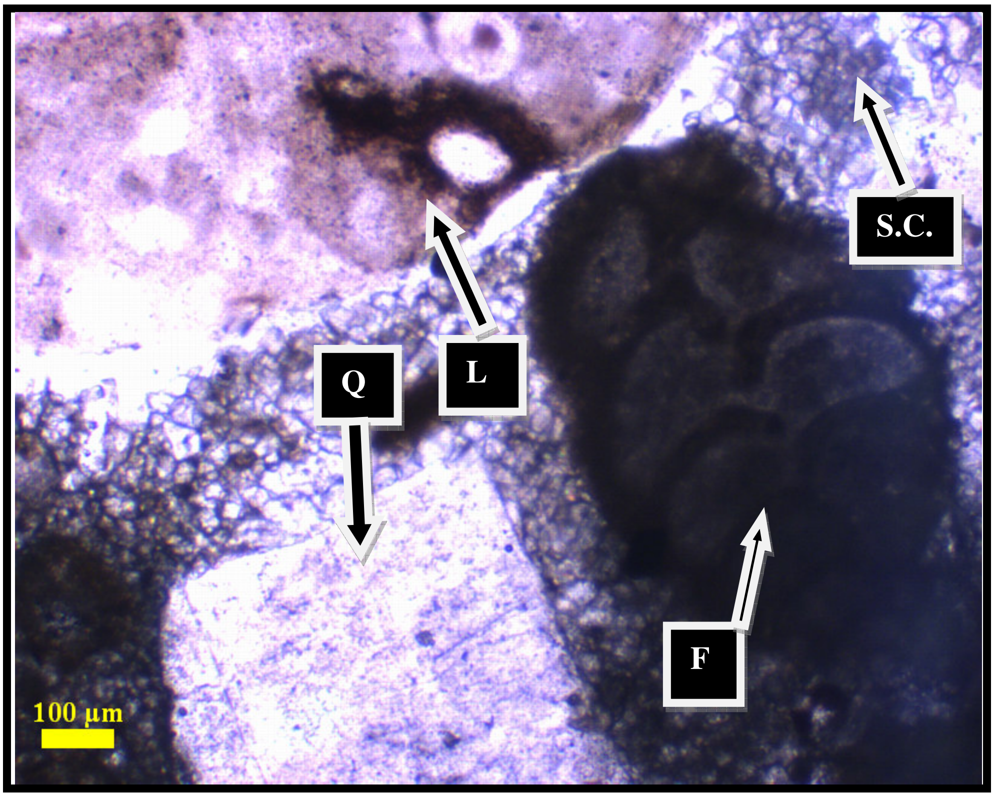

Figure 21. Photomicrograph of a conglomerate: (Q-quartz, L-rock fragment, F-foraminifer, S.C.-sparry calcite cement). Sandy conglomerate deposited in marine environment (KRF-16). Plane polarized. Barscale below 100 μm.

3.1.4 Mudrocks

Indurated, massive mudstones and marls were classified during the field works and in the laboratory, by visual estimation and modal analyses. As the upper part of Kartal Formation shows the abundance of continental sediments, mudrocks here may be associated with floodplains (after Tucker 2001). On the other hand, some of the mudrocks along the measured section contain vertical ichnofacies, which, according to Demircan (1994) suggests a shallow marine environment of deposition (For details see subchapter 3.4.)

Red and gray coloured mudrock have been observed along all measured section and documented in 12 samples (Sample No: 18A, 30, 36, 37, 41, 45, 46, 49, 50, 53, 57, 63) (Appendix B). Two classifations were applied for mudrocks: Pettijohn (1975) and McKee and Weer (1953) (Figure 22, Figure 23, Appendix B). Following Pettijohn's classification, mudrocks were classified as mudstones. Silt-sized quartz grains are presented in all samples and range between 2.5-26.5 %, with an average of 13 % (Figure 24). According to McKee and Weer's classification (1953) based on the quartz percentage within a rock, mudstones were defined as very fine (Sample No: 45, 63), fine (Sample No: 18A, 30, 46, 50, 53, 57) and coarse (Sample No: 36, 37, 41, 49) (Appendix B). Mudstones contain an average of 73.5 % and a maximum 77% of clay matrix stained with iron oxide.

3.1.4.1 Marls

According to Pettijohn (1975) marl is applied for mudrocks containing 35-65% clay and 65-35% carbonate. Calcareous mudrocks-marls are observed in the middle and lower parts of the measured section and were documented in four levels (KRF-17, 39, 51, 55). Intensive bioturbation and parallel lamination was seen on marls in the outcrop. Marls contain an average of 45% of limemud and 55% of clay matrix with iron stains. Quartz, rock fragments and feldspar were rarely observed in marls.

Quartz content	Mudrocks	
	fissile	non-fissile
>40% quartz	flaggy siltstone	massive siltstone
30-40% quatz	very coarse shale	very coarse mudstone
20-30% quartz	coarse shale	coarse mudstone
10-20% quartz	fine shale	fine mudstone
<10% quartz	very fine shale	very fine mudstone

Figure 22. McKee and Weer classification based on the amount of quartz components within a mudrock (1953).

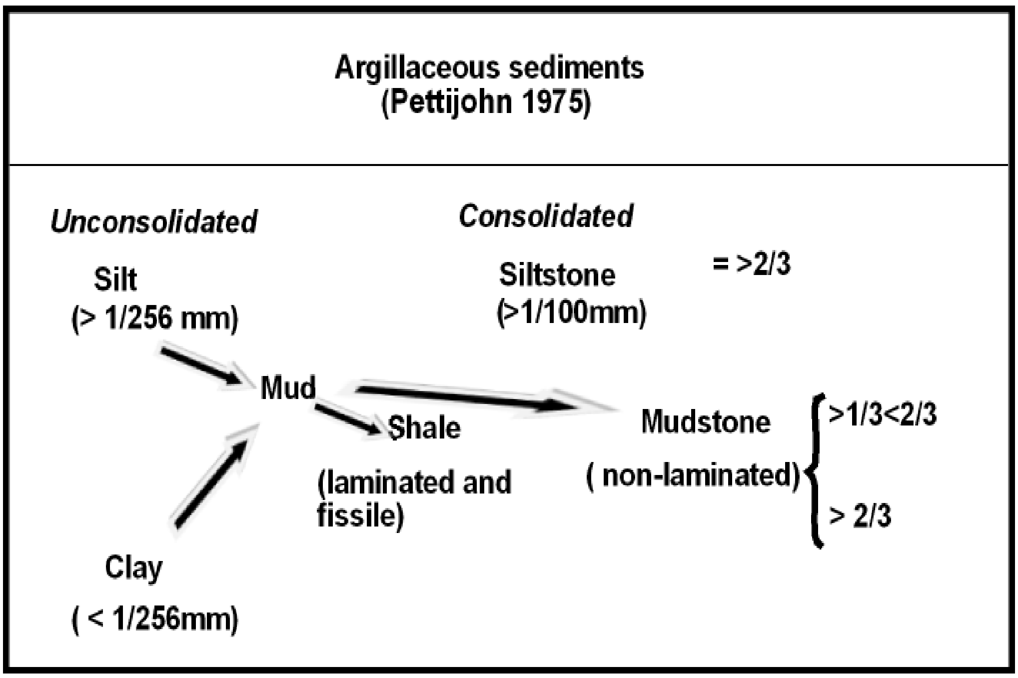

Figure 23. Classification of mudrocks based on clay/silt ratio within a rock (after Pettijohn, 1975).

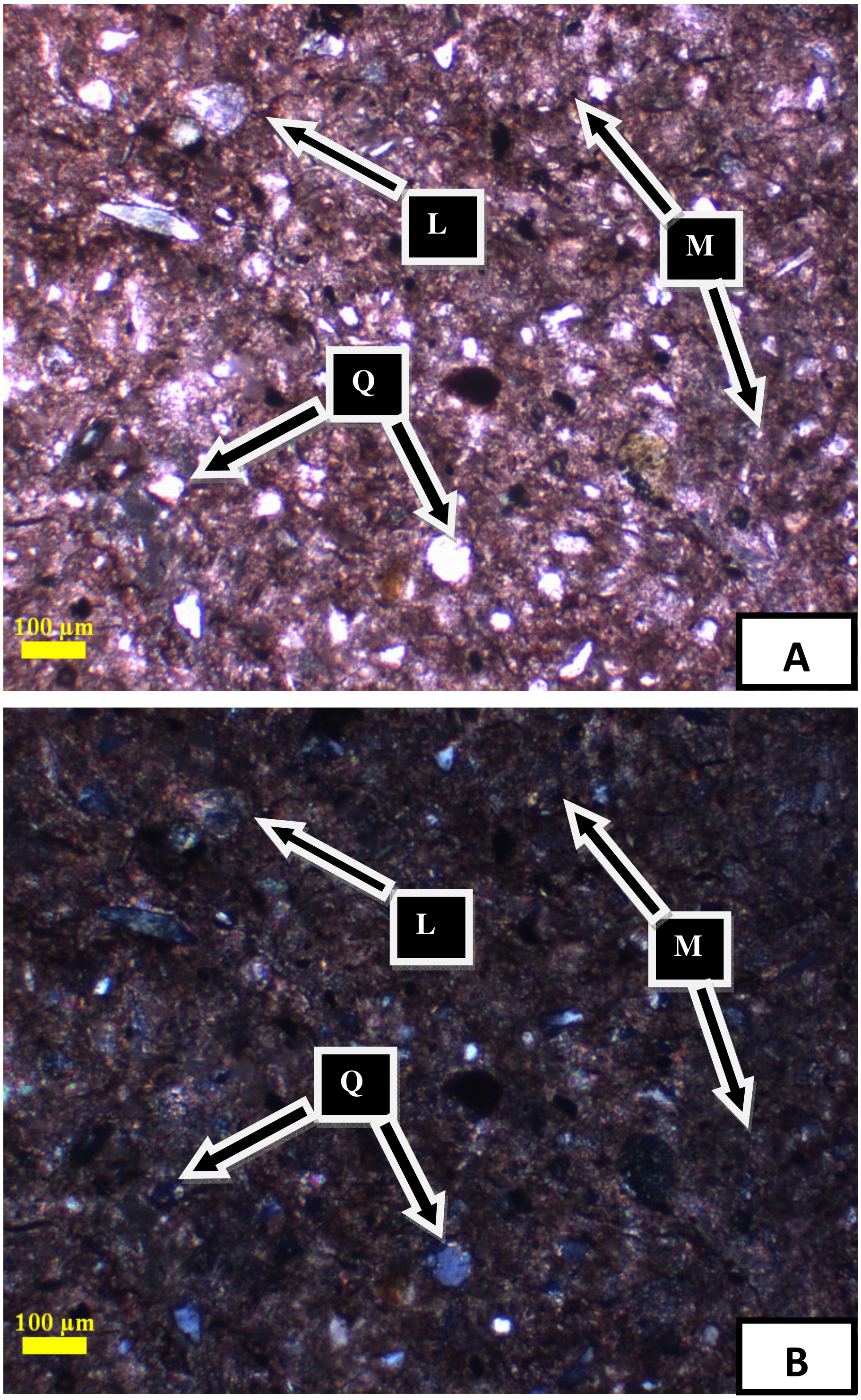

Figure 24. Photomicrographs of mudrocks (Q - quartz, M - matrix, L – rock fragment). A- Transmitted normal, B- Plane polarized. (KRF-37). Barscale below 100 μm.

3.2 Analyses of Grain Parameters

The size of detrital grains within sediment is proportional to the available materials and to the amount of energy imparted to the sediment (Folk, 1974). There is also a close correlation between the grain size and sorting of sandstone. Because the size and sorting of sediment grains may reflect sedimentation mechanisms, grain size data can be used to interprete the depositional environment of sedimentary rocks (Tucker, 1988). In order to obtain grain size, roundness, sphericity, skewness, kurtosis parameters for sandstones and grain shape for conglomerates, grain size analyses was performed on 16 sandstone samples and 3 conglomeratic beds. 200 individual grains were measured in each sample using projection techniques (Appendix C). The histogram and cumulative frequency curves were constructed in order to obtain the end parameters (Appendix D).

The effect of measuring grain size in thin section should be to increase the relative number of very fine grains, and a sieve analysis should never result in a higher percentage of fines than comparable grain size analysis (Friedman, 1962). The Φ (phi) scale introduced by Krumbein and Sloss (1963) is a more convenient way of presenting data than if the values are expressed in mm, and was thus used.

The grain size of the sand fraction in sandstones has commonly been measured by sieving dissaggregated samples (Johnson, 1994). Converting of thin section data to its sieve equivalent has been performed using mathematical equations suggested by Johnson (1994). The empirical equation proposed by Johnson (1994) (Equation 1) was used in this study to obtain mean true nominal diameter of grains from 2D measurements.

$$\overline{D_\phi} = \overline{d'_\phi} - 0.4\left(\overline{a'_\phi} - \overline{d'_\phi}\right)^2$$

Equation 1. True Nominal diameter of ellipsoidal quartz grain (D), $\overline{d}$ - mean nominal diameter and $\overline{a}$ - major axes of the central section (after Johnson, 1994).

Long, intermediate and short ellipsoid axis lengths here correspond to L, I, S with ***a*** and ***b*** representing the long and short axes of cross sections through ellipsoid (Johnson, 1994). According to the empirical equation, mean nominal diameter (D) of ellipsoidal grain, obtained from sieve analysis, can be defined in thin sections from mean nominal sectional diameters (d') and major axes (a') of the central section (derived from the observed values by subtracting 0.2023 from the means) (Johnson, 1994).

Median diameter represents the midpoint of grain size distribution, but is not as useful as the mean grain size (Boggs, 2001). Its size is determined by the 50% line of the cumulative frequency curve (Tucker, 2001). The mean size is the arithmetic average of all the particle sizes in a sample (Boggs, 2001). Where a grain–size distribution is perfectly normal and symmetrical, then the median, mean values are the same. The sorting is a measure of the range of the grain sizes present and the magnitude of the spreads of these sizes around the mean size. It is one of the most useful parameters because it indicates the effectiveness of the depositional medium in separating grains of different classes. Skewness is a measure of the symmetry of the distribution. Skewness is also a descriptive factor for depositional environments: sediment becomes more negatively skewed and finer grained along its transport path, whereas the source sediment becomes more positively skewed and relatively coarse (Tucker, 2001). Kurtosis is the quantitative measure used to describe the departure from normality (Boggs, 2001). Although kurtosis is commonly calculated along with other grain-size parameters, the geological significance of kurtosis is less than that of sorting and skewness (Boggs, 2001). The grain-size frequency curve showing the relationship of standard deviation to the mean and median size was constructed in order to calculate mean and median, sorting, skewness and kurtosis (after Folk and Ward, 1957) (Appendix D). The 5th, 16th, 25th, 50th, 75th, 84th, 95th percentile values of the Φ were used for calculations by graphical-statistical methods (Table 1). Grain size parameters for sandstones were calculated using Folk and Ward formulae (1974) and cumulative percent log. (Table 1, Appendix D). Results of the grain size parameters are shown in the Table 2.

The grain-size characteristics reflect conditions of the depositional environment. Some techniques for utilizing grain size data to interpret depositional environment have been used. The techniques are based on scatter diagrams that compare median grain size versus skewness relationship and sorting versus skewness for distinguishing between beach, dune and river sands (Tucker,

Table 1. Formulae for the calculation of grain–size parameters from a graphic presentation of the data in a cumulative frequency plot.

Parameter formula	Folk and Ward (1957)
Median	$Md = \phi_{50}$
Mean	$M = \frac{\phi_{16} + \phi_{50} + \phi_{84}}{3}$
Sorting	$\sigma\phi = \frac{\phi_{84} - \phi_{16}}{4} + \frac{\phi_{95} - \phi_{5}}{6.6}$
Skewness	$S_{K1} = \frac{\phi_{16} + \phi_{84} - 2\phi_{50}}{2(\phi_{84} - \phi_{16})} + \frac{\phi_{5} + \phi_{95} - 2\phi_{50}}{2(\phi_{95} - \phi_{5})}$
Kurtosis	$K_G = \frac{\phi_{95} + \phi_{5}}{2.44(\phi_{75} - \phi_{25})}$

Table 2. Grain size parameters derived graphically, using Folk and Ward formulae (1957).

Sample No.	Grain size par		Sorting	Skewness	Kurtosis
	median	mean			
12	2.1	2.0	0.71 (moderately)	- 0.11(coarse)	1.09(mesocurtic)
13	2.4	2.4	0.51 (moder. well)	- 0.15(coarse)	1.16 (leptocurtic)
14	2.7	2.7	0.45 (well sorted)	0.16 (fine)	1.23 (leptocurtic)
20	2.2	2.17	0.61(moder. well)	-0.06(near.sym)	0.87 (platycurtic)
27	2.5	2.5	0.46(well sorted)	0.15 (fine)	1.39 (leptocurtic)
34	1.5	1.37	0.62(moder. well)	-0.24 (coarse)	1.23 (leptocurtic)
35	2.5	2.5	0.70(moder. well)	0.02(near. sym)	1.35 (leptocurtic)
38	2.3	2.2	0.66(moder. well)	- 0.23 (coarse)	0.87(platycurtic)
40	1.6	1.73	0.68(moder.well)	0.11(fine)	1.33(leptocurtic)
42	2.2	2.10	0.65(moder.well)	-0.21(coarse)	0.74(platycurtic)
48	2.80	2.93	0.59 (moder.well)	0.25 (fine)	0.97 (mesocurtic)
52	1.7	1.8	0.61(moder well)	0.19(fine)	0.97(mesocurtic)
54	2.4	2.27	0.62(moder.well)	- 0.31(v.coarse)	0.82(platycurtic)
56	2.4	2.43	0.37(wel sortedl)	0.11(fine skew)	1.33(leptocurtic)
58	1.7	1.8	0.74(moderately)	0.10(fine)	0.89 (platycurtic)
64	1.7	1.83	0.70(moder well)	0.12 (fine)	0.94(mesocurtic)

Table 3. Terms used to describe sorting, skewness and kurtosis values.

Φ	Sorting
< 0.35	very well sorted
0.35 - 0.50	well sorted
0.50 - 0.70	moderately well sorted
0.70 - 1.0	moderately sorted
1.0 - 2.0	poorly sorted
2.0 - 4.0	very poorly sorted
>4.0	extremely poorly sorted
Sk	**Skewness**
>0.30	strongly fine-skewed
+0.30 to 0.10	fine skewed
+0.10 to -0.10	near-symmetrical
-0.10 to -0.30	coarse-skewed
< -0.30	strongly coarse-skewed
Kg	**Kurtosis**
<0.67	very platykurtic
0.67- 0.90	platykurtic
0.90-1.11	mesokurtic
1.11 - 1.50	leptokurtic
1.50 - 3.00	very leptokurtic
>3.00	extremely leptokurtic

1988). Interpretation of depositional environment in the upper portion of the Kartal Formation is discussed in the depositional environment subchapter.

Figure 25 illustrates the heterogeneous sublitharenitic sandstone. According to depositional environment interpretation obtained from scattered diagrams, the rock's main transportation mode was saltation (after Visher, 1969) and it was deposited by waves (after Stewart, 1958) (subchapter 3.6). Along the measured section, mean grain size of sandstones varies from 1.3 to 2.93 Φ (Appendix C). The sandstones are moderately- to well-sorted and the sorting value varies from 0.37 to 0.74 (Tables 2, 3). There is fine to coarse skew that varies from -0.31 to 0.25 (Tables 2, 3). Kurtosis values vary from platykurtic (0.67-0.90) to mesokurtic (0.90-1.11) and leptokurtic (1.11-1.50), with values ranging from 0.87 to 1.39 (Tables 2, 3). As marine carbonates are predominantly biogenic sediments, the size and the type of carbonate sediments is largely controlled by the original size, rather than by any size reduction process that might take place during transport (Flügel, 2004). Depositional environment of sandstones and limestones is discussed further in the depositional environment subchapter.

The morphology of a grain depends upon the mineralogy, nature of the source rock, degree of weathering and degree of abrasion during transport (Tucker, 2001).

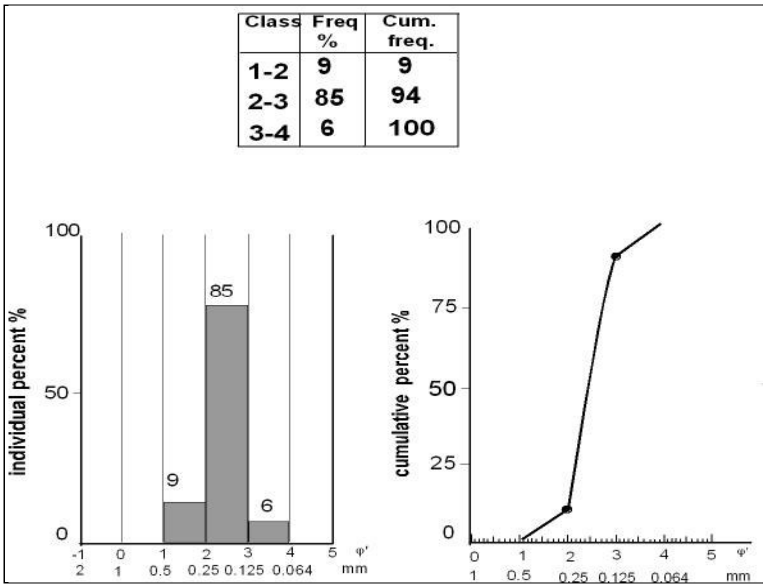

Figure 25. Graphic presentation of grain size data for a sample KRF-56 (Left-histogram.

These factors are reflected in the roundness and sphericity of a grain. Sphericity is a measure of how closely the grain shape approaches that of a sphere. Roundness is a level of curvature of the corners of a grain (Tucker, 2001). Sphericity and roundness analyses were carried out on 16 sandstone samples. Riley's (1941) equation for two dimensional grain images has been used to calculate sphericity of the samples (equation 2).

$$S_R = \sqrt{D_i / D_c} \quad (2)$$

Average sphericity ranges from 0.69-0.75, and varies between subequant to very equant in all samples (after Folk, 1974) (Tables 4, 5 and Appendix C). Roundenss analyses were performed for 16 samples. Dobkins and Folk (1970) formula was used to calculate the parameter (Equation 3). Roundness varies from subangular to subrounded and in average, the roundness is 0.27 for all samples (Tables 4, 5 and Appendix C).

$$R_F = D_K / D_i \quad \textbf{(3)}$$

End results of sphericity and roundness suggest high level of abrasion during transportation.

Scattered diagram representing relationship between roundness, matrix content and sorting data have been used to determine the maturity of the sandsones (Figure 26). Maturity of sandstone varies from immature to mature.

Most of the ooids within grainstones of the measured section are spherical. The shape of ooids often results from the shape of the nuclei (Flügel, 2004). Ooid size within a sediment is controlled by the supply of nuclei (Bathurst, 1979), growth rate (Swett and Knoll, 1989) and mobilization and agitation (Carozzi, 1989).

Table 4. Roundness and sphericity values derived from equations (after Dobkins and Folk, 1970; Riley, 1941)

Sample No.	Roundness (average)	Sphericity (average)
KRF12	0.32 (subrounded)	0.74 (equant)
KRF13	0.32 (subrounded)	0.71 (subequant)
KRF14	0.33 (subrounded)	0.70 (subequant)
KRF20	0.38 (subrounded)	0.73 (equant)
KRF35	0.32 (subrounded)	0.70 (subequant)
KRF48	0.24 (subangular)	0.69 (subequant)
KRF52	0.19 (subangular)	0.74 (equant)
KRF54	0.22 (subangular)	0.70 (subequant)
KRF64	0.35 (subrounded)	0.74 (equant)
KRF34	0.27 (subrounded)	0.76 (very equant)
KRF38	0.22 (subangular)	0.75 (equant)
KRF56	0.29 (subrounded)	0.75 (equant)
KRF27	0.19 (subangular)	0.73 (equant)
KRF40	0.25 (subrounded)	0.74 (equant)
KRF42	0.23 (subrounded)	0.73 (equant)
KRF58	0.21 (subrounded)	0.73 (equant)

Table 5. Terms used to describe roundness and spericity.

Roundness		Sphericity	
0.60 - 1.00	well rounded	<0.6	very elongate
0.40 - 0.60	rounded	0.6 - 0.63	elongate
0.25 - 0.40	subrounded	0.63 - 0.66	subelongate
0.15 - 0.25	subangular	0.66 - 0.69	interdiate
0- 0.15	angular	0.69 - 0.72	subequant
		0.72 - 0.75	equant
		>0.75	very equant

Sample No	12,48,52,54, 34,42	13,20,38,40,58 ,64	14,20,56,27	
	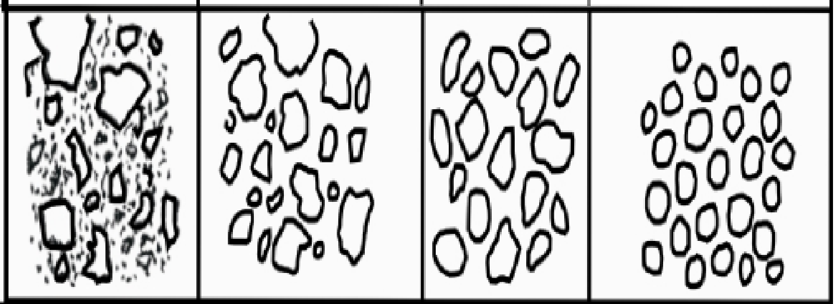			
	IMMATURE	SUBMATURE	MATURE	SUPERMATURE
Clay matrix	> 5%	< 5%		
Sorting	> 0.5 phi		< 0.5 phi	
Roundness	$R_f < 0.35$			$R_f > 0.35$

Figure 26. Textural maturity of siliciclastic sedimentary rocks.

Population of grain sizes may be defined by dynamic considerations, or by supply characteristics (McManus *et al*., 1980). Distribution of the grain size population was obtained using Visher's (1969) scattered diagram, which is based on the three subdivisions of the mode of transportation. The results obtained from the diagram shows that most of the sandstone grains were transported by saltation mode (Figure 27).

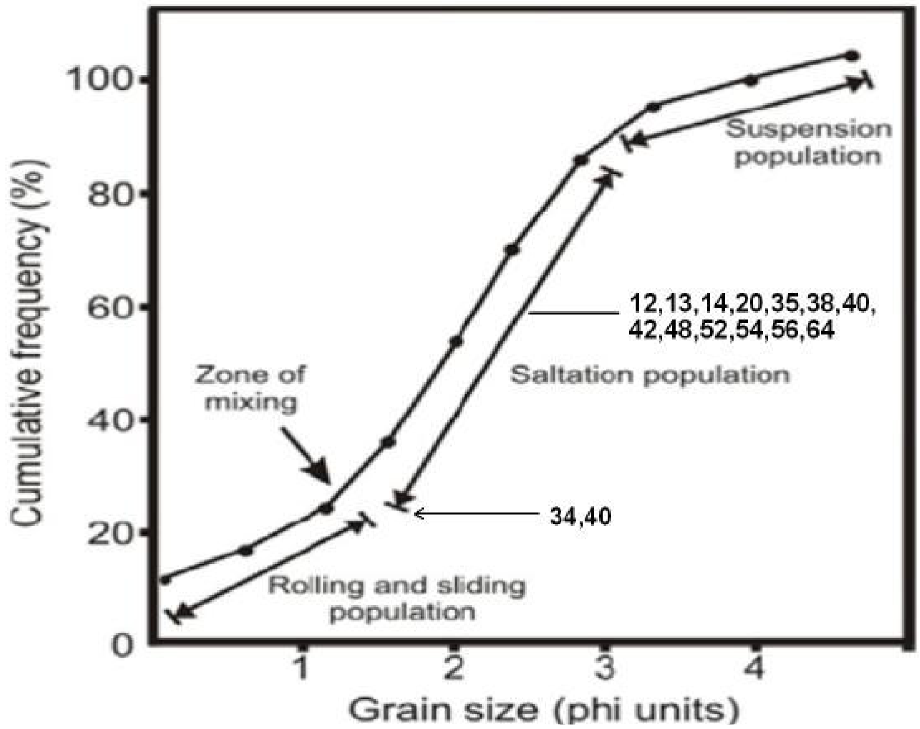

Figure 27. Transport modes in relation to size distributions (Friedman and Sanders, 1978).

Sphericity analyses have also been performed for three conglomeratic successions. Form analyses were based on ratios of the long (L), intermediate (I) and short (S) axes of pebbles collected from the field. In our analyses, sphrericity was calculated based on the Sneed and Folk (1958) formula shown below:

$$\mathbf{SPH} = \sqrt[3]{S^2 / LI}$$

The results of these calculations are shown in (Appendix E). On average, the sphericity is 0.71 for three beds, which results in the particles are being compact. Oblate–Prolate index calculations (OP index) have been performed for these beds. OP index is closely related to form, but it is obtained by a different formula, as shown below:

$$\mathbf{OP = (10L\ (L\text{-}I)/S\ (L\text{-}S)) - (5L/S)}$$

The OP index data is plotted against the diagram proposed by Dobkins and Folk (1970), which developed the OP index of shape to distinguish beach gravel from stream gravel (Figure 28, Figure 29, Figure 30). It can be observed from the OP index diagram, that in all three beds peak position corresponds the range between 2 and 4, which means that the river environment gravels are dominate (after Dobkins and Folk, 1970). In general, as we may observe, gravels in these beds are more likely to be a mixture of beach and river types. Certainly, the gravels deposited within the conglomerates in the Kartal Formation indicates both beach and river environments. Roundness for these three conglomeratic beds has been interpreted by visual estimation and they were found to be sub- to very well-rounded indicating a considerable distance of transportation for most of the pebbles.

Additionally, form of the pebbles within each conglomeratic bed has been revealed using scattered diagarams proposed by Zingg (1935) and Illenberger (1991). According to Zingg's diagram average amount of I/L and S/I ratios were used to obtain average shape of pebbles within each bed (Figure 31, Appendix E). Illenberger's (1991) diagram based on disc rod and shape indexes gives more precise information about form of the pebbles (Figure 32, Figure 33, Figure 34, Appendix E). Affromentioned form analyses revealed that the majority of the pebbles are compact and spherical. This factor can be evidence for long term channel transportation and minor wave influence of pebbles.

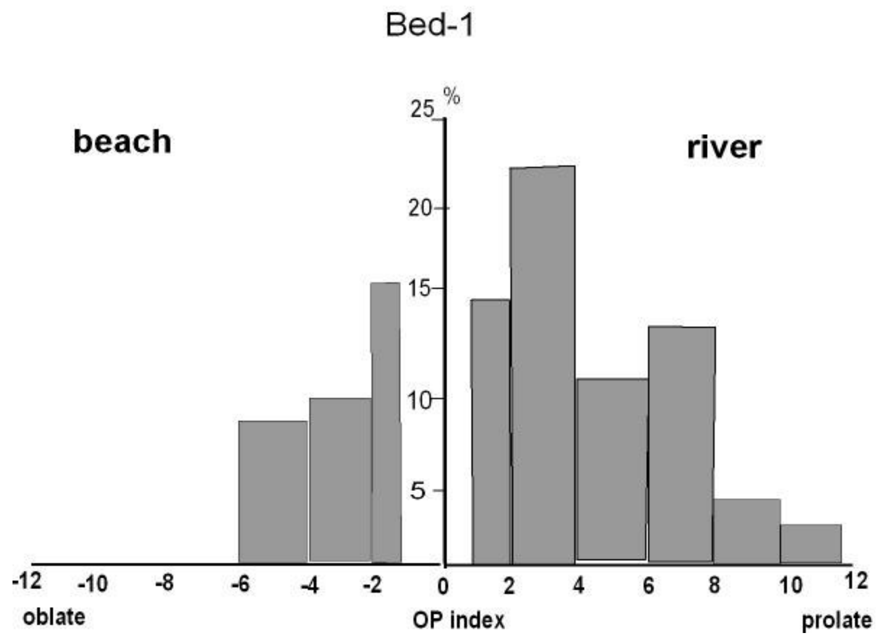

Figure 28. OP index diagram for Bed-1 (after Dobkins and Folk, 1970).

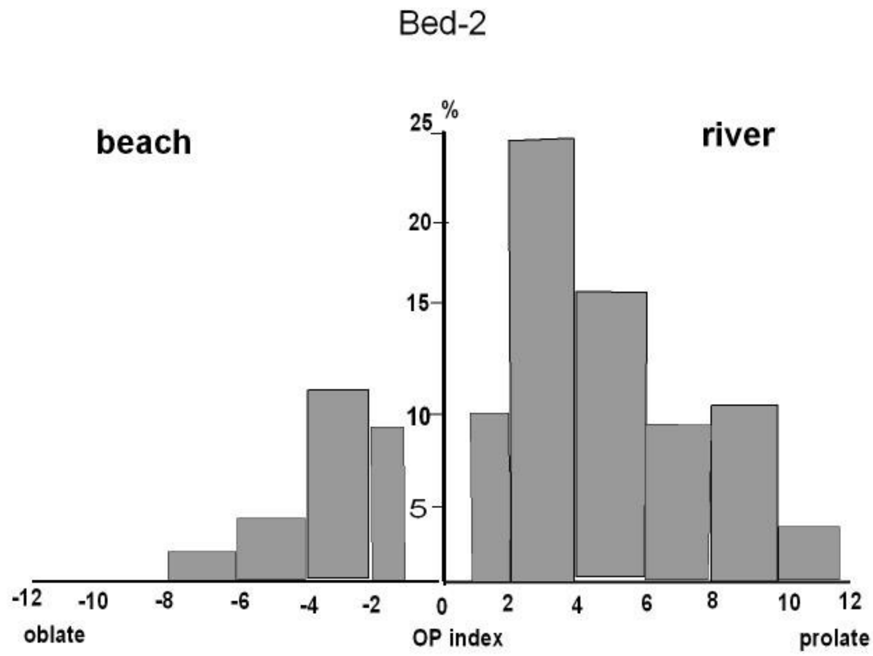

Figure 29. OP index diagram for Bed-2 (after Dobkins and Folk, 1970).

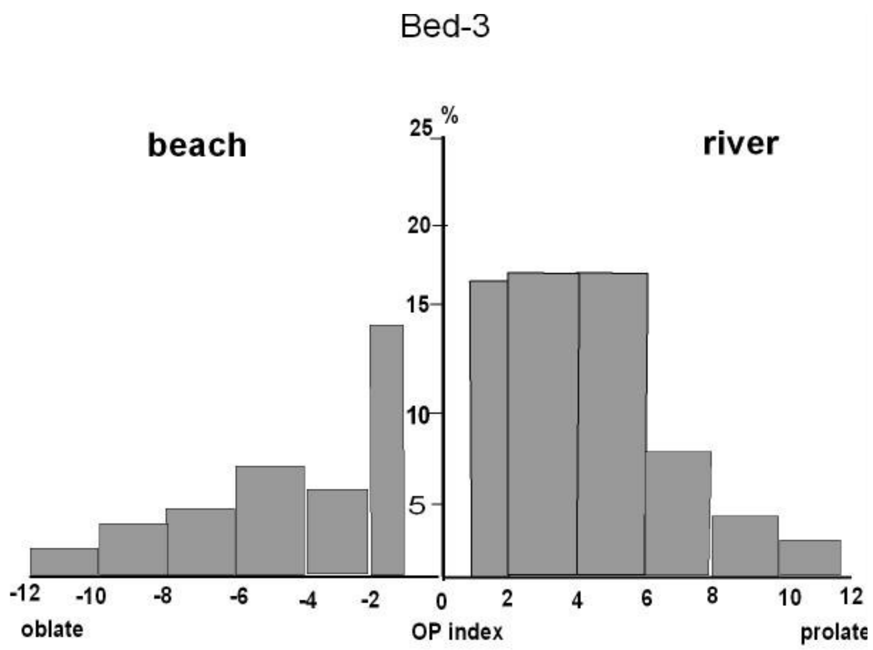

Figure 30. OP index diagram for Bed-3 (after Dobkins and Folk, 1970).

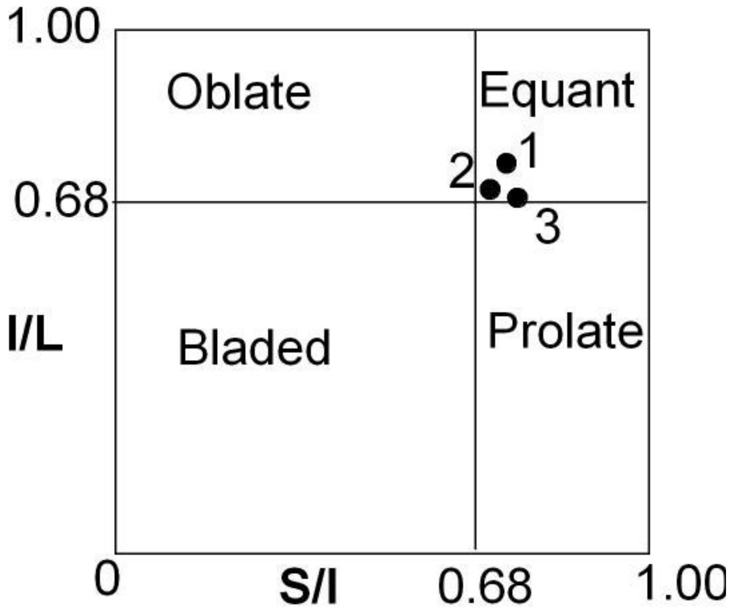

Figure 31. Grain form description according to Zingg (1935).

	Spheres		32%
BED 1	Compact	Discs	9%
		Blades	33%
		Rods	11%
	Discs		1%
	Blades		10%
	Rods		3%
	Extreme	Discs	
		Blades	1%
		Rods	

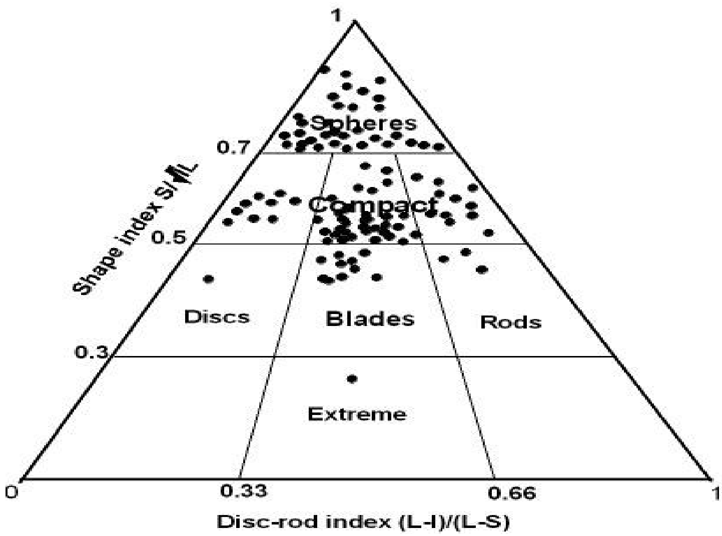

Figure 32. Grain shape description for Bed-1 (after Illenberger, 1991).

BED 2	Spheres		20%
	Compact	Discs	13%
		Blades	23%
		Rods	11%
	Discs		3%
	Blades		18%
	Rods		10%
	Extreme	Discs Blades Rods	2%

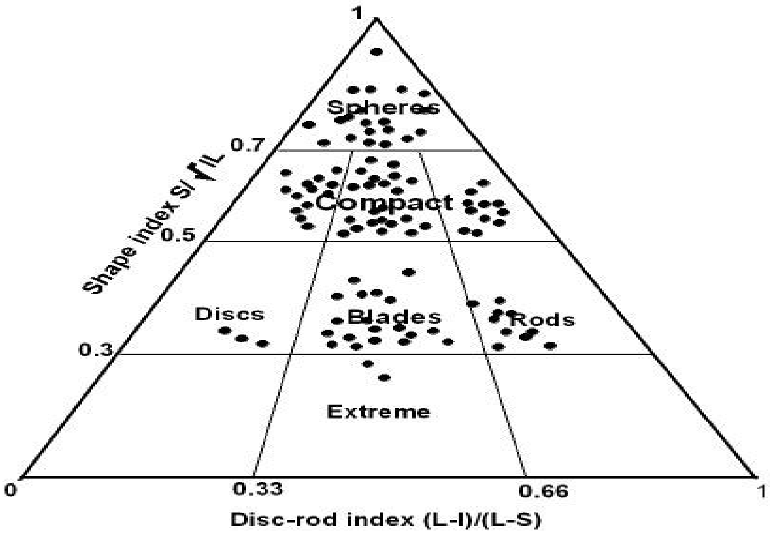

Figure 33.Grain shape description for Bed-2 (after Illenberger, 1991).

BED 3	Spheres		24%
	Compact	Discs	6%
		Blades	10%
		Rods	16%
	Discs		14%
	Blades		2%
	Rods		5%
	Extreme	Discs Blades Rods	4%

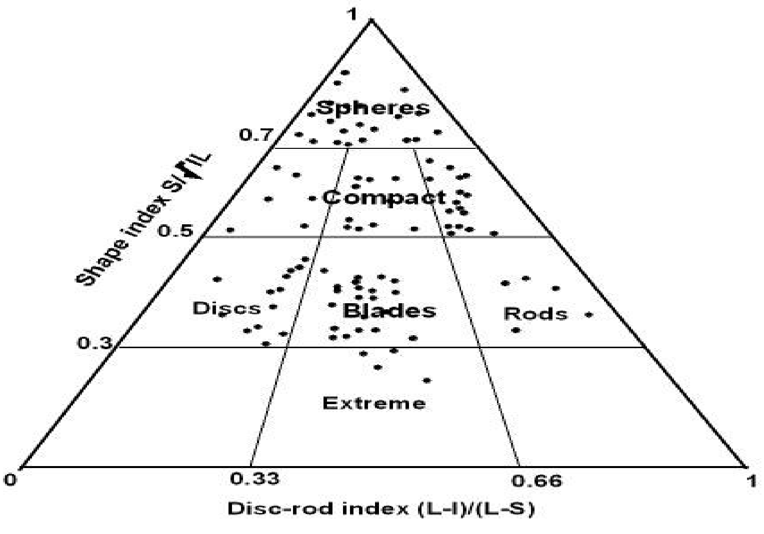

Figure 34. Grain shape description for Bed-3 (after Illenberger, 1991).

3.3 Provenance Analysis

Provenance studies of sandstone sequences can be made using modal composition plus maturity indicators (i.e. sorting, roundness) (Valloni, 1985; Dickinson, 1985). Sandstone sequences are the result of both provenance and tectonic environment, modified by climate, depositional environment and later diagenetic events. Provenance determinations of sandstones also can be made from examination of individual quartz, feldspar and lithic grains (Krynine, 1946). Dickinson (1985) distinguished four major provenance terrains for sandstones: stable craton, basement uplift, magmatic arc and recycled orogen. In order to perform provenance analysis, 16 sandstone samples were used, after obtaining data from microfacies analysis. Samples were chosen on the criteria of Cox and Lowe (1996), who suggested using sandstones with less than 15% of matrix content for such purposes. Dickinson's triangular diagram (1985) was used, which plots Qm (monocrystalline quartz), F (total feldspar), Lt (total lithic fragment), including Qp (polycrystalline quartz) with lithic grains to determine the source. Detritus from the various provenance terrains generally has a particular composition, as the debris is deposited in associated sedimentary basins, which occur in a limited number of plate–tectonic settings (Tucker, 2001). In this modal analysis of sandstone samples, the percentages of various combinations of grains are plotted on a triangular diagram. According to Tucker (2001), at least 300 samples are required from different places within one layer to obtain precise results.

In order to give at least some information about possible tectonic setting of sandstones and detect relative change along the section, limited amount of samples (16) samples were selected (Figure 35).

Thin–section analyses of the samples show that the sandstones are mainly composed of monocrystalline quartz, volcanic and sedimentary rock fragments and a small quantity of feldspars. Limited data plotted on a ternary diagram reveals that sandstones are mainly related to combination of recycled orogen and transitional arc (Figure 35). Detritus derived from the recycling of orogenic belts is varied in composition, reflecting the different types of orogen (e.g. continent-continent or continent-ocean collisions) (Tucker, 2001). Sediments from recycled

Sample no.	Quartz %	Feldspar %	Rock fragments %
KRF-12	30	4	66
KRF-13	38	7	55
KRF-14	45	5	50
KRF- 20	49	11	40
KRF-27	53	8	39
KRF- 34	37	14	49
KRF-35	53	2	45
KRF-38	45	5	50
KRF- 40	36	4	60
KRF- 42	38	5	57
KRF- 48	46	4	50
KRF-52	38	2	60
KRF-54	44	0	56
KRF-56	81	3	16
KRF-58	30	8	62
KRF-64	30	8	62

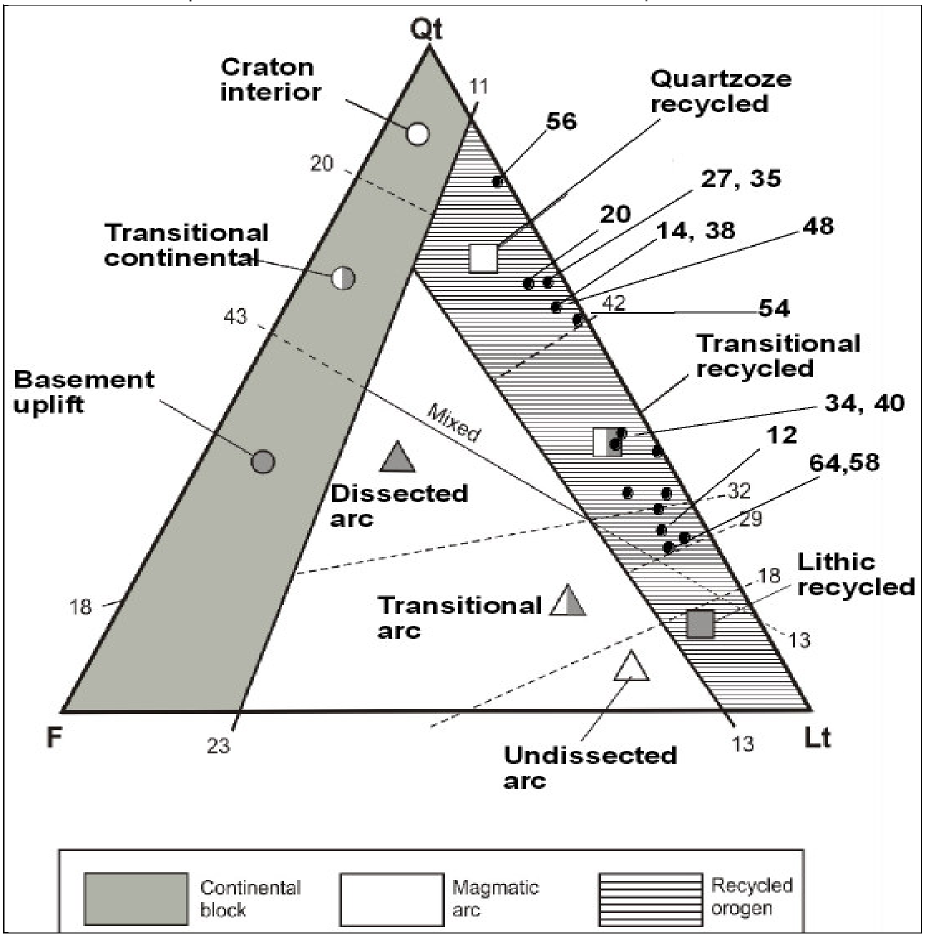

Figure 35. Triangular diagram showing average compositions of sand derived from different provenance terrains (after Dickinson, 1985).

orogen may fill adjacent foreland basins or be transported by major river systems to more distant basins in unrelated tectonic settings. Sediments from transitional arcs have a high percent of volkanic rock fragments, and they dissect down to more plutonic roots. Such sands are usually deposited in forearc basins i. e. Haymana–Polatlı basin (after Tucker, 2001). Among the lithic fragments, volcanic rock is dominant; most probably these fragments derived from the basement of the Sakarya Continent and/ or Tertiary calcalkaline volkanism i.e. Galatian volcanic arc. (Ünalan *et al.*, 1976; Görür and Derman 1978; Norman, 1984; Koçyiğit, 1991).

Demirel and Şahbaz (1994) studied petroleum potential and provenance charcteristics of the Haymana-Polatlı basin. The same provenance results were obtained in their study: recycled orogen and transitional arc.

3.4 Sedimentary structures

The majority of sedimentary structures form by physical processes, before, during and after sedimentation, whereas others result from organic and chemical processes (Boggs, 2001). In this study, sedimentary structures were documented from the outcrop studies. More than 50 sedimentary structures were observed and they are documented along the measured section. In the uppert part of the measured section where carbonate rocks, pebbly sandstones and conglomerates are common, burrow structures, graded bedding, cross bedding and cross lamination were mainly observed (Figure 36, Figure 37). Massive bedding in mudrocks and limestones without any apparent internal structures is also common along the measured section. According to Demircan (1994), who studied ichnofacies (*Skolitos SP/Planoolitos*) of the upper part of Kartal Formation, it was possible to distinguish between continental, shallow coastal and marine bioturbations. Vertical burrowing is the evidence of a marine environment, oblique of transitional or shallow coastal, and horizontal of continental environment (Figure 37A). Measurements made showed that in general, the ichnofacies varied from 5 to 15 cm in length and from 1-2 cm in diameter. Cross-

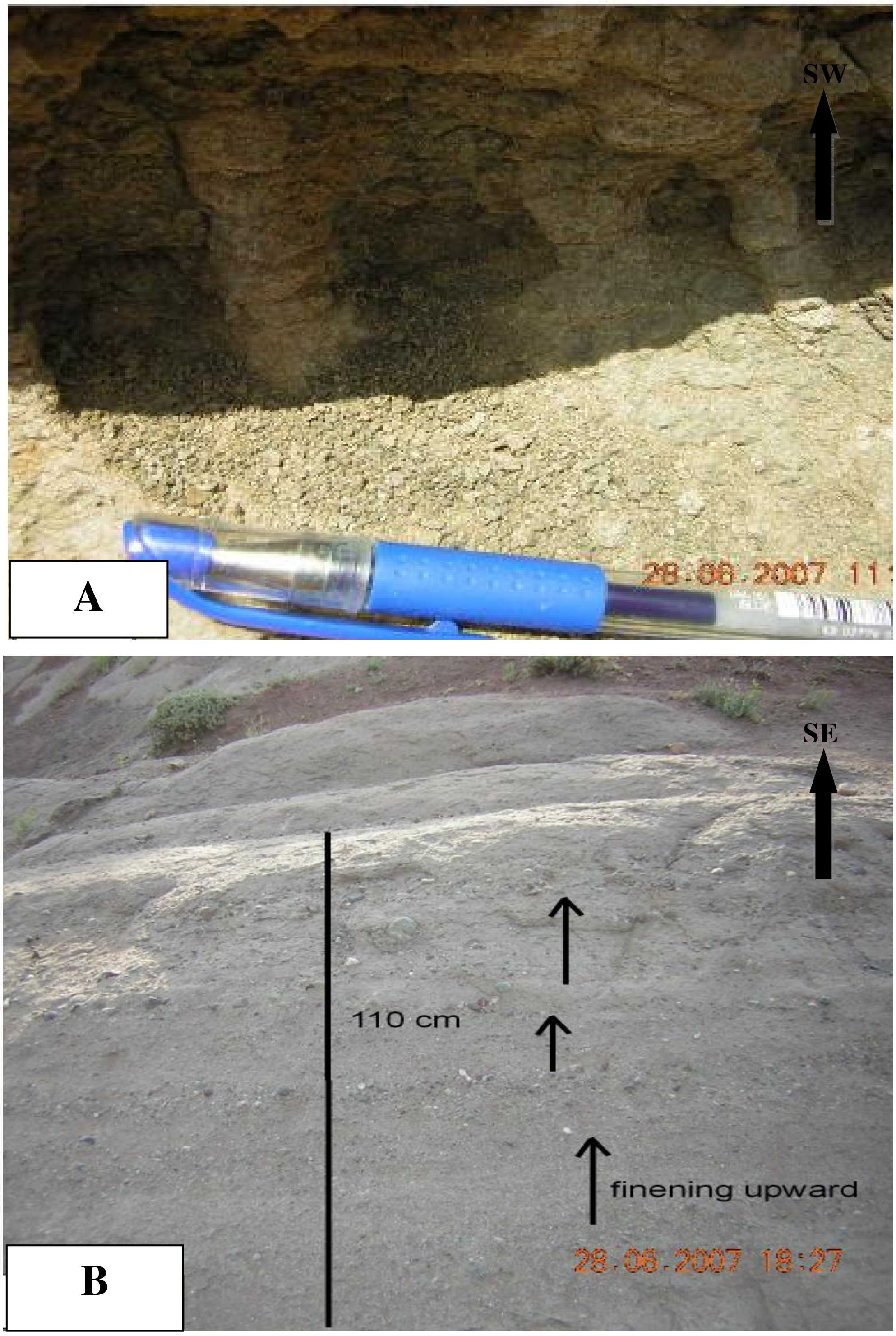

Figure 36. Photographs of sedimentary structures observed in the field; A – Burrowed limestone (KRF-11); B – Three sets of graded bedding within 110 cm thick conglomeratic bed (KRF-18)

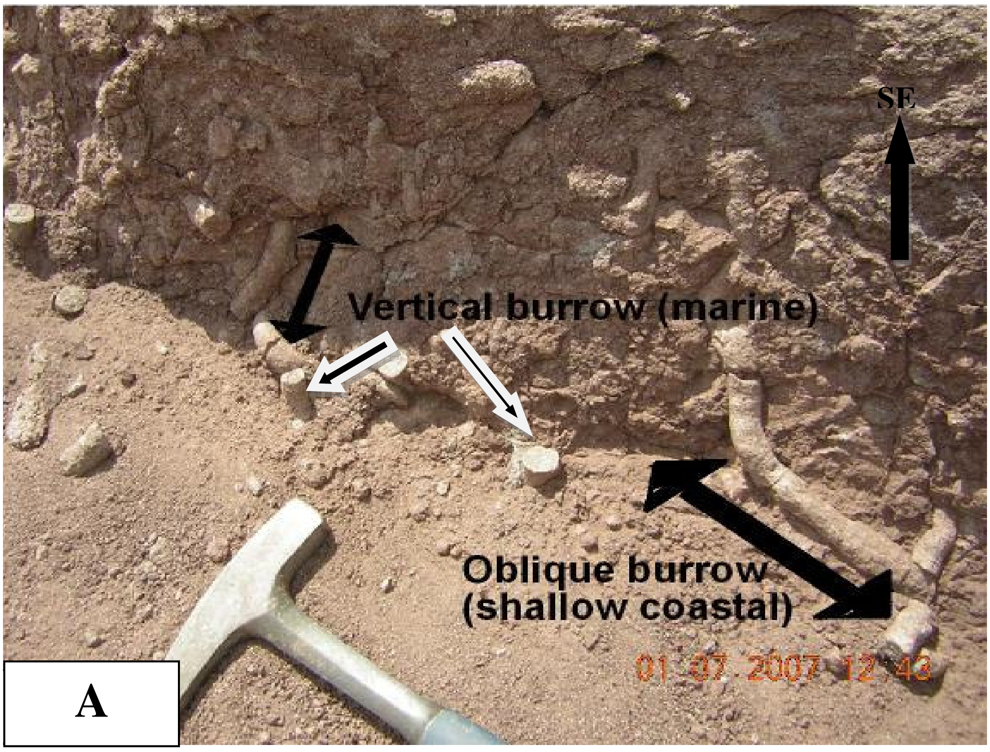

Figure 37. Photographs of sedimentary structures observed in the field; A- Vertically and obliquely burrowed mudrock (KRF-30) (after Demircan, 1994). B – Cross-laminated sandstone bed (KRF-19).

bedded sandstones are commonly observed in the upper and lower parts of the measured section and can be associated with downstream migration of dunes and/or bars (after Tucker, 2001) (Figure 38A). Ancient channels, showing the pathways for sediment and water transport over considerable period of time, are represented with materials coarser than the underlying beds (after Tucker, 2001). The typical evidence of a channel structure is represented by conglomeratic bed (KRF 31) that cuts into underlying cross bedded sandstone (Figure 38A). Scour base is also observed in conglomeratic beds overlying sandstone successions (Figure 38B). According to Boggs (2001) scours are formed by short lived channel erosional events.

Normal grading is common in most of the conglomerates along the measured section (Figure 36 B). According to Tucker (2001) grading may be associated with changes in flow conditions. Some sandstones in the lower part of the measured section show bimodal cross stratification, with a reactivation surface in between. Such sediments are deposited under a tide or wave influence (after Tucker, 2001) (Figure 39A).

Abrupt transition from coastal to marine environment, where limestone overlies cross-bedded conglomerate and massive sandstone, is also observed in the lower part of the section (Figure 40A). In the middle and lower parts of the measured section low angle cross bedded beach sandstones are abundant (Figure 38 B, Figure 39B). According to Tucker (2001) such structures are formed when waves move sediment to shallow depth or shore. Additionally, in the lower part of the section, community of pebbly limestones is also presented. Pebbles or calcarudites are mostly presented by algal remains and oncoids (Figure 40B) (after Blair, 1999). According to depositional environment interpretation these limestones are probably deposited by a high energy wave agitation (after Flügel, 2004).

Taking in to account affromentioned interpretations of sedimentary structures, transitional depositional environment can be stated for the upper 283 meters of the Kartal Formation.

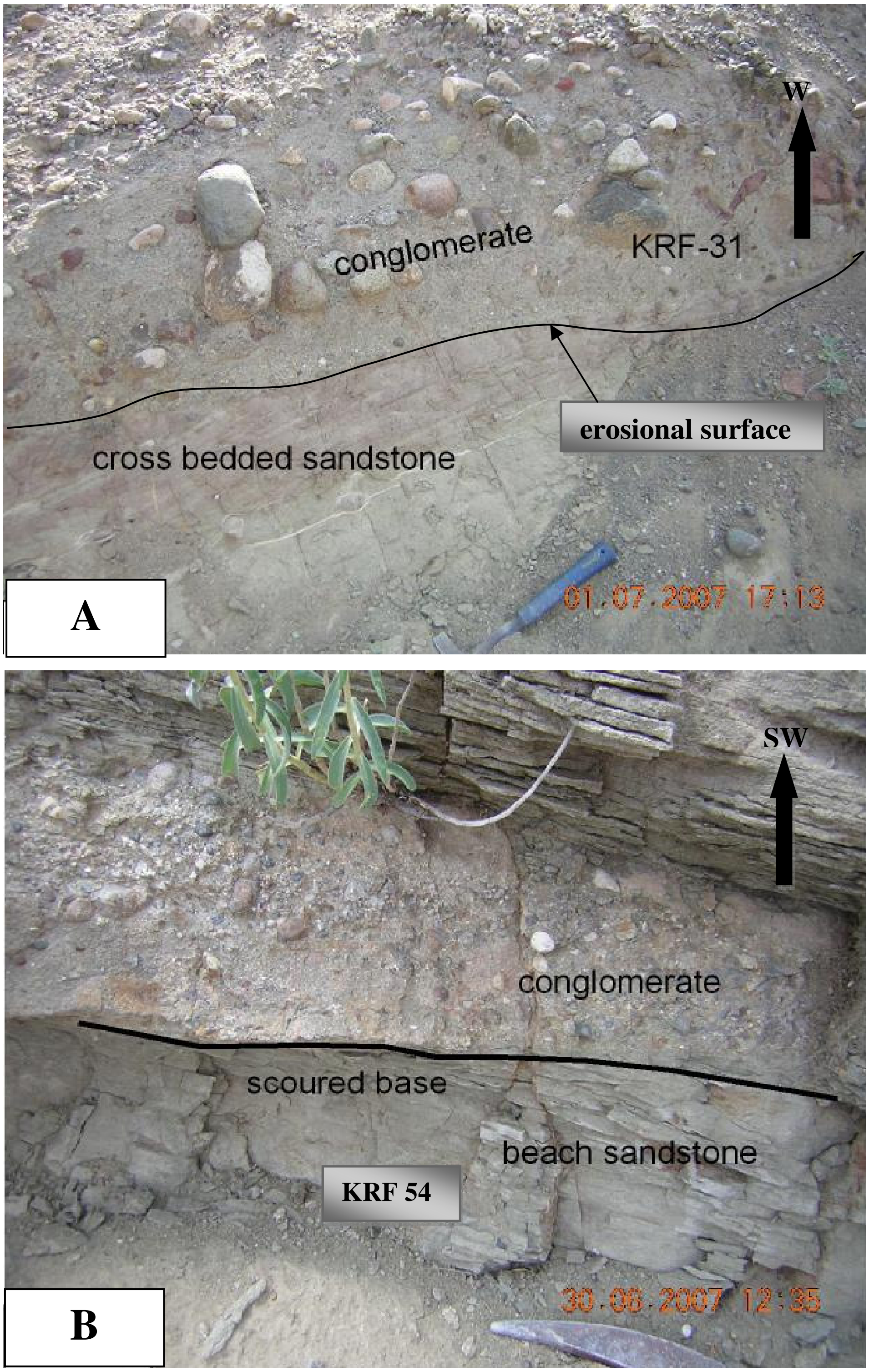

Figure 38. Photographs of sedimentary structures observed in the field. A-Channel structure. B-Scour-base conglomerate (short lived channel erosional event)

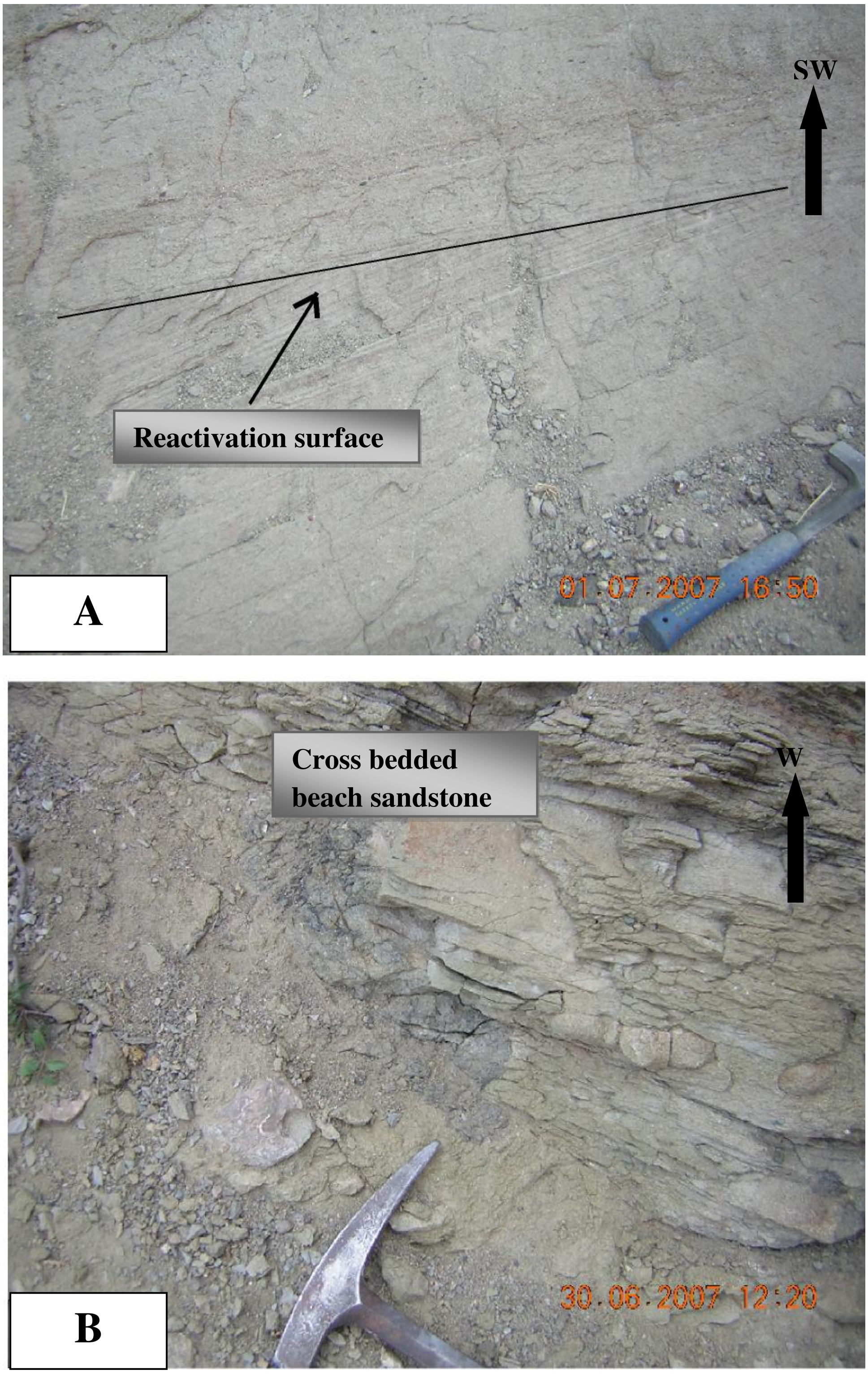

Figure 39. Photographs of sedimentary structures observed in the field. A-Herringbone cross stratification in sandstone. B-cross bedded beach sandstone (KRF-56)

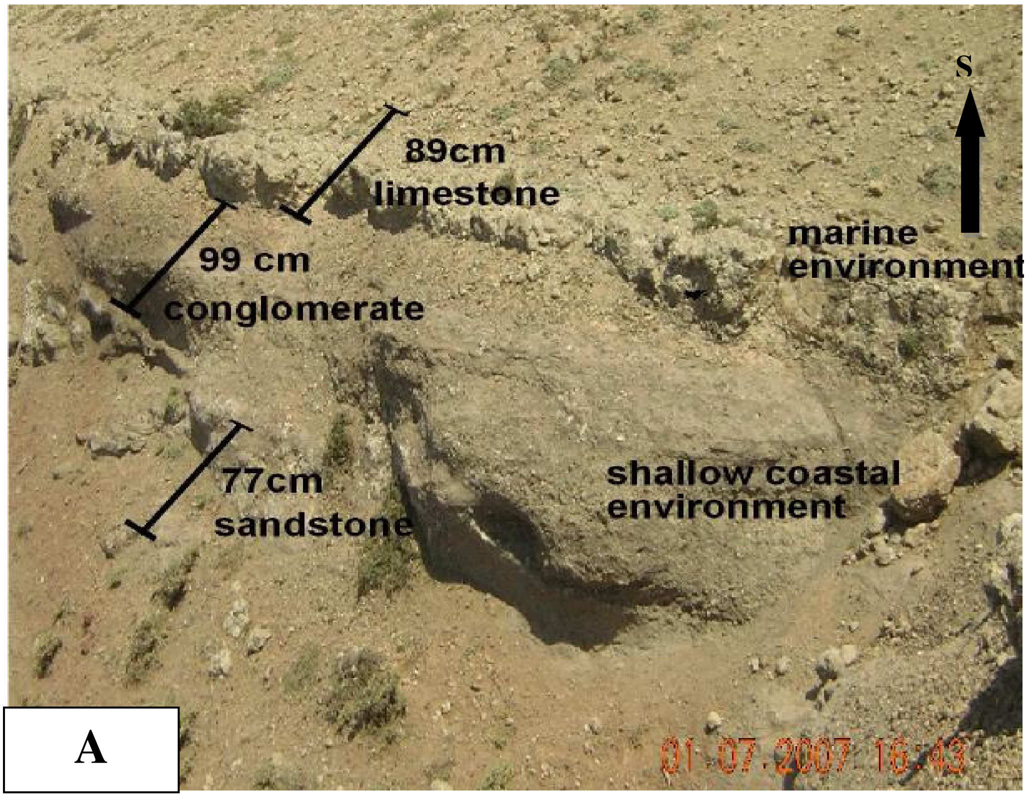

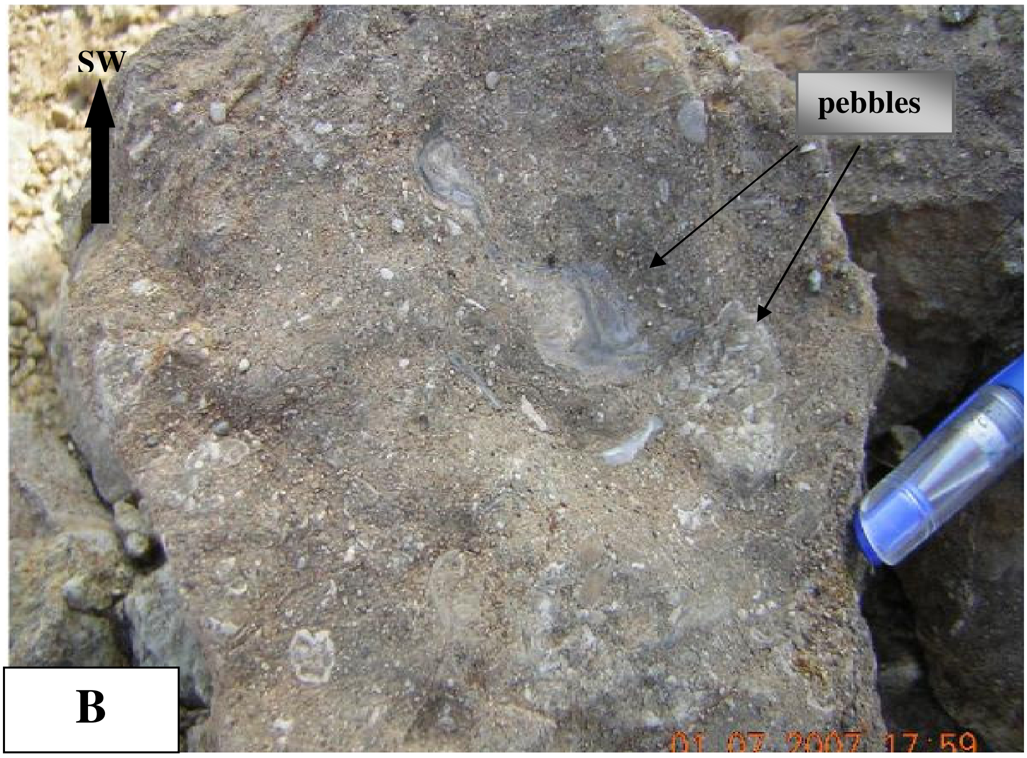

Figure 40. Photographs of sedimentary structures observed in the field. A- Transition from continental to marine environment.B. Pebbly rudstone (after Embry and Klovan, 1971)

3.5 Palaeocurrent Analysis

The measurement of paleocurrent is an important item in study of sedimentary rocks, since they provide information on the paleogeography, palaeoslope, current and wind directions and they are useful in facies interpretation. Many different features of a sedimentary rock can be used as paleocurrent indicators, as some structures record the direction of movement (azimuth) of the current whereas others only record the line of the movement (trend) (Tucker, 2003). According to Tucker (2003) the most useful indicators of paleocurrent are cross bedding and sole structures (flute and groove casts). Grain size analysis performed on sandstone samples and conglomeratic beds along with outcrop observations revealed that the distributary channel system was the major transportation agent for the sediments' deposition.

In the Kartal Formation, measurements were taken from two cross bedded sandstones by measuring vector mean and from six conglomeratic beds by measuring tentative pebble imbrication in the lower, middle and upper parts of the studied section. According to Tucker (2001) prolate pebbles in fluvial deposits produce normal-to-current orientation. In the entire measured section majority of pebbles represented almost the same orientation within each bed. Additionally, a bimodal conglomeratic bed located 2 levels below KRF 57 comprizes symmetrical ripples with paleocurrent values 270º N and 120º N.

Obtained measurements have been plotted on rose diagram (Table 6, Figure 41). As observed from the diagram, the major transport direction was towards SE (unidirectional) and source area is located in the NW. According to Tucker (2001), small dispersion on rose diagram, indicates deposition by low sinuosity rivers. The typical vertical sequence of low sinuosity rivers usually represented by repeated succession of finining-upward gravel-sand sequences, 1 to 3 m thick (Figure 42). These successions are very common along the measured section. Study of sedimentary structures and results of grain analysis also indicated deposition of sediments by river systems (For details see subchapters 3.4 and 3.2). Additionally, according to scattered diagrams of Bjorlykke (1984) and Stewart (1958) the majority of the sandstones were deposited by rivers (For details see subchapter 3.6). Taking affromentioned factors in to account, deposition by low sinuosity channels may be suggested for most of the sandstones and all of the conglomerates along the measured section. However whether the deposition occurred by low sinuosity meandering or by distibutary braided channels is still questioned.

Table 6. Measurements plotted on rose diagramm

Bed No.	Measurements	Paleocurrent
1.	pebble imbrication	185° N
2.	pebble imbrication	133° N
3.	pebble imbrication	155°N
4.	cross bedding	150°N
5.	pebble imbrication	154° N
6.	cross bedding	154°N
6.	pebble imbrication	170°N
7.	symmetrical ripple (bimodal)	270°N / 120°N

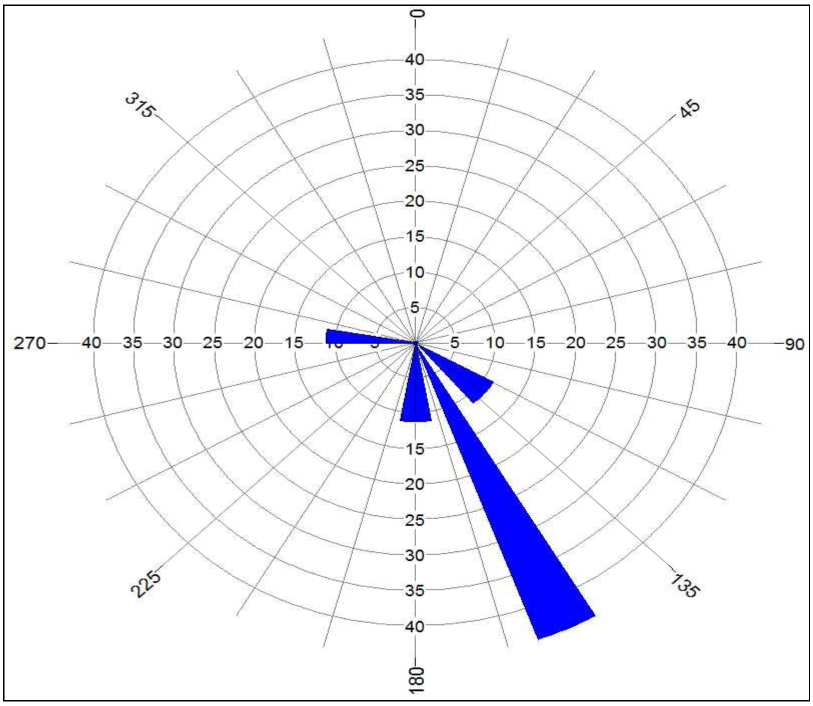

Figure 41. Rose diagram, illustrating palaecurrent direction for all beds

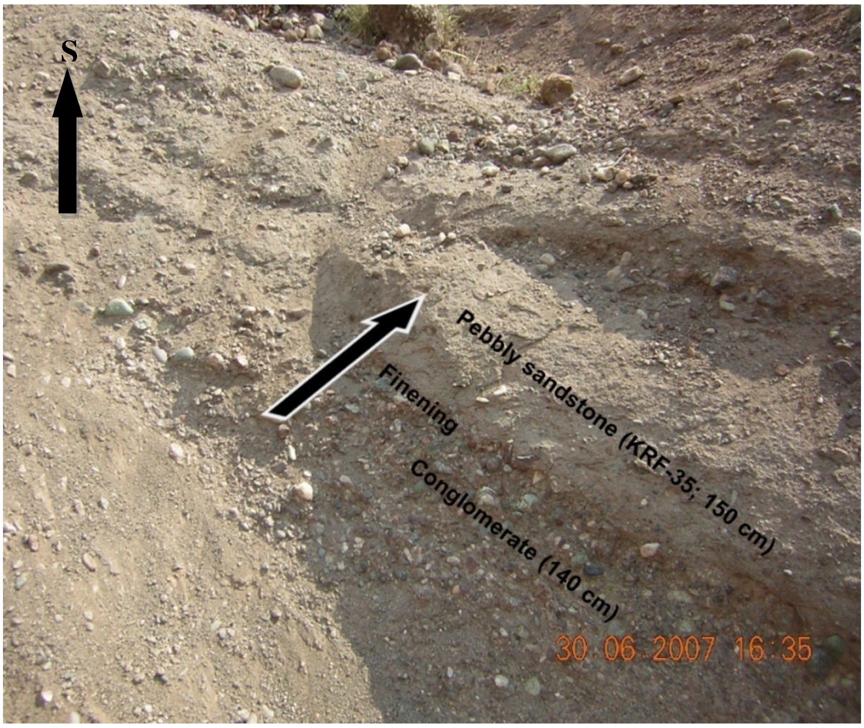

Figure 42. Field photographs of the rock units recognized along the measured section. Vertical succession of finening upward gravel-sand units, typical for low sinuosity channel system (after Einsele, 2000)

3.6 Depositional Environment

Interpretation of depositional environment of the sediment is the one of the most important tools for sedimentological analysis. A depositional environment is characterized by a particular geomorphologic setting in which a particular set of physical, chemical, and biological processes operates to generate a certain kind of sedimentary deposit (Boggs, 2001). Previous studies interpreted depositional environment of the Kartal Formation as transitional-deltaic (Sirel, 1975; Ünalan *et al*., 1976). However typical succession produced by delta progradation were not observed in the upper part of the Kartal Formation (after Battacharya and Van Wagoner, 2006). Though, field and laboratory studies suggest transitional environment of the deposition.

The red color of the most of clastic sediments within Kartal Formation is probably related to the presence of iron oxide (after Tucker, 2001). In many cases, these rocks were deposited in continental environment, most probably a floodplain. Micron-size oxidized crystals of iron, even in small amount (0.1 %), are enough to give red colour to sediment (Mücke, 1994).

Based on petrographic data, sands are mainly litharenites. Sedimentary structures interpreted along the studied section are commonly cross-lamination, planar and herringbone cross-bedding, which are typically related to sandstone deposition in fluvial and wave realms (see section 3.4). Grain size parameters, such as those based on skewness versus median diameter (Stewart, 1958), sorting versus skewness (Bjorlykke, 1984) and coarsest class percentile versus median diameter scatter diagrams (Passega, 1964), show that grains were mainly transported by wave and river action (Figure 43, Figure 44) and deposited in the beach (Figure 45). Additionally, field studies indicated that the beach environment signatures such as the presence of macrofossils within sandstones, oblique burrowing within mudstones, wave-generated cross-bedding are common along the measured section (Section 3.4; Appendix A)

Oolites are valuable paleoenvironmental proxies for water energy, salinity, temperature and depth. The paleoenvironmental interpretations of ancient ooids should be done with caution; the transport of ooids from the areas in which they were produced to the depositional areas is often underestimated (Flugel, 2004).

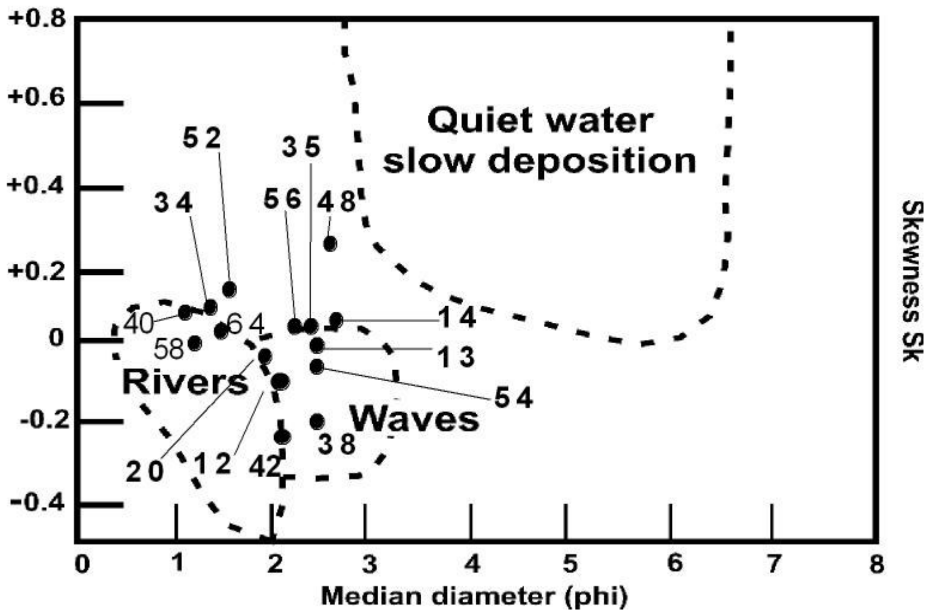

Figure 43. Scattered diagram of median versus skewness (Stewart, 1958)

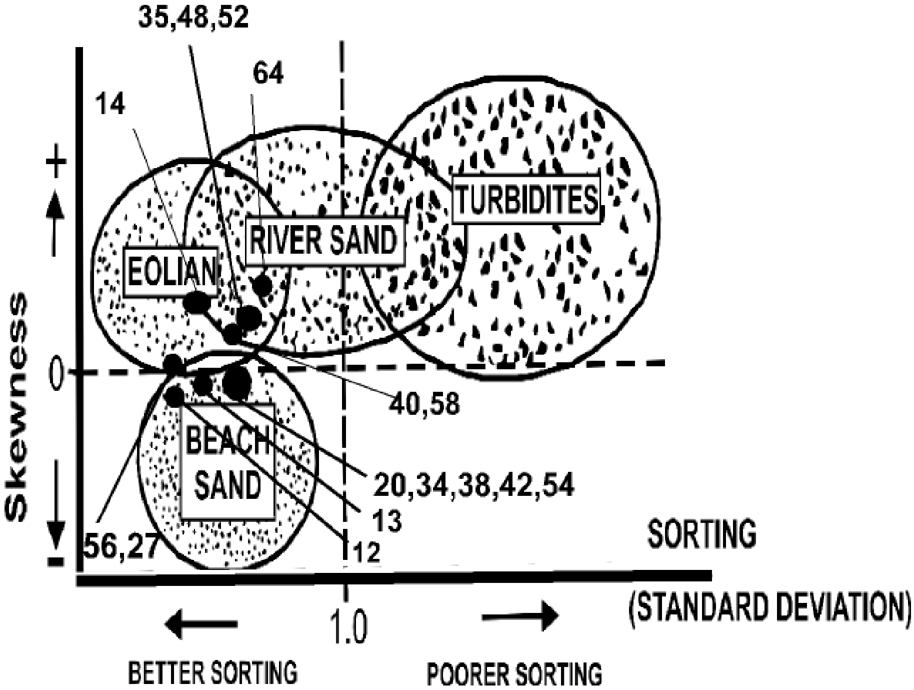

Figure 44. Sorting and skewness of grain size distribution parameters. (Bjorlykke, 1984).

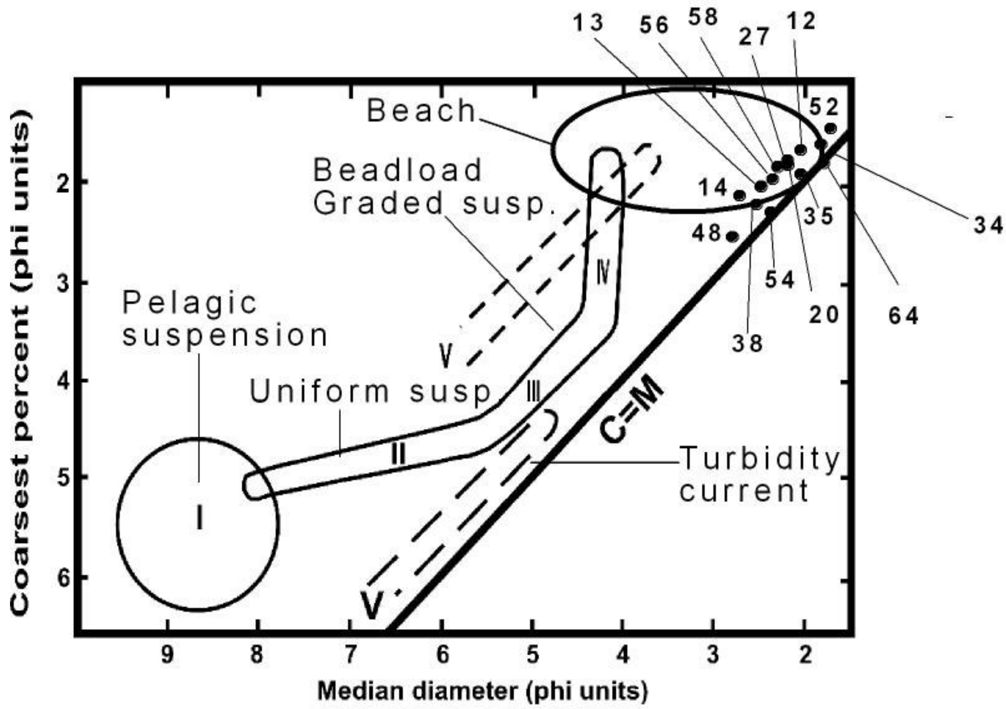

Figure 45. Scattered diagram of coarsest class percentile versus median diameter, indicating environment of deposition (Pasega, 1964)

Additionally the microfacies analyses performed for limestones, proved the shallow marine environment. From the above mentioned, we may conclude that the measured section represented by transitional environment.

Accordingly to interpretation of depositional environment of limestone facies within upper portion of the Kartal Formation, oolitic grainstones most probably were deposited in shallow marine environment (after Flügel, 2004). As the ooids within grainstones are represented by micritic laminae, they are best associated with shallow marine environment. Additionally some ooidal grainstones contain meniscus cement, that can be evidence of vadoze-diagenetic alteration (after Flügel, 2004).

The minor bioclastic grainstones represented within Kartal Formation, constitute high energy skeletal banks and sheets, most probably deposited seaward of ooid shoals in wave-agitated settings (after Flügel, 2004).

Depositional environment of rudstones may be related to agitated shallow subtidal and/or beach environment (Golubic *et al*., 1984; Richter and Sedat, 1983).

Dolomitic limestone, which was only represented in one sample (KRF-32), was probably deposited in near-surface vadose zone (after Kenny, 1992), as calcite cement and bioclastic shells are replaced by dolomite with idiotopic mozaic (Figure 22B).

Clast-supported conglomerates and also some better-sorted pebbly sandstones with floating larger clasts within measured section record bedload deposition from stream flows (after Reading, 1996). Conglomerates are commonly characterized by lenticular bedding and erosion surface with conspicuous relief and some of them are deposited in marine environment (see subchapter 3.4). Form analyses of the pebbles confirmed that the majority of the clasts within conglomerates are deposited by streams (see subchapter 3.2). The presence of foraminifers within conglomerates and siliclastic fragments within limestones is further evidence of a transitional environment (Figure 20, Figure 21). Additionally, Demırcan (1994) identified caliche nodules within sandstones and mudstones in the lower part of the Kartal Formation. This factor is the further evidence of the continental deposition for the part below of our studied section.

According to affromentioned results, outcrop observations, sedimentary structures study, grain size and microfacies analysis, the studied interval of the Kartal formation might be interpreted as a transition between shallow coastal (beach) and shallow marine environments of deposition (Figure 46).

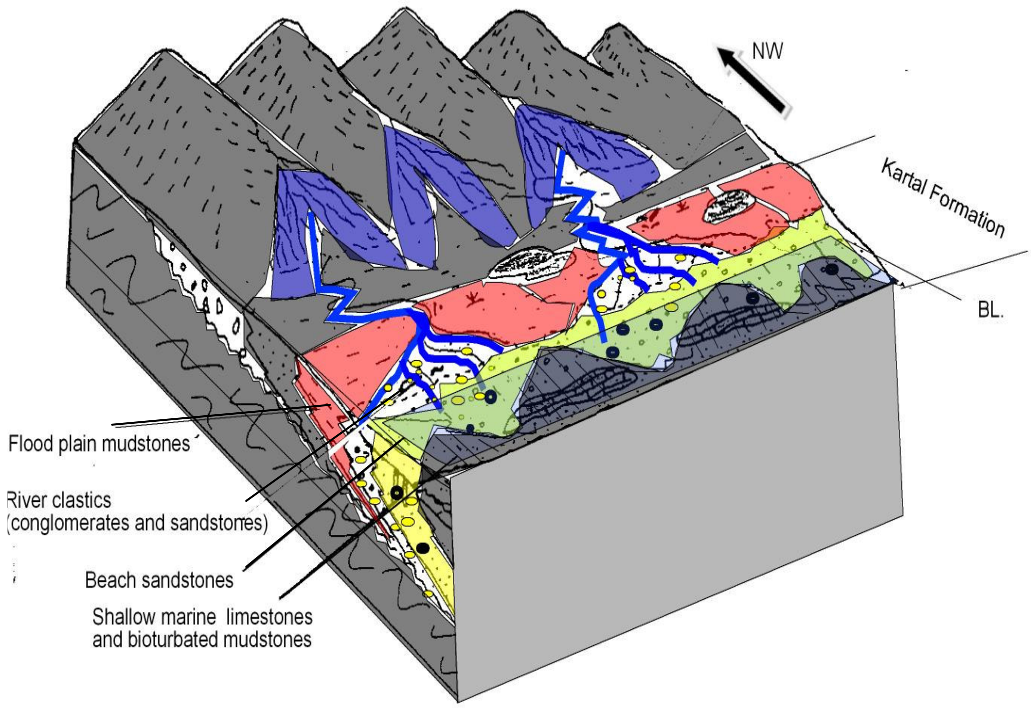

Figure 46. Depositional environment (not to scale) of the Kartal Formation (modified from Demircan, 1994).

CHAPTER 4

CYCLOSTRATIGRAPHY

Cyclostratigraphy is the study of cyclic depositional patterns produced by climatic and tectonic processes (Schwarzacher, 1993). It deals with minor, relatively short-period (high-frequency) sedimentary cycles (mainly Milankovitch cycles) and has become a field of great interest because of its link with climate change and potential to complement and refine chronostratigraphy and stratigraphic correlation (Einsele, 2000). The term ‘‘cycle’’ universally used for describing repetition of more than 2 lithological patterns, refers to measured thicknesses between repetitions and to time cycles when this is relevant (Schwarzacher, 2000).

Cyclic bedding originates with slow, gradual, periodic variations in primary sediment composition and sedimentation rates. These lead to a vertical sedimentation buildup that changes smoothly with time and is characteristic for various sediment types (after Einsele, 2000). Rhythmic bedding results from such repeated episodic phenomena as storms, turbidity currents and river floods and characterized by the repetition of 2 lithological patterns (Einsele, 2000).

Rhytmic and cyclic sediments are subdivided into four groups: the varve-scale laminations, bed-scale rhytms and cycles, field-scale cycles and various orders of macro-scale cyclic sequences (Einsele *et al.*, 1991). Because of meter-scale cycles are not the products of one specific process in a certain environment, each of them may represent quite different time periods. The term sedimentary cycle do not represent equivalent time periods but it’s used as a convenient way to describe repeated successions of certain lithologies and depositional events (Einsele *et al.*, 1991).

The measured section is represented by meter-scale cyclic beds, which according to Beerbower (1964) termed autocyclic and controlled by processes taking place in the sedimentary prism itself (e.g. within a basin or part of it).

Cyclic successions in fluvial environment show limited stratigraphic continuity and related with the migration and superposition of channel and lobe system (Beerbower, 1964; Einsele *et al*., 1991). According to Allen (1965) ancient fluvial fining upward cycles represented by the fine grade member succeding gradationally a coarse grade member which rests on an erosional and often channel surface. The coarse member here represented by conglomerates, pebbly, cross-bedded and parallel laminated sandstones, whereas fine member represented by massive to laminated flood plain mudstones (Allen, 1965).

In coastal environment, terrigenous input can show the alternation with limestone beds representing the flactuations of the sea level (Einsele *et al*., 1991). The flactuations are caused by external factors, such as climate and tectonics.

. Sirel (1975) assigned Montian age for the whole Kartal Formation (≈4 My; 62 ± 0.2 to 58 ± 0.2 Ma), however according to recent geological time scale this period of time roughly corresponds to Selandian (≈3 My; 61.7 ± 0.2 to 58.7 ± 0.2 Ma (Van Eysinga, 1975; Gradstein *et al*., 2004). It is assumed that the lower part of the Formation which is below the measured section was deposited very quickly and represented by continental sediments. Hence the studied interval is characterized by terrestrial siliciclastics and marine carbonate alternation and may roughly correspond to the half of the Selandian age (≈1.5 My), because of the limestone successions dominate towards the upper part of the Formation. This property may lead to consider the longer duration of carbonate deposition compared to terrestrial siliciclastics and in turn help to interpret the time span for this part of the Formation.

According to detailed lithofacies analyses, the whole section, which is 283 m thick, was divided into large-scale hierarchies which comprise smaller-scale repeated cyclic and rhythmic beds.

4.1 Hierarchy in cycles

According to litofacies analysis 6 large scale hiehrarchies were distingueshed along entire measured section. Each hierarchy starts with sandstone or mudrock and fnishes with thick limestone succession representing highstand of sea level (Figure 47, Figure 48). **HC**.-1 starts at the lowest point of the measured section below which only continental sediments were deposited. Its thickness is about 20 m. **HC**.-2 represented by 35 m thick succession of meter scale rhytmic and cyclic beds. **HC**.-3 represented by 24 m thick succession of cyclic and rhytmic beds. **HC**-4 is 24.5 m in thick. **HC**-5 is the thickest of all hierarchies (120 m). Taking into account that the cyclic and rhytmic lithofacies within 120 m thick **HC**-5 are represented by conglomerates, sandstone and red mudstones, so rapid continental deposition can be suggested for **HC**-5. **HC**-6 represented by 15 m thick succession of cyclic and rytmic beds.

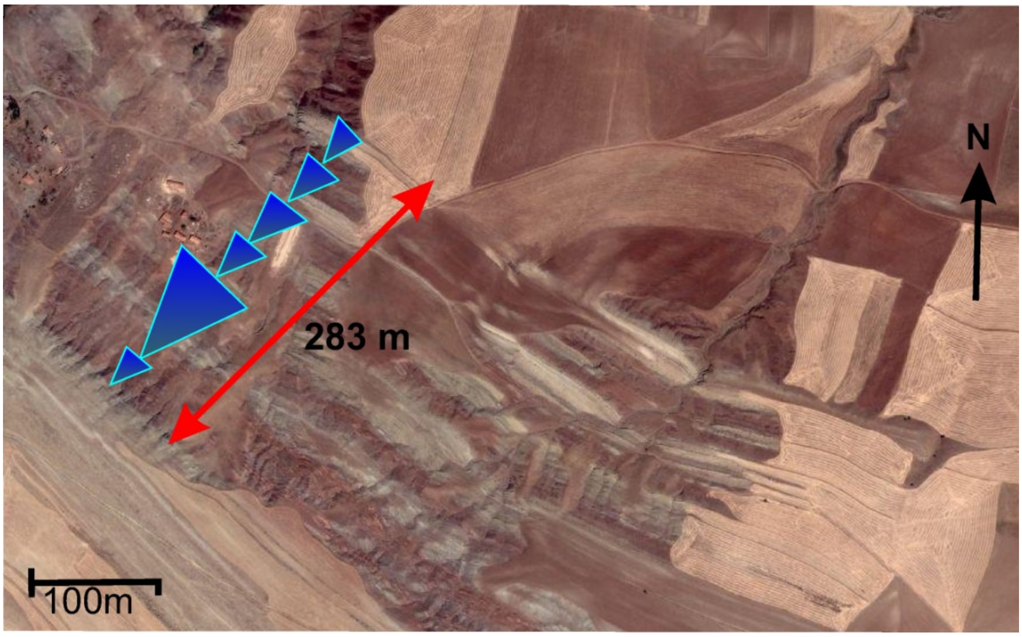

Figure 47. Satelite image illustrating location of studied section (red line); hierarchy cycles (blue triangles). (snapshot taken from Google Earth, www.earth.google.com).

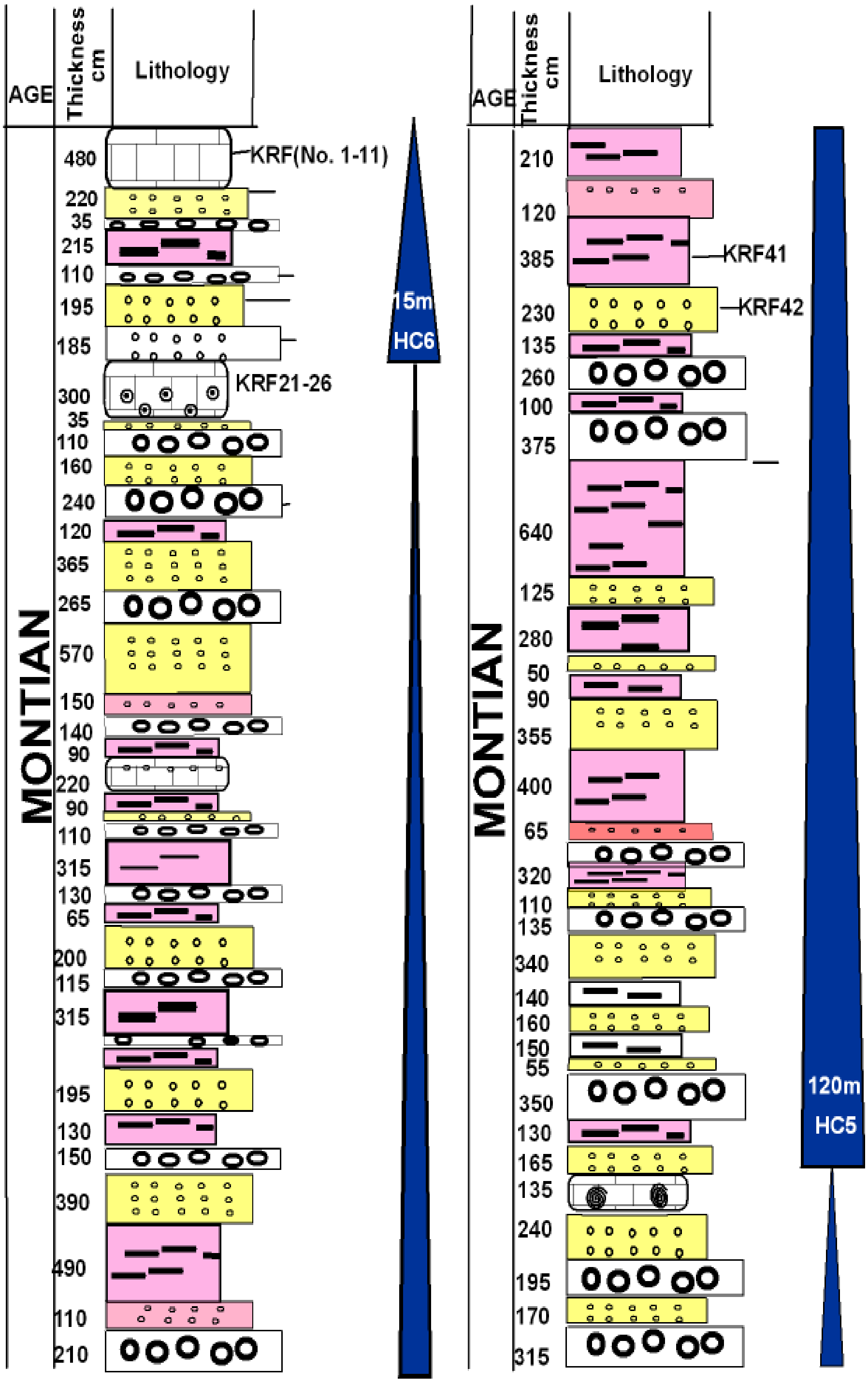

Figure 48. Simplified measured section showing large scale hierarchies in cycles

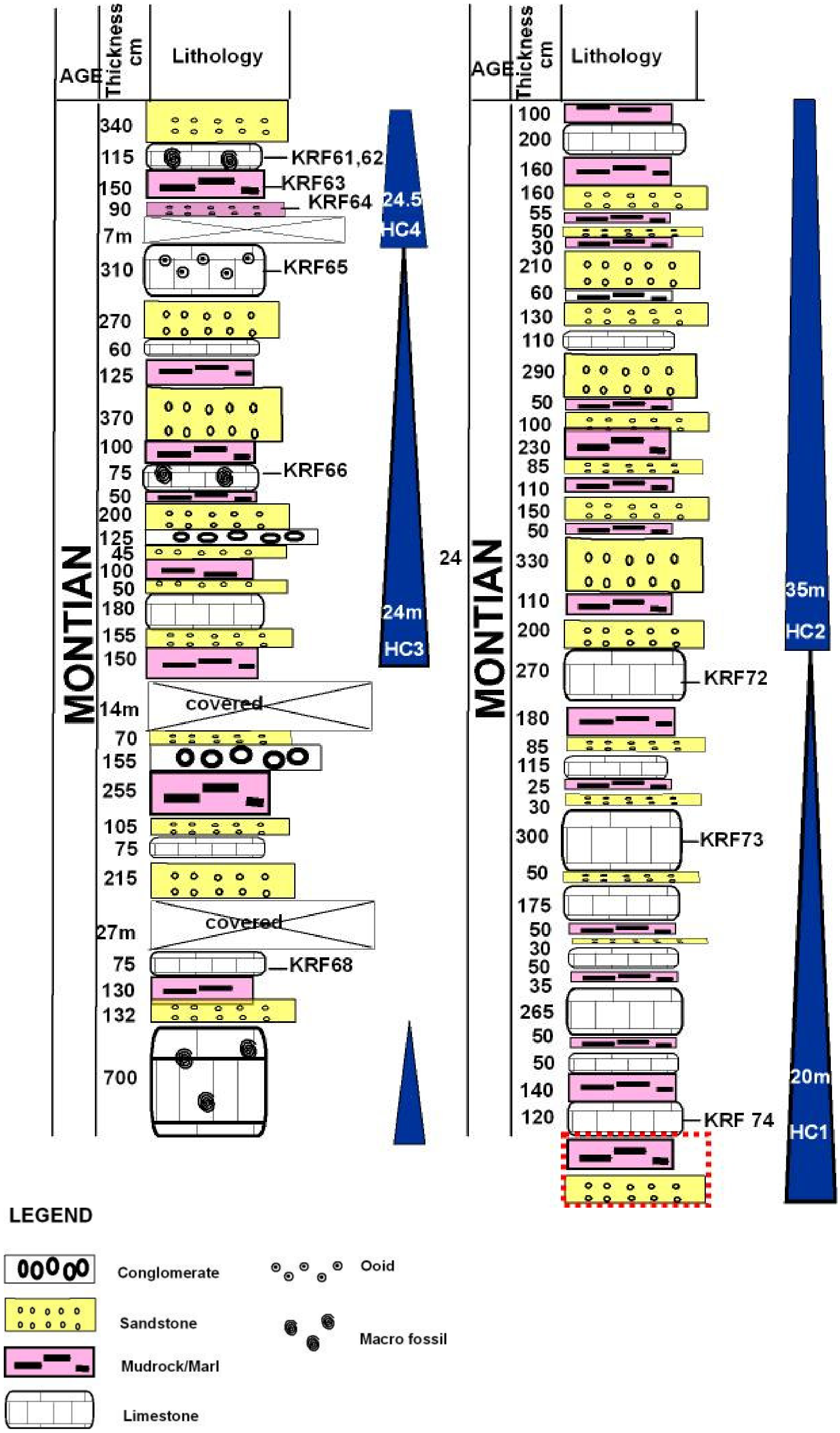

Figure 48. Continued

4.2 Meter-Scale Cyclic and Rhytmic Beds

According to detailed lithofacies analyses and their vertical association, the whole section, which is 283 m thick, is represented by meter-scale fining and deepening upward cycles and rhytmic beds. According to lithofacies association, three types of meter-scale cycles and six types of rhytmic units were determined along the measured section (Figure 49).

Fining upward **A** type cycle and rhytmic units represented by coarse sediments at the base which rests on an erosional often channel surface and overlying by fine sediments (Figure 49; Appendix A). Type **A1** cycle starts with conglomeratic bed passes in to finer sandstone and finishes with flood-plain mudstone and its thickness is 3.5-5 m. This type of cycles represents ancient fluvial fining upward cycle and nine times repeated along the measured section (after Allen, 1965; Çiner, 1996). **A1** cycle is limited at the bottom and top by the **B** or **C** type rhytmic units, which also represented by fining upward successions (1.5-3.5 m) (Appendix A). Type **A** cyle comprises **A2** and **A3** incomplete subtypes, which represented by fining upward succession of two lithological patterns (after Einsele *et al*., 1991). **A2** and **A3** start with erosive base conglomerate passing in to fine sandstone and flood plain mudstone respectively (1.5-3.6 m) (Appendix A). Periodic deposition of **A** type cycle and rhytmic units is best associated with the migration and superposition of channel and lobe system (after Beerbower, 1964; Einsele *et al*., 1991).

Deepening upward **D** type cycles and rhytmic beds (units) represented by coarse clastic bed at the base, which passes in to the finer sediment and finishes with thick limestone succession (Figure 49; Appendix A). Deepening upward cycles characterized by a rise of the sea level and reduction in terrigenous input (Einsele *et al*., 1991). Based on facies variation within **D**, two types of cycles and three types of rhytmic units were defined. Type **D1** cycle starts with erosive base conglomeratic bed, which passes in to the sandstone and finishes with thick limestone succession and its thickness is 3.5-5.5 m (Figure 49; Appendix A). Along the measured section **D1** and **D2** type cycles repeated seven and eight times respectively (Appendix A). Type **D2** cycle starts with coarse sandstone bed, passes in to marine mudstone (marl) and finishes with limestone (3.5-6 m). **D1** and **D2** type cycles are limited at the top by B or C type rhytmic units, which represent subsequent fall of the sea level and increase in terrigenous input (Einsele *et al*., 1991). **D2** type cycle comprises **D3** and **D4** rhytmic subtypes, representing transition from sandstone to limestone and from marine mudstone to limestone respectively.

The lower part of the section corresponding to HC-1 represented completely by deepening upward cycles and can be associated with sea level fluctuations. HC-2 mainly consists of B type fining upward rhytmic beds, starting with B type and finishing with D3 type rhytmic succession (Appendix A). HC-3 is limited by deepening upward D3 units at the bottom and top, whereas the middle part of the hierarchy represented by deepening upward D1 cycles and fining upward incomplete B and C units. HC-4 is limited by deepening upward D2 cycles at the bottom and top, whereas the middle part represented by fluvial fining upward A2 and C rhytmc units. HC-5 is the largest of all hierarchies comprises fining upward fluvial cycles and rhytmic beds. HC-6 is the smallest of all hierarchies starts at the bottom with fining upward C unit passes in to fining upward A2, A3, C units and is capped by thick deepening upward D1 cycle.

According to facies association the lower part of the measured section is mostly represented by deepening upward cycles and rhytmic units, whereas central and upper parts are enriched by fluvial fining upward cycles and rhytmic beds (after Allen, 1965). The uppermost part of the measured section represented by thick deepening upward D1 cycle (5.5 m), indicating transition from continental to shallow marine environment at the boundary with overlying Kırkkavak Formation (Appendix A).

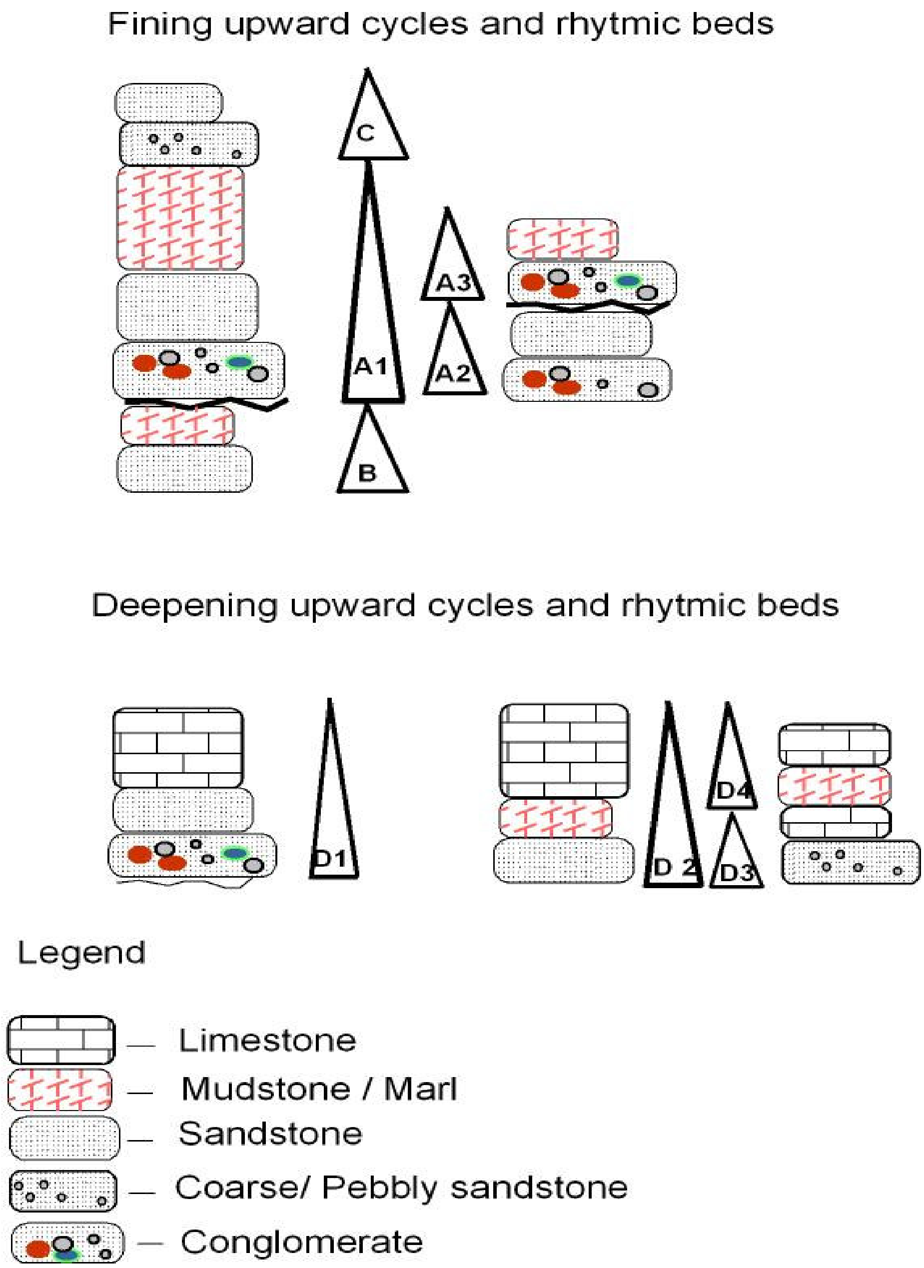

Figure 49. Determination of meter-scale Cyclic and rhytmic beds within large scale cycles (hierarchies).

CHAPTER 5

CONCLUSION AND RECOMENDATION

1. 283 m thick stratigraphic section was measured within upper portion of the Kartal Formation in the Haymana-Polatlı basin. Studied section comprises sandstone, mudrock, limestone, and conglomerate successions and represents well developed cyclic pattern just below the boundary with overlying Kırkkavvak Formation.
2. According to previous studies, the depositional environment of the whole Kartal Formation was interpreted as transitional-deltaic (Sirel, 1975; Ünalan et al., 1976). Based on the field works and detailed lithofacies analyses, our observations suggest that, the uppermost 283 meters of the Formation represented by coastal and shallow marine environments of the deposition. And no deltaic evidences were observed along the measured section.
3. Detailed petrographic, sedimentologic analyses were carried out in 283 m (starting from the top) of the total measured section. According to modal analyses sandstones were interpreted as litharenites, lithic graywackes and as a sublitharenite (after Pettijohn *et al*., 1987). Limestones were interpreted as oolitic granestones (oosparites), bioclastic grainstones (biosparites), rudstones (biosparites), packstone (biomicrite) and dolomitic sandy limestone (after Dunham, 1962; Folk, 1959). Mudrocks were interpreted as very fine, fine and coarse mudstones (after Pettijohn, 1975; McKee and Weer, 1953). Conglomerates were interpreted as orthoconglomerates (Boggs, 1992).
4. Analysis of grain parameters showed that the grain size distribution along the measured section displayed the distribution of very fine to coarse sands. Sorting of sandstones varies from moderately well to well sorted, skewness from fine to coarse skewed and kurtosis from leptokurtic to platykurtic. Dominant transportation mechanism as been revealed as saltation. Maturity of the sandstones varies from immature to mature according to sorting and sphericity analysis. According to interpretations of depositional environment and grain parameters results, the main transportational agents for the

sandstones were rivers and waves, which deposited them in the beach environment. Channel and wave created sedimentary structures also suggest affromentioned results (i.e. herringbone cross bedding, cross bedded beach sandstones, graded bedded conglomerates). Modal analyses of carbonates suggest their shallow water deposition.

5. The provenance of sandstones based on modal analysis of 16 samples has been used to obtain the tectonic setting of the basin and source rocks. After plotting on Dickinson (1985) terniary diagram the provenance of sandstones corresponds to recycled orogen and transitional arc. According to Koçyiğit (1991) Haymana-Polatlı basin is forearc basin. However Okay and Tüysüz (1998) indicated that the Haymana-Polatlı is a composite basin. Additionally Demirel and Şahbaz (1994) revealed the same result as in our study. So the obtained provenance and tectonıc results correspond to the prevıous works and most probably studied sandstone fragments derived from the basement of the Sakarya Continent and/ or Tertiary calcalkaline volkanism i.e. Galatian volcanic arc. According to paleocurrent analyses the major transport direction was towards SE (unidirectional) and source area is located in the NW.
6. Cyclostratigraphic and field studies revealed 6 hierarchy cycles corresponding to fifth order. Hierarchy cycles start with sandstone bed and ends with limestone varying 20-120 m in thickness. Each hierarchy cycle comprises meter-scale fining and deepening upward cyclic and rhytmic units. Environmental interpretation of fining upward cyclic and rhytmic beds suggest the migration and superposition of channel and lobe system, whereas deepening upward cycles and rhytmic units suggest a rise of the sea level and reduction in terrigenous input (Beerbower, 1964; Allen, 1965; Einsele *et al*., 1991; Çiner, 1996).

Sirel, (1975) identified *Rotalia trochidiformis* and *Missisipina binkhorsti* in the upper part of the Kartal Formation and assigned the entire 1326 meter thickness to the Montian-age. However the lower part of the Formation was not examined in terms of its age. As a recomendation for further work, determination of the age for the whole formation, detailed sedimentologic and sequence stratigraphic works for the rest part of the Formation may be suggested.

REFERENCES

Akarsu, I., 1971, 2. Geological report of the AR/TPO/747 area. TPAO. (non published).

Allen, J.R.L., 1965. Fining-upward cycles in alluvial successions. Geological Journal, vol. 4, p. 229-243.

Bathurst, R.G., 1979. Diagenesis in carbonate sediments: a review. Geol. Rundschau Stuttgart, vol. 68, pp. 848-855.

Battacharya, J.P., Wagoner Van J.C., 2006. Delta facies models revisited. S.E.P.M. Special Publication No 84, p. 237-292.

Beerbower, I.R., 1964. Cyclothems and cyclic depositional mechanism in alluvial plain sedimentation: Kansas Geological Survey Bulletin, vol. 169 (1), p. 31–32.

Bjorlykke, K., 1984, Sedimentology and petroleum geology: Springer-Verlag, Berlin, 370 p.

Blair, T. C., McPherson, J.G., 1999. Grain-size and textural classification of coarse sedimentary particles. Journal of Sedimentary Research, vol. 69, p. 6-19.

Boggs, S. Jr., 1992. Petrology of sedimentary rocks. Macmillan Publishing. 665 p.

Boggs S. Jr., 2001. Principles of sedimentology and stratigraphy, Prentice Hall publishing, 688 p.

Brinkman, R., 1932. Stratigraphy and its conditions. Journal of Geology and Paleontology, vol. 11, p 187–202.

Carozzi, A.V., 1989. Carbonate rock depositional model: a microfacies approach. Prentice Hall Publishing. 604 p.

Cater, J.M.L, Hanna, S.S., Ries, A.C., Turner, P., 1991. Tertiary evolution of the Sivas Basin, central Turkey. Tectonophysics, vol. 195, pp 29-46.

Chaput, E., 1936. Voyages d'etudes tectoniques et geomorphogeniques em Turquie (In french). Paris.

Cox, R., Lowe, D.R., 1996. Quantification of the effect of secondary matrix on the analysis of sandstone compositional and a petrographic – chemical technique for retrieving original framework grain models of altered sandstones: Journal of Sedimentology Research, vol. 66, p. 548 – 558.

Çiner, A., 1996. Distribution of Small Scale Sedimentary Cycles Throughout Several Selected Basins. Turkish Journal of Earth Sciences, vol. 5, p. 25-37.

Çiner, A., Deynoux, M., Koşun, E., 1996. Cyclicity in the Middle Eocene Yamak turbitite complex of the Haymana basin, Central Anatolia, Turkey. International Journal of Earth Sciences, vol. 85 (4), p. 669-682.

Çiner, A., Deynoux, M., Ricou, S. and Koşun, E. 1996. Cyclicity in the middle Eocene Cayraz carbonate formation, Haymana Basin, Central Anatolia, Turkey. Paleogeography, Paleoclimatology, Paleoecology, vol. 121, p. 313-329.

Çiner, A., Deynoux, M., Koşun, E. and Gündoğdu, N. 1993. Sequence stratigraphic analyses of the Beldede braid-delta complex: Polatli-Haymana Basin, (Middle Eocene), Central Anatolia, Turkey, (in turkish). Bull. of Earth Sciences of Hacettepe University, vol. 16, p. 67-92.

Çiner, A., 1992. Sedimentology and sequence stratigraphy of the Middle Eocene part of the Haymana basin. Central Turkey. Louis Pasteur University. Strasbourg. 190 p. (In french).

Demirel, İ.H., Şahbaz, A., 1994. Reservoir potential, lithofacies and provenance characteristics of Haymana, Paşadağ-Aladağ basins, Turkish Petroleum Congress 10, p. 5-19. (in Turksh)

Demircan H., 1994. Environmental analysis of Paleocene Kartal Formation's sediments according to trace fossils, Eski Köseler (south of Polatlı). Master thesis, Ankara University. 45 p. (in Turkish)

Dickinson, W.R. 1985. Interpreting provenace relations from detrital modes of sandstones. In: Provenance of Arenites (Ed. G.G. Zuffa): Reidel, Dordrecht, p. 333 – 361.

Dobkins, J. E., Folk, R. L., 1970, Shape development on Tahiti-Nui: Journal of Sedimentary Petrology, vol. 40, p. 1167-1203.

Drummond, C.N., Wilkinson, B.H., 1993. Carbonate cycle stacking patterns and hierarchies of orbitally forced eustatic sealevel change. Journal of Sedimentary Petrology, vol. 63, p. 369–377.

Dunham, R.J., 1962, Classification of carbonate rocks according to depositional texture: Amercan Association of Petroleum Geologists, p. 108-121.

Einsele, G. 2000. Sedimentary Basins: Evolution, Facies, and Sediment Budget: Springer, 792 p.

Einsele, G., Ricken, W., Seilacher, A., 1991, Cycles and events in stratigraphy. Springer, 955 p.

Embry, A.F. and Klovan, J.E., 1971. A Late Devonian reef tract on the Northeastern Banks Island, NWT: Canadian Petroleum Geology Bulliten, vol.19, p. 730 – 781.

Erol, O., Weingart, W., 1955, Geological correlations within 57/1, 57/3 taps of the Ankara region's map. M.T.A. Report No.2473. Ankara (In Turkish).

Flügel, E., 2004. Microfacies of carbonate rocks: Analysis, Interpretation and application. Springer-Verlag, Berlin, 976 p.

Folk, R.L., 1959**,** Practical petrographic classification of limestones: American Association of Petroleum Geologists Bulletin, vol. 43, p. 1-38.

Folk, R. L., 1974, Petrology of Sedimentary Rocks: Hemphill Publishing, Austin**,** 184 p.

Folk, R. L., Ward, W. C., 1957. Brazos River bar: a study in the significance of grain size parameters: Journal of Sedimentary Petrology, vol. 27, p. 3-26.

Forquin, C., 1975, North-West Anatolia, Tectonic evolution of the south margin of the European continent during Tertiary time. Bulletin of the Geological Society of France, vol..17. p. 1058-1070. (In french).

Friedman, G.M., 1962, Comparision of moment measures for sieving and thin section data for sedimentary petrological studies: Journal of sedimentary petrology, vol. 37, p. 15-25.

Friedman, G.M., and Sanders, J.E., 1978. Principles of sedimentology: New York, John Wiley and Sons, 792 p.

Gale, S.J.,1990. The shape of beach gravels: American Association of Petroleum Geologists. 5 p.

Ginsburg, R.N., 1971. Landward movement of carbonate mud: New model for regressive cycles in carbonates: American Association of Petroleum Geologists Bulletin, vol. 55, p. 340.

Golubic, S., Campbell, S.E., Drobne, K., Cameron, B., Balsam, W.L., Cimerman, F., Dubois, L., 1984. Microbial endoliths: a benthic overprint in the sedimentary record, and a paleobathymetric cross-reference with foraminifera. Journal of Paleont., vol. 58, pp. 351-361.

Gradstein, F.M., Ogg, J.G., and Smith, A.G., Agterberg, F.P., Bleeker, W., Cooper, R.A., Davydov, V., Gibbard, P., Hinnov, L.A., House, M.R., Lourens, L., Luterbacher, H.P., McArthur, J., Melchin, M.J., Robb, L.J., Shergold, J., Villeneuve, M., Wardlaw, B.R., Ali, J., Brinkhuis, H., Hilgen, F.J., Hooker, J., Howarth, R.J., Knoll, A.H., Laskar, J., Monechi, S., Plumb, K.A., Powell, J., Raffi, I., Röhl, U., Sadler, P., Sanfilippo, A., Schmitz, B., Shackleton, N.J., Shields, G.A., Strauss, H., Van Dam, J., van Kolfschoten, T., Veizer, J.,Wilson, D., 2004. A Geologic Time Scale 2004. Cambridge University Press, 589 p.

Grovel, W.K., Silverman, R.M., Rasmussen, R.D., Penfield, T.G., Gurnert, R.W., Grateral, V., 2000. AAPG Regional international conference, Istanbul Turkey.

Gökçen, S. L., Kelling, G., 1983. The Paleogene Yamak sand-rich submarine-fan complex, Haymana basin, Turkey. Journal of Sedimentary Geology, vol. 34, pp. 219-243

Göncüoglu, M.C., 1992, Structural and stratigraphical framework of the Central Anatolian Tertiary Basins. Guide Book: Introduction to the Early Paleogene of the Haymana-Polatlı Basin, p. 1-11.

Görür, N., Oktay, F.Y., Seymen, I., Sengör, A.M.C., 1984. Paleotectonic evolution of the Tuzgölü basin complex, Central Turkey: sedimentary record of a Neo – Tethyan closure. In: Dixon, J.E., Robertson, A.H.F., (eds) The geological evolution of the eastern Mediterranean. Geol Soc Lond, vol. 17, p. 467 - 482.

Görür, N., 1981, Petrology of the Çaldağ limestone of the Haymana-Polatlı basin: Istanbul University Earth Science Review, vol.2, p 193-201.

Görür, N., Derman, A.S., 1978. Stratigraphic and tectonic analysis of the Tuzgölü-Haymana basin (In turkish). TPAO report, No, 1514 (non published)

Harland, W.B., Armstrong, R.L., Cox, A.L., Craig, L.E., Smith, A.G., 1989. A geologic time scale. Cambridge University Press. 279 p.

Illenberger, W., 1991, Pebble shape and size: Journal of Sedimentary Petrology, vol. 61, p.756-767

Johnson, M.R., 1994. Thin section grain analysis revised: Sedimentology, vol 41. p. 985-999

Kenny, R., 1992. Origin of disconformity dedolomite in the Martin Formation (Late Devonian, northern Ariozona). Sedimentary Geol. Amsterdam, vol. 78, p. 137-146.

Koçyiğit, A., 1991. An example of an accretionary fore–arc basin from northern Central Anatolia and its implications for the history of subduction of Neo –Tethys in Turkey. Geol Soc Am Bull, vol. 103, p. 22 - 36.

Koçyiğit, A., Lünel, T., 1987. Geology and tectonic setting of Alci region, Ankara. Journal Pure Appl Sci Ankara, vol. 20, p. 35 - 57.

Koçyiğit, A., Özkan, S., Rojay, F.B., 1988. Examples from the fore-arc basin remnants at the active margin of northern Neo –Tethys; development and emplacement ages of the Anatolian nappe, Turkey. Journal Pure Applied Science Ankara, vol. 21, p. 183 - 210.

Krumbein, W. C., and Sloss, L. L., 1963. Stratigraphy and sedimentation: Sun Francisco. KH. Freeman and Co., 660 p.

Krynine, P.D., 1946, The tourmaline group in sediments, Journal of Geology, vol. 54, pp. 65–87.

McKee, E. D., Weir, G. W., 1953, Terminology for stratification and cross-stratification in sedimentary rocks: Geological Society of America, vol. 64, p. 381-90.

McManus, J., Buller, A.T., Green, C.D., 1980. Sediments of the Tay Estuary. Proceedings of the Royal Society of Edinburgh, vol. 78, pp. 133–154.

Meriç, E., Görür, N., 1979., Age of the Çaldağ limestone of the Haymana-Polatlı basin. MTA report 93/94, pp. 137-142. (In turkish)

Moore, C.H., 2001, Carbonate reservoirs porosity evolution and diagenesis in a sequence stratigraphic framework: Elsevier, Amsterdam. 444 p.

Mücke, A., 1994. Post-diagenetic ferruginization of sedimentary rocks, including a comparative study of reddening of red beds. In Diagenesis 4 (editors: Wolf, K. H., Chillingarian, G. V.). Elsevier, Amsterdam, vol. 48, pp.361-423.

Norman, T., 1975, Flow features of Ankara melange. 9th International Congress on Sedimentology, Nice (France), vol. 4, p. 261-269.

Norman, T., 1984, The role of the Ankara melange in the development of Anatolia (Turkey), in Doxon, J.E. and Robertson, A.H.F., eds. Geol. Soc. of London. vol. 17, p. 441-447.

Okay, A. I., Tüysüz, O., 1998. Tethyan sutures of northern Turkey. Eurasian Institute of Earth Sciences and Geological department. 86 p.

Okay, A. I., Tüysüz, O., Tansel, I., 2001. Obduction, subduction and collision as reflected in the Upper Cretaceous–Lower Eocene sedimentary record of western Turkey. Geological Magazine UK, vol**.** 138 (2), pp. 117–142.

Özcan, E., Özkan-Altıner, S.A., 1997. Late Campanian – Maastrichtian evolution of orbitoidal foraminifera in Haymana Basin successions (Ankara, Central Turkey). Revue Paleobiol., Geneve, 16, vol. 1, p. 271 – 290.

Özcan, E., Özkan, S., 1999. The genera *Lepidorbitoides* and *Orbitoides:* evolution and stratigraphic significance in some Anatolian basins. Geological Journal, vol. 34, p. 275 – 286.

Özkan-Altıner, S. Özcan, E., 1999. Upper Cretaceous planktonic foraminiferal biostratigraphy from NW Turkey: calibration of the stratigraphic ranges of larger benthonic foraminifera. Geological Journal, vol. 34, 287 – 301.

Özcan, E., Özkan-Altıner, S.A., 2001. Description of an early ontogenetic evolutionary step in Lepidorbitoides: Lepidorbitoides bisambergensis asymmetrica subsp. n., Early Maastrichtian (central Turkey). Rivista Italiana di Paleontologia e Stratigrafia, vol. 107, p. 137-144.

Özcan, E., Sirel, E., Özkan-Altıner, S.A. and Çolakoğlu, S., 2001. Late Paleocene Orthophragminae (foraminifera) from the Haymana – Polatli Basin, (central Turkey) and description of a new taxon, Orbitoclypeus haymanaenis. Micropaleontology, vol. 47, p. 339 - 357.

Passega, R., 1964, Grain size representation by CM patterns as a geological tool: Journal of Sedimentary Petrology. vol. 34, p. 840-847

Pettijohn, F. J., Potter, P.E., Siever, R., 1987. Sand and sandstone: Springer – Verlag, New York.

Pettijohn, F. J., 1975. Sedimentary Rocks: Harper and Row Publishing, New York, 628 p.

Reading, H.G., 1996. Sedimentary environments: processes, facies, stratigraphy, Blackwell Publishing, 593 p.

Reckamp, J.U. and Özbey, S., 1960, Petroleum geology of Temelli and Kugtepe structures, Polatlı area: Pet. îş. Gen. Md., Ankara (non published)

Richter, D.K., Sedat, R., 1983. Brackishwater oncoids composed of blue-green algae and red algae from a Pleistocene terrace near Corinth, Greece. - In: Peryt, T. (ed.): Coated grains. Berlin, Springer Publishing, vol. 6, p. 299-307.

Rigo de Righi, M. and Cortesini, A., 1959, Regional studies of central Anatolian basin, progress report 1, Turkish Gulf Oil Com.: Pet. is. Gen. Md., Ankara (non published).

Riley, N. A**.,** 1941**.** Projection sphericity: Journal of Sedimentary Research, vol. 11(2), p. 94-95

Schimidt, G. C., 1960, AR/MEM/365-366-367 areas' report. Turkish Petroleum administration report. Ankara. (non published)

Schwarzacher, W., 1993. Cyclostratigraphy and the Milankovitch theory: Elseveier London, 11 p.

Schwarzacher, W., 2000. Repetitions and cycles in stratigraphy: Elseveier Northern Ireland, United Kingdom, vol. 50, p 51-75.

Sirel, E., 1975. Stratigraphy of the region south of Polatlı (SW Ankara) (in Turkish). Türkiye Jeoloji Kurumu Bülteni.18, 181–92.

Sirel, E., 1999. Four new genera (*Haymanella, Kayseriella, Elazigella and Orduella*) and one new species of *Hottingerina* from the Paleocene of Turkey Micropaleontology, vol. 42, p. 113 – 137.

Sneed, E. D., Folk, R. L., 1958, Pebbles in the lower Colorado River, Texas: a study in particle morphogenesis: Journal of Geology, vol. 66, p. 114-150.

Spears, D.A., 1980, Towards a classification of shales: Journal of the Geological Society, vol. 137 p. 125-129.

Stewart, H.B., 1958, Sedimentary reflections on depositional environments: American Assosiacion of Petroleum Geologists, vol. 42, p. 2567-2618.

Swett, K., Knoll, A.H., 1989. Marine pisolites from Upper Proterozoic carbonates of East Greenland and Spitsbergen. Journal of Sedimentology Oxford, vol. 36, p.75-93.

Şenalp, M., Gökçen, L.S., 1978. Sedimentological Studies of the Oil-Saturated Sandstones of the Haymana Region. Bull Geol Soc Turkey, vol. 21, p. 87 – 94 (in Turkish).

Şengör, Ç.A., Yılmaz, Y., 1981. Tethyan evolution of Turkey, a plate tectonic approach. Tectonophysics vol. **75**, p. 181–241.

Şengör, A.M.C., 1984. The Cimmeride Orogenic System and the Tectonics of Euroasia. Geol. Soc. Am. Spec. Pap., vol. 195, 82 pp.

Toker, V., 1979. Upper Cretaceous Planktonic Foraminifera and the biostratig-raphic investgations of the Haymana area. Bulliten of the Geological Society of Turkey, 22, 121 – 132 (in Turkish).

Tucker, M.E., Wright, V. P., 2004. Carbonate sedimentology: Blackwell Publishing, 482 p.

Tucker, M.E., 1988. Techniques in sedimentology: Blackwell Publishing, 394p.

Tucker, M.E., 2001. Sedimentary petrography: Blackwell Publishing, 262 p.

Tucker, M.E., 2003. Sedimentary rock in the field. John Wiley & Sons Publishing, 244 p.

Turgay, M. I., Kurtuluş, C., 2000, Seismic reflection studies in Polatlı region, Turkey. M.T.A. report. 103-104, p. 41-49.

Ünalan, G., Yüksel, V., Tekeli, T., Gönenç, O., Zinet, S., Hüseyin, S., 1976. Upper Cretaceous – Lower Tertiary stratigraphy and paleogeographic evolution of Haymana – Polatli region (SW Ankara). Turkish Geol Soc Bull, vol. 19, p. 159 - 176 (in Turkish).

Valloni, R., 1985, Reading provenance from modern marine sands. In: Provenance of Arenites (Edited by Zuffa, G.G.): NATO ASI Series, vol. 148, p. 309 – 332.

Visher, G.S., 1969, Grain size distribution and depositional processes: Journl of Sedimentary Petrology, vol. 39, p. 1074- 1106.

Vail, P.R., Michum, R. M. Jr., Todd, R.G., Widmier, J.M., Thompson, S., Sangree, J.B., Budd, J.B., Hatlied, W.G., 1977. Seismic stratigraphy and global changes of sea level. American Association of Petroleum Geologists Memoir, vol. 26, p. 47-212

Van Eysinga, F.W.B., 1975, Geological time scale. Elsevier, 3-rd edition.

Yüksel, S., 1970. Geological study of the Haymana region (Central Turkey). Thesis. Univ.Nancy, 179 P.

Zingg. T., 1935, Beitrage zur Scotteranalyse (in German). Min. Petr Mittl Schweiz, vol. 15, p. 39-140

APPENDIX A

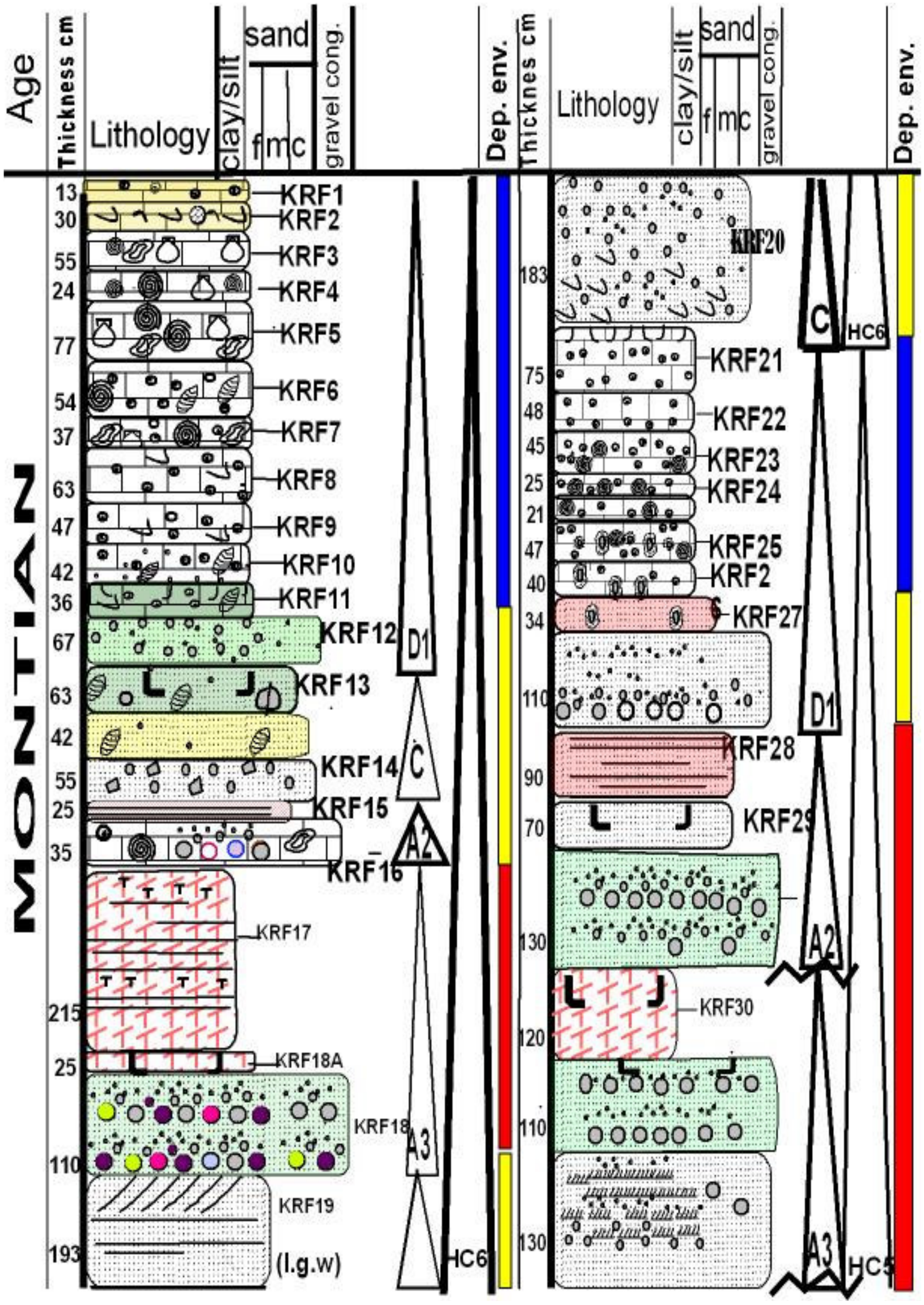

Figure A1. Detailed measured section (From top to bottom).

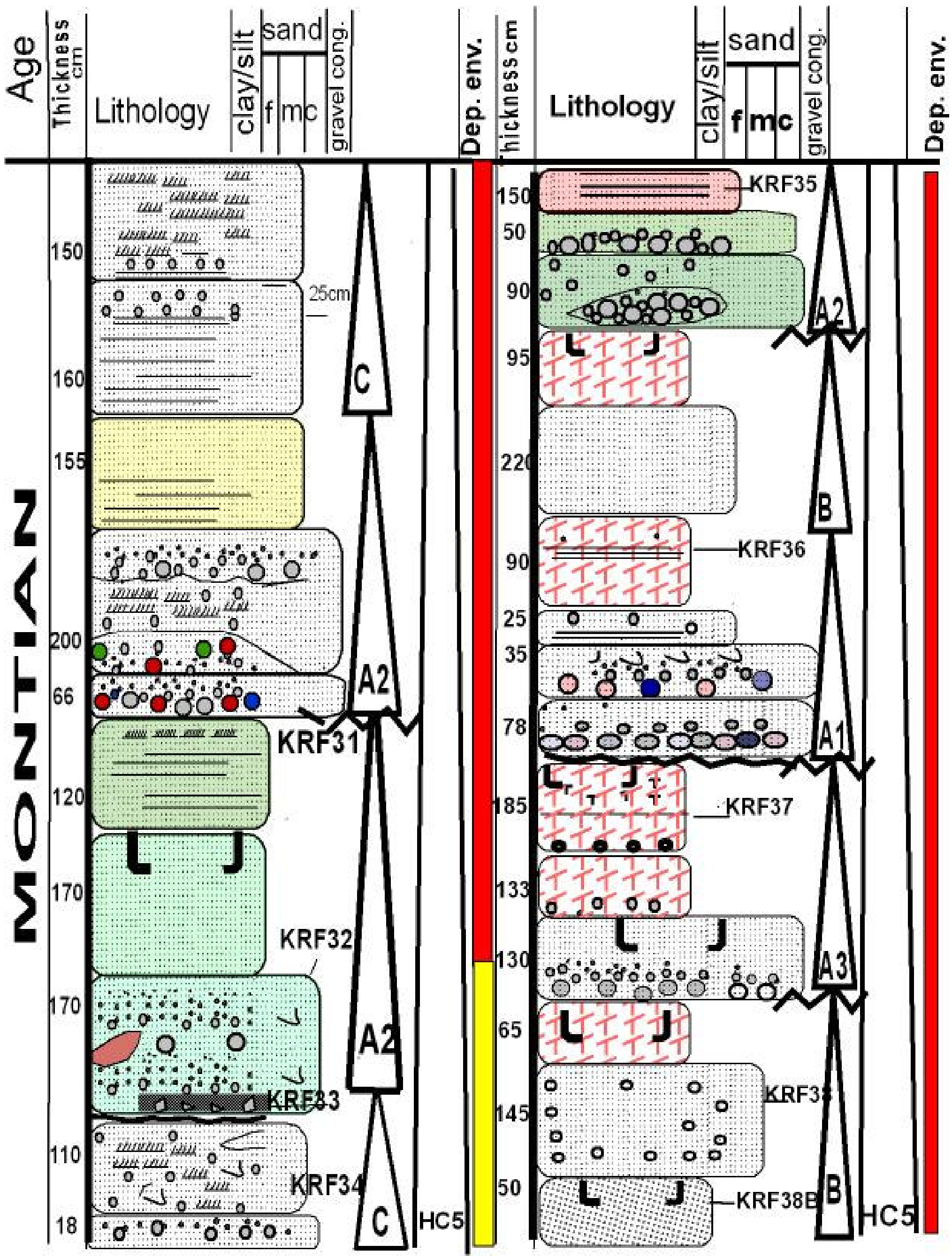

Figure A2. Detailed measured section (continued)

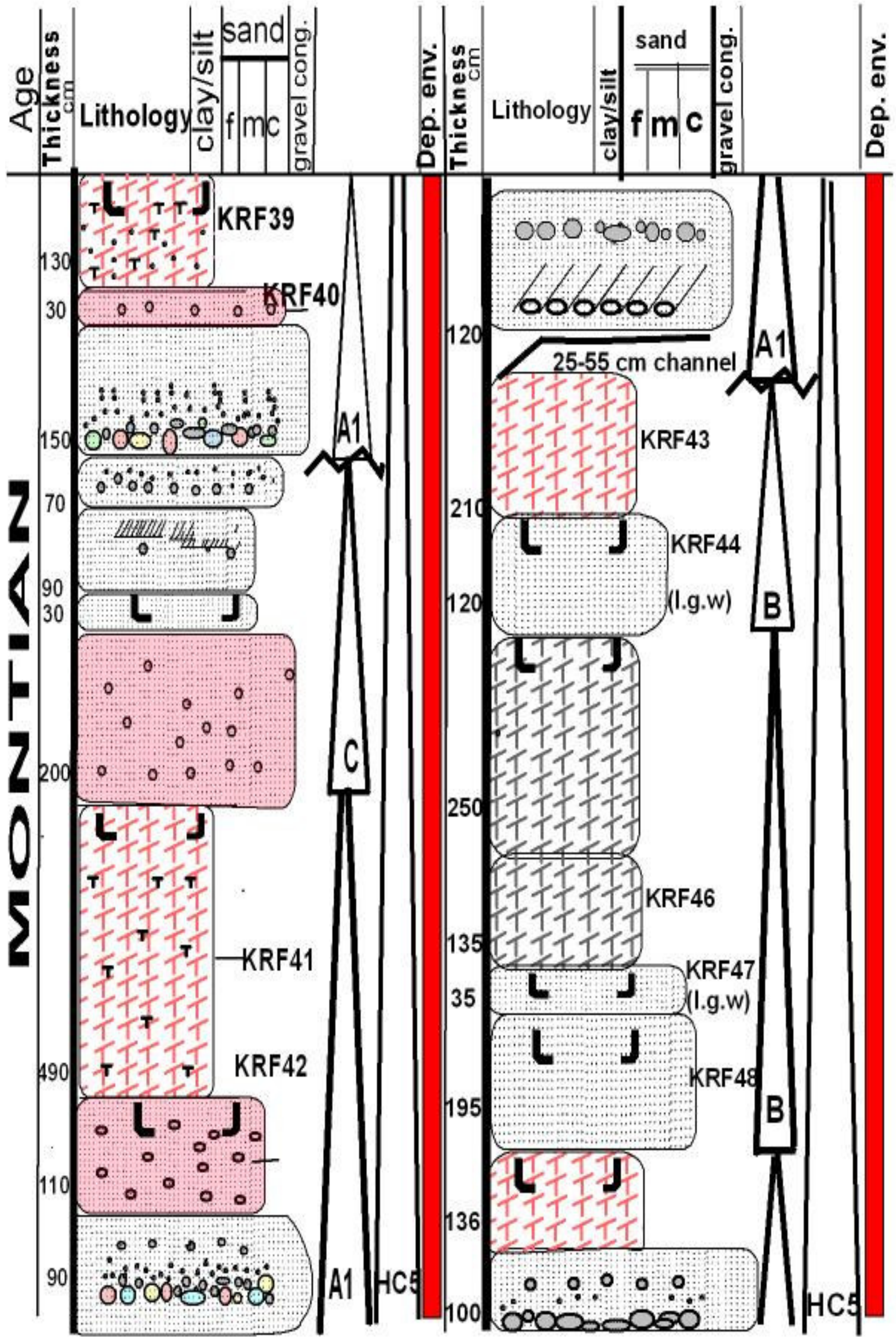

Figure A3. Detailed measured section (continued)

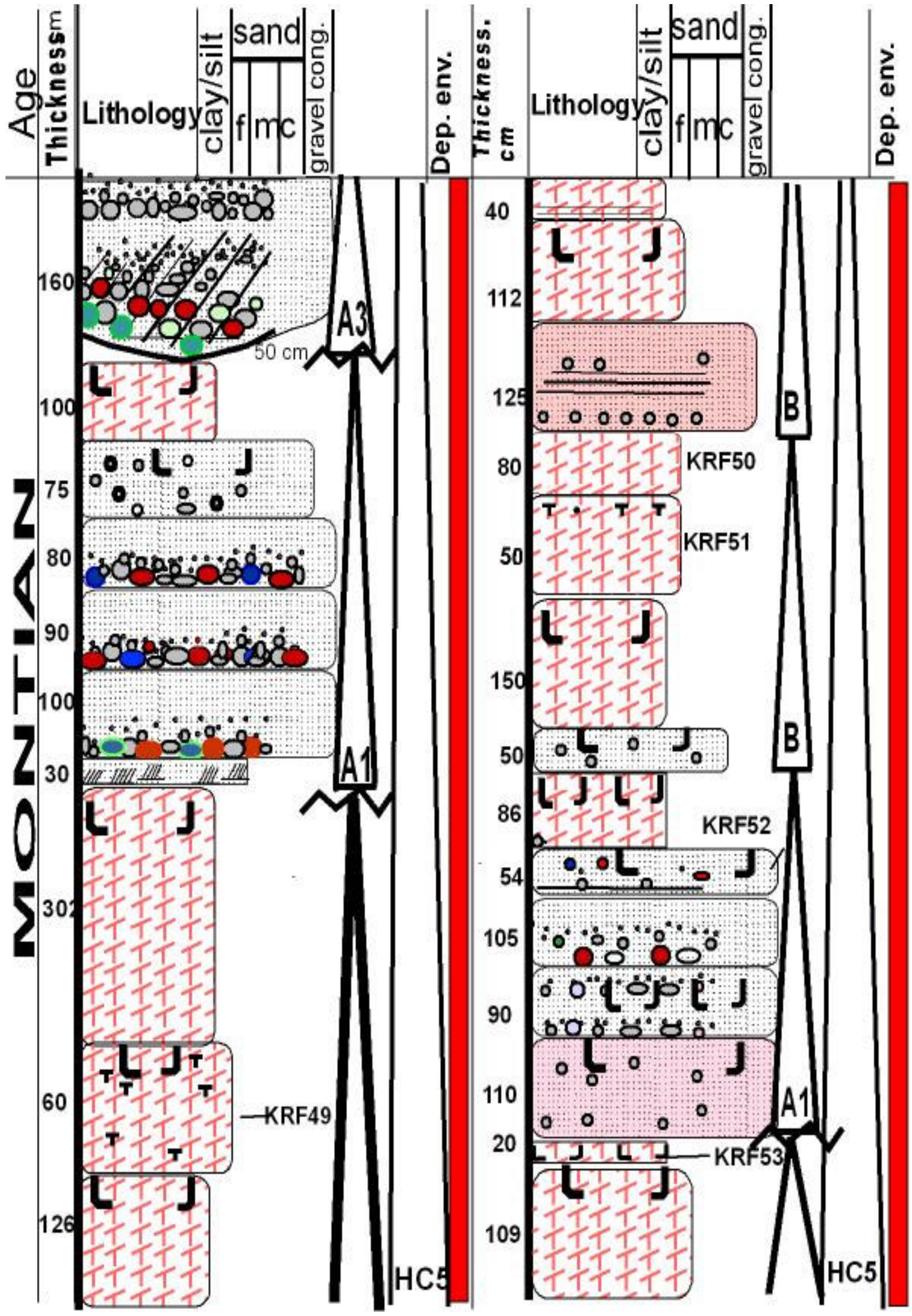

Figure A4. Detailed measured section (continued)

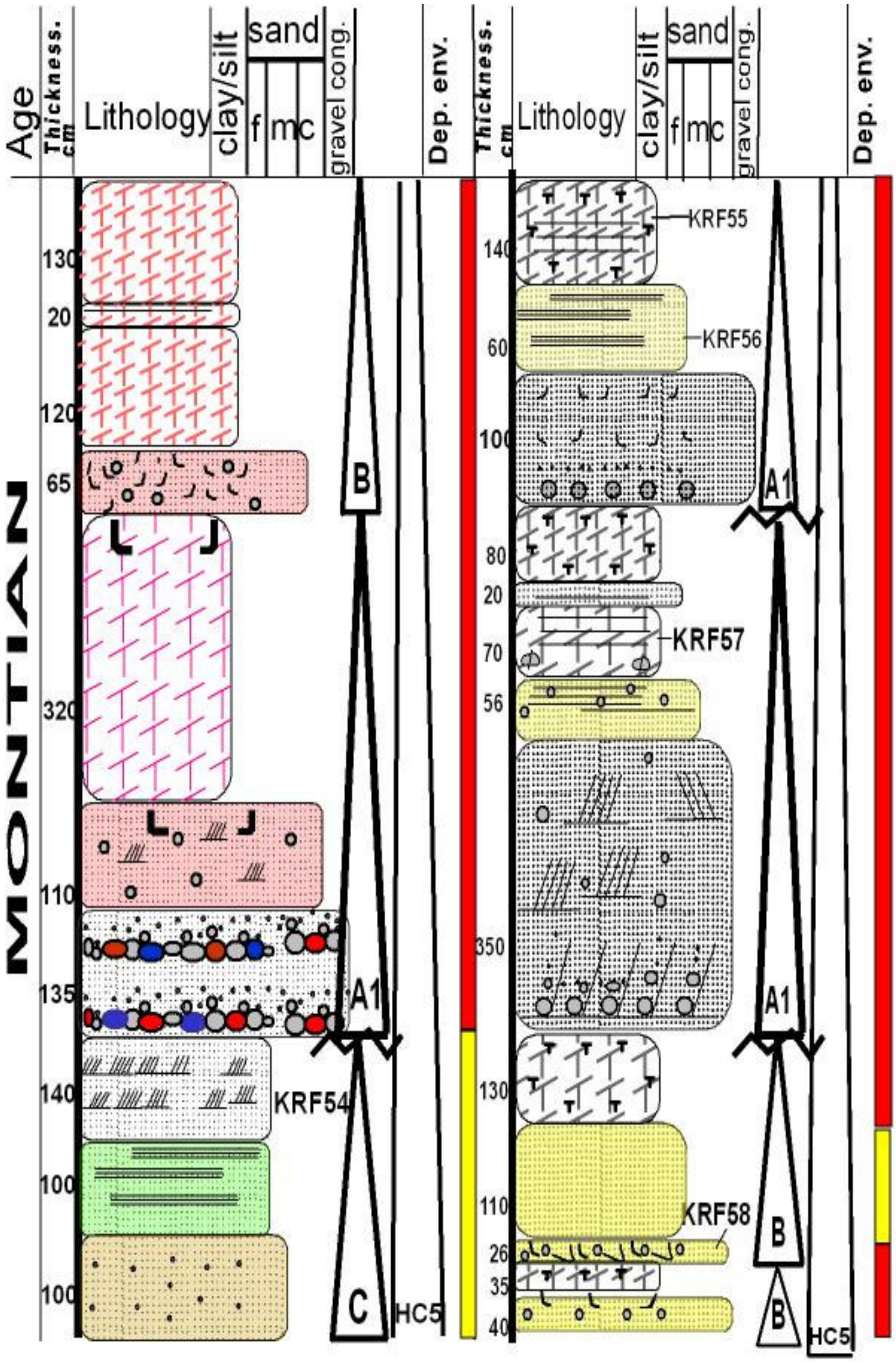

Figure A5. Detailed measured section (continued)

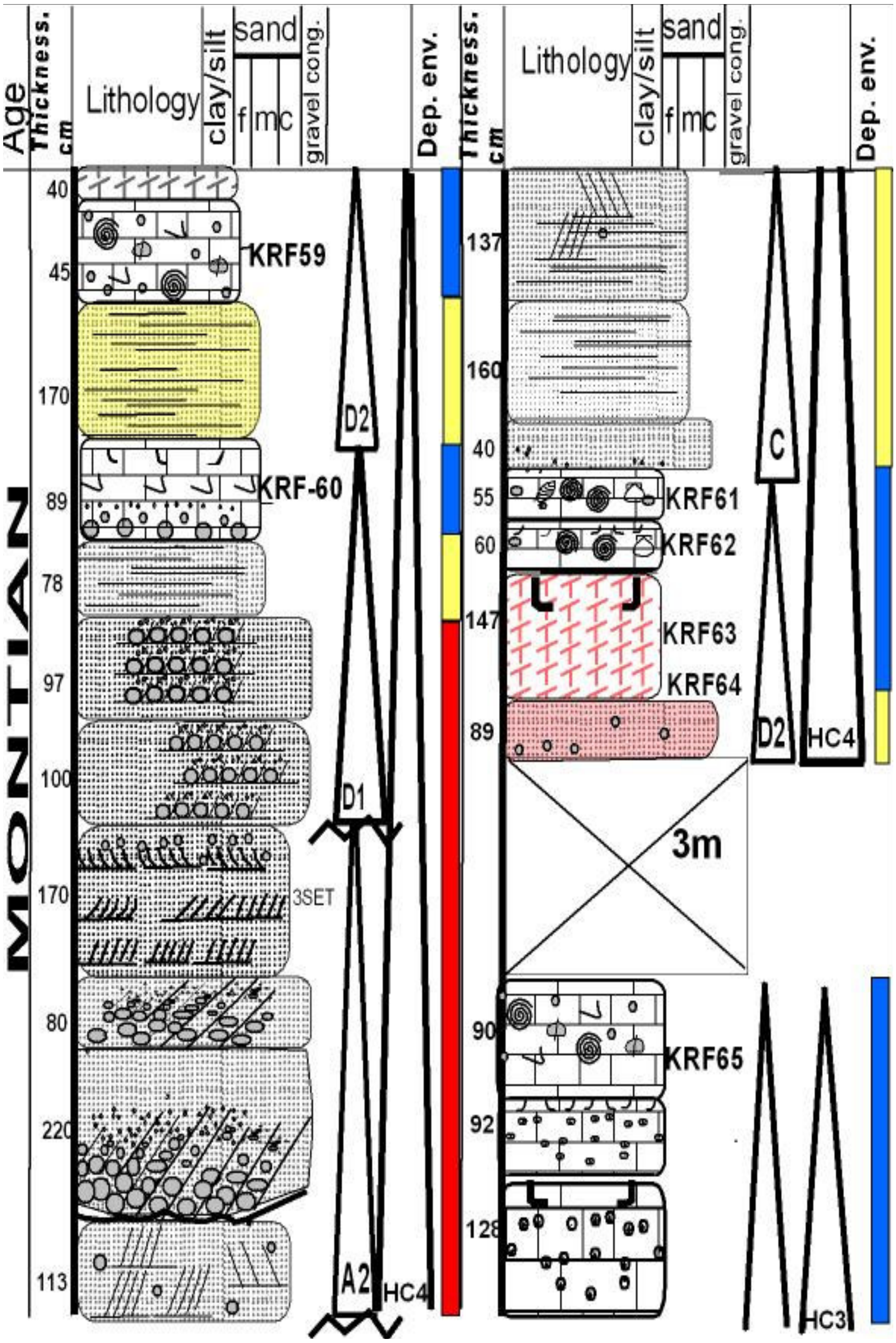

Figure A6. Detailed measured section (continued)

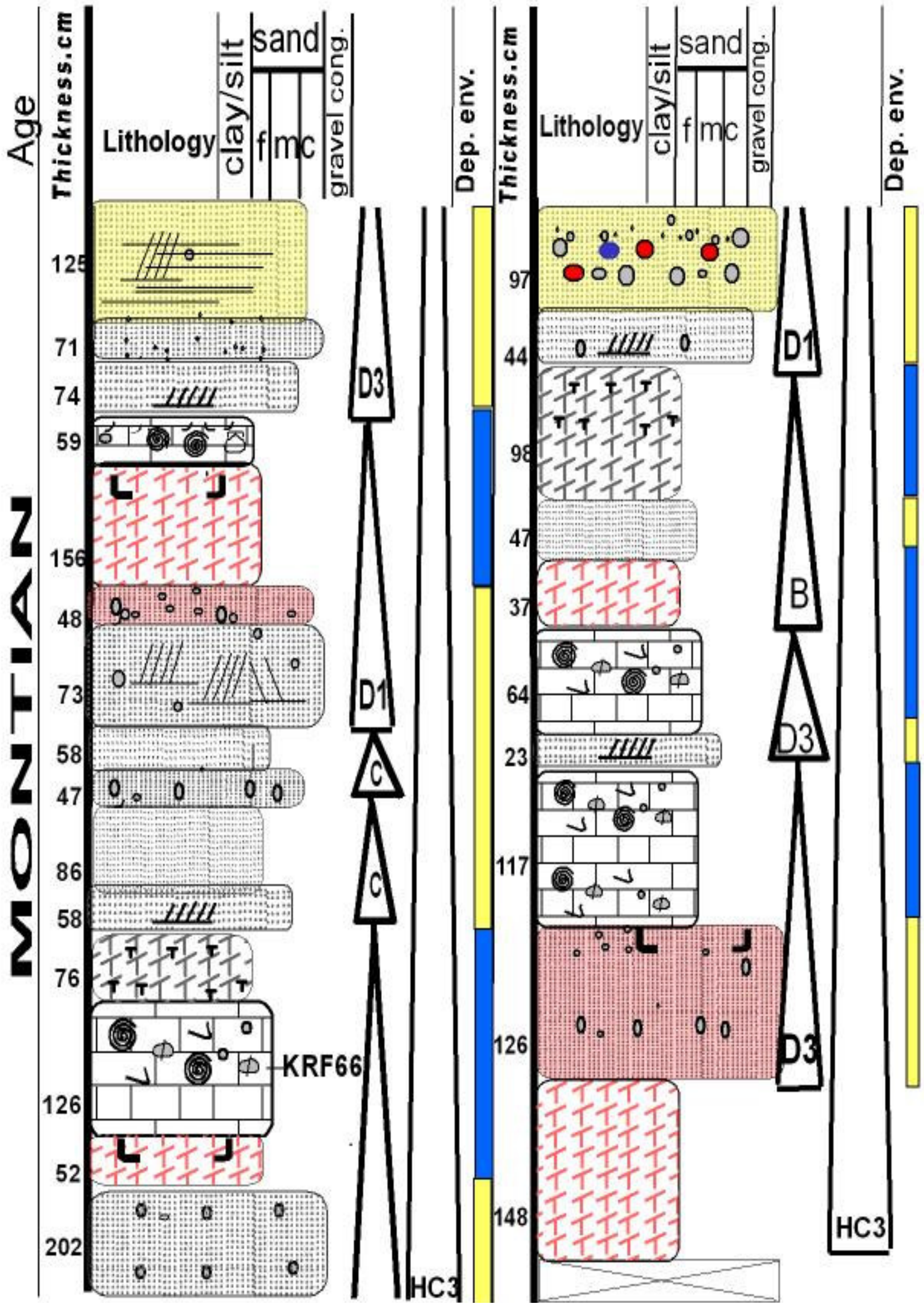

Figure A7. Detailed measured section (continued)

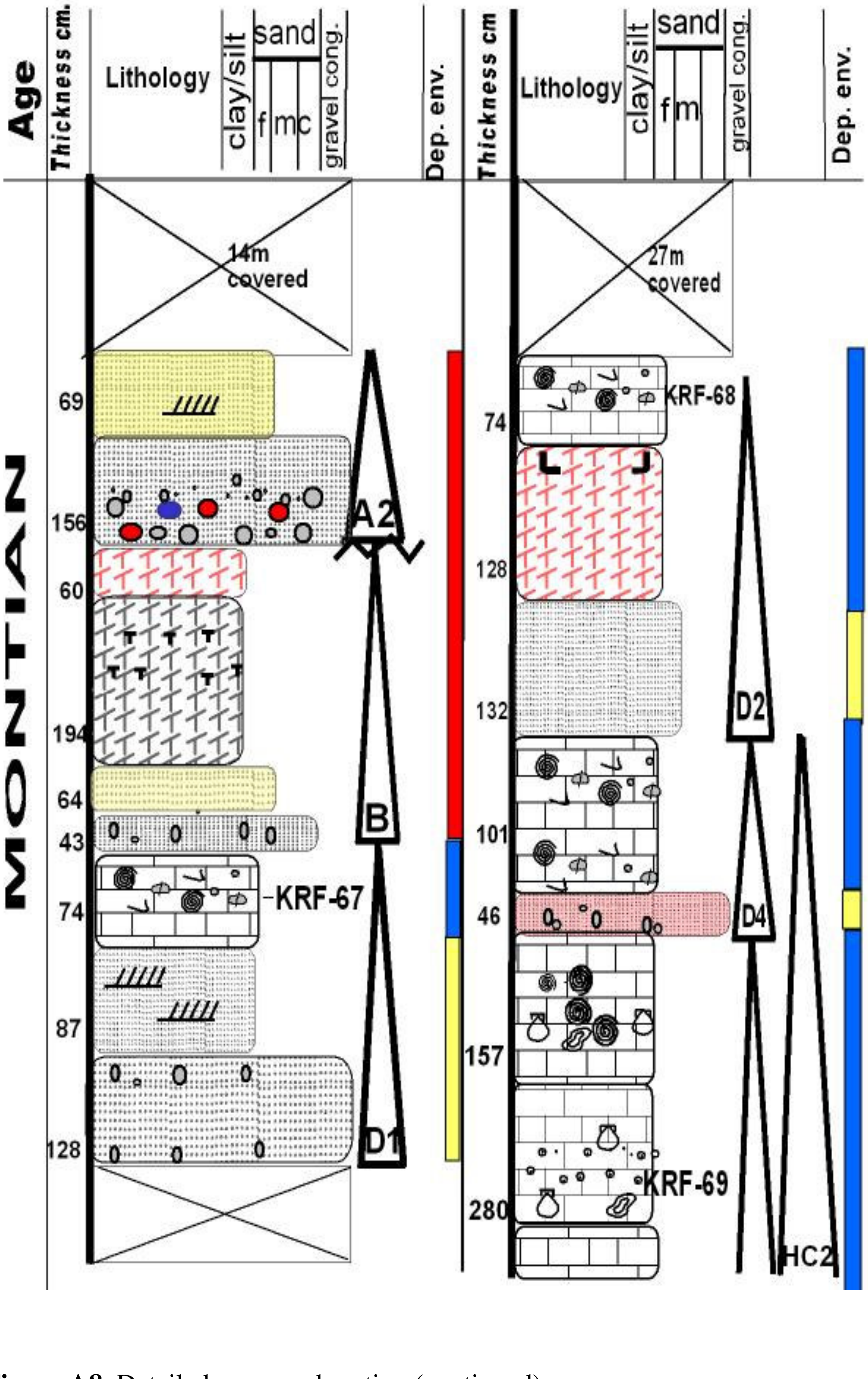

Figure A8. Detailed measured section (continued)

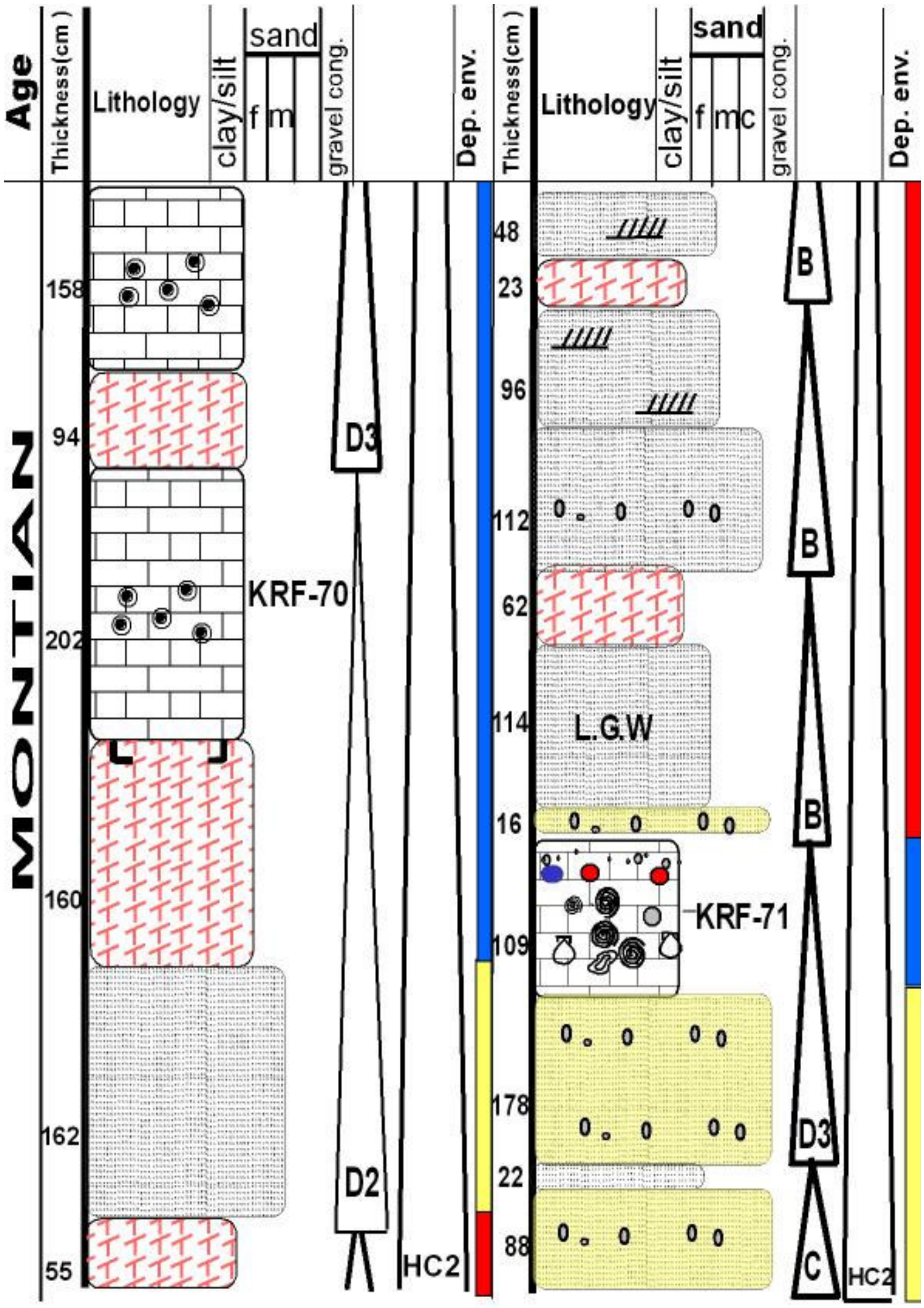

Figure A9. Detailed measured section (continued)

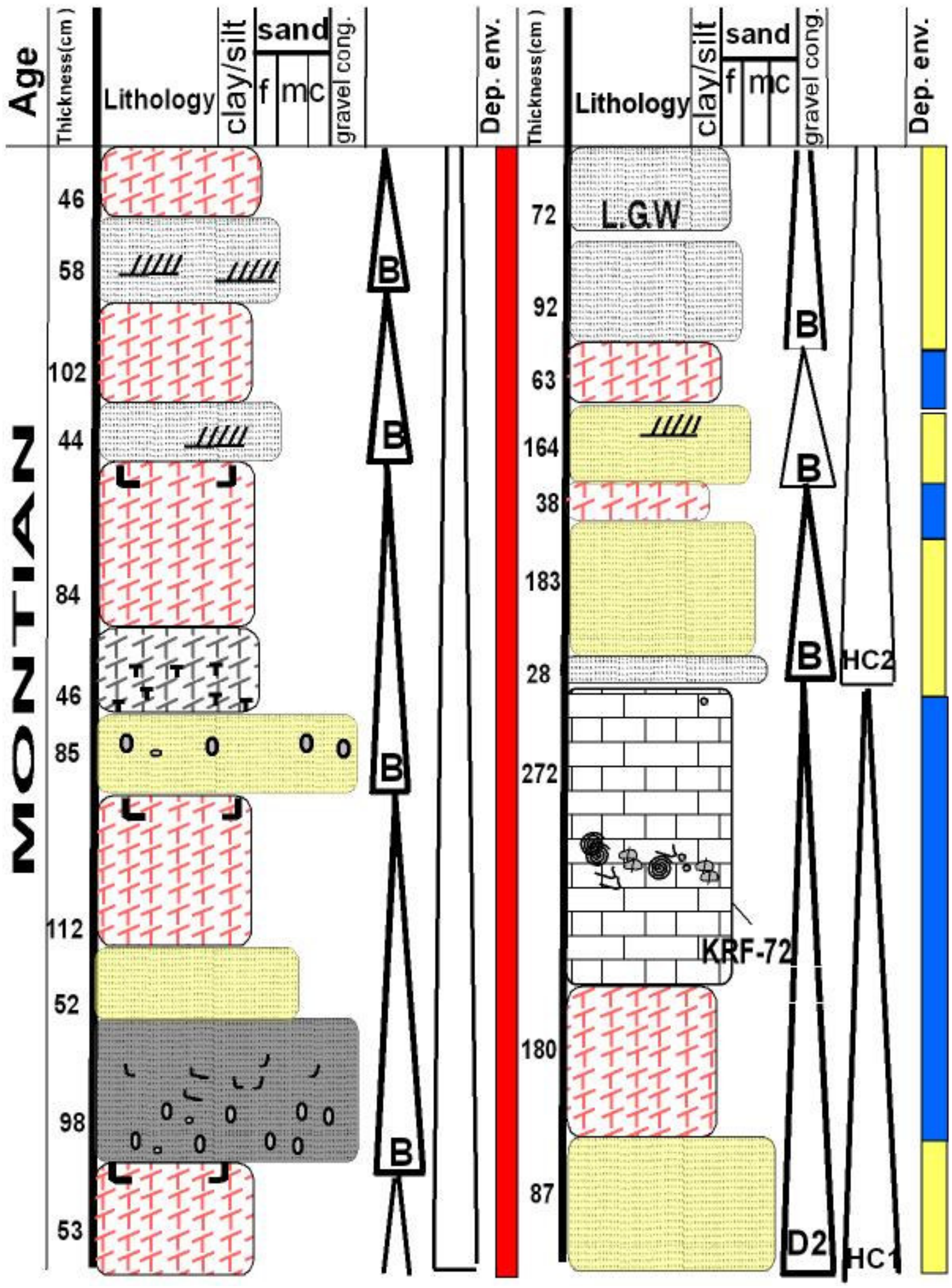

Figure A10. Detailed measured section (continued)

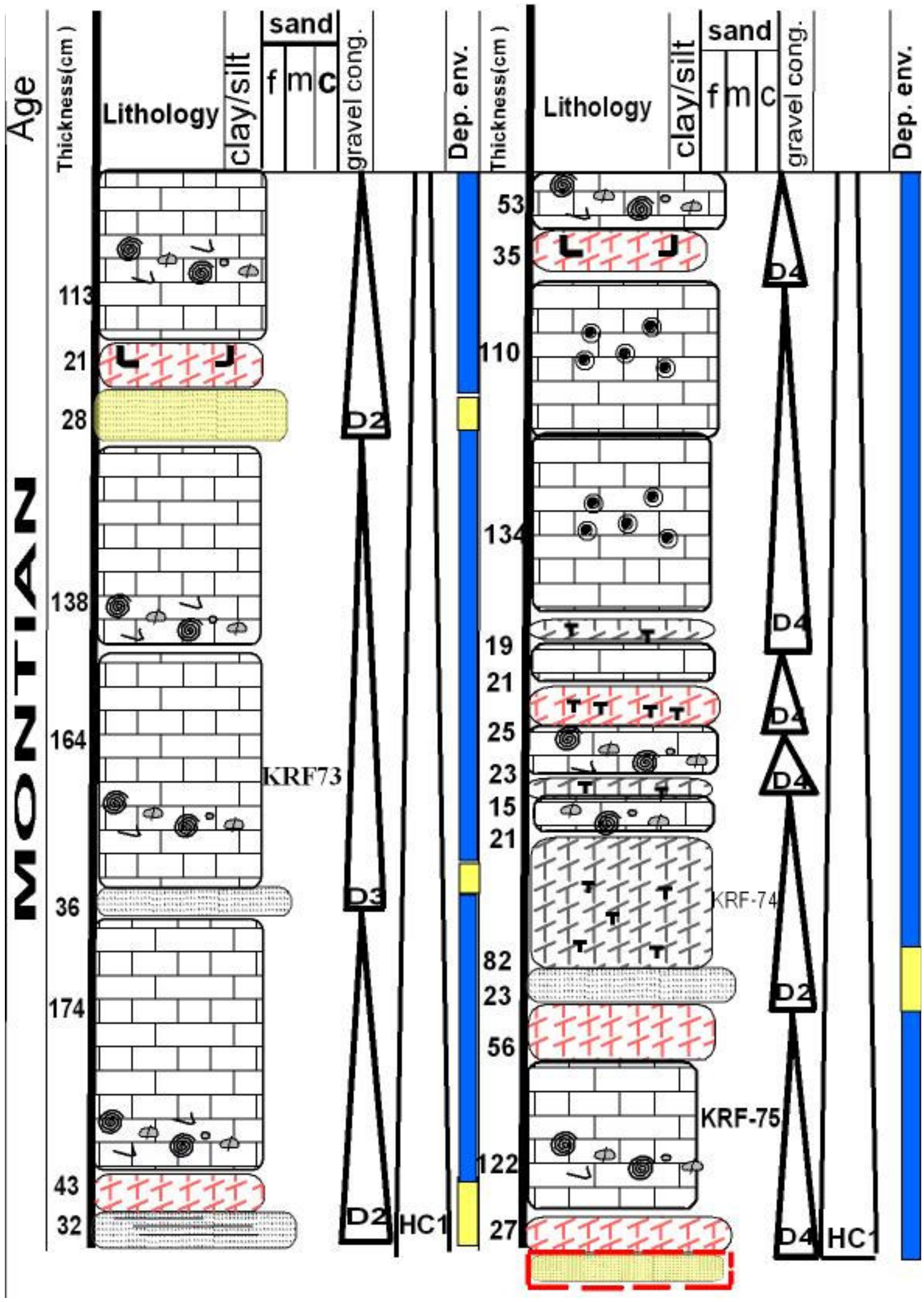

Figure A11. Detailed measured section (continued)

Legend

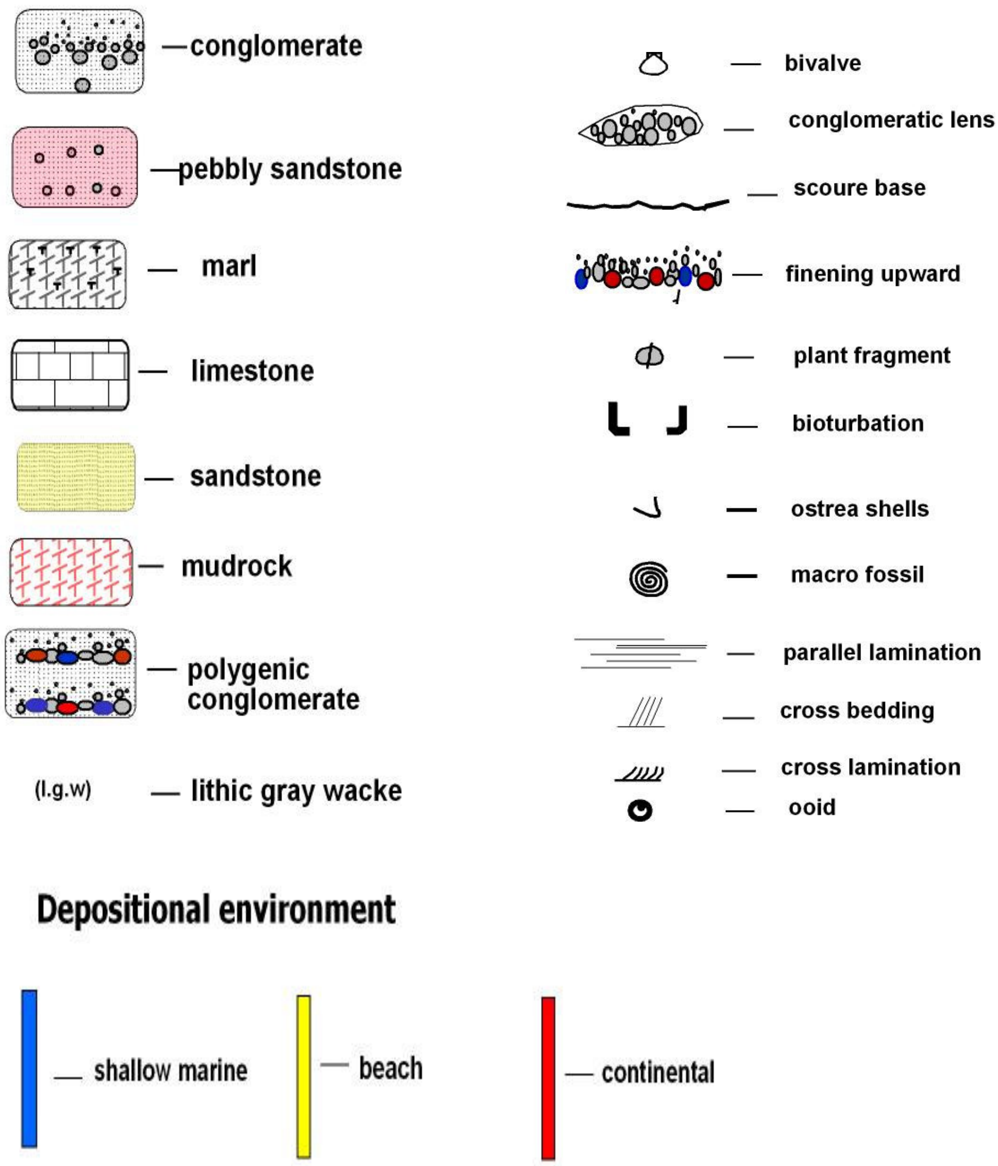
conglomerate
pebbly sandstone
marl
limestone
sandstone
mudrock
polygenic conglomerate
(l.g.w)
lithic gray wacke
bivalve
conglomeratic lens
scoure base
finening upward
plant fragment
bioturbation
ostrea shells
macro fossil
parallel lamination
cross bedding
cross lamination
ooid
Depositional environment
shallow marine
beach
continental

APPENDIX B

Table B1. Point counting data derived from the samples of studied section sandstones

SANDSTONES

Samples No.	Quartz	Rock fr.	Feldspar	Cement(calcite)	Matrix	Opaque	Muscovite	Bioclast	Ooid	Facies	Classification
	%	%	%	%	%	%	%	%	%		Pettijohn *et al*., (1987)
KRF-12	16.2	35.3		24	7.1				10.5	Sandstone with carb.	Litharenite
KRF-13	18.4	26.4	3.4	32.2	4.2				11.8	Sandstone with carb.	Litharenite
KRF-14	23.4	20.9	4.2	27.7	3.1	10.8		5.5	3.6	Sandstone	Litharenite
KRF-15	31	21.8	1.8	6.2	16.4	21.4	0.2	1.2		Sandstone	Lithicgraywacke
KRF-19	36.6	24	3.5	14.4	16.6	4.9				Sandstone	Lithicgraywacke
KRF-20	28.4	23.3	6.6	27.7	1.9	2.6	0.7	2.5		Sandstone with carb.	Litharenite
KRF-27	26.5	19.4	3.3	32.2	11.2			7.4		Sandstone with carb.	Litharenite
KRF-28	24.2	17.4	2.4	23.5	32.6					Sandstone	Lithicgraywacke
KRF-33	16.3	19.8	2.4	24.7	36.5					Sandstone	Lithicgraywacke
KRF-34	27.4	36.4	10.4	19.8	6					Pebbly sandstone	Litharenite
KRF-35	42.5	35.7	2	18.3	1.5					Sandstone	Litharenite
KRF-38	20.7	22.2	2.3	53.4	1.3					Sandstone	Litharenite
KRF-38B	20.8	26	2		30.1		0.7			Sandstone	Lithicgraywacke
KRF-40	14.6	23.2	1	57	4.2					Sandstone	Litharenite
KRF-42	22.1	33.2	3.1	27.4	12.9					Sandstone	Litharenite
KRF-44	21.2	27.5	1.7	8.9	38.2	2.5				Sandstone	Lithicgraywacke
KRF-47	16.4	32.3			50.1					Sandstone	Lithicgraywacke
KRF-48	28.5	31.1	2.6	18.2	12.1	6.4	1.1			Sandstone	Litharenite
KRF-52	27	42.5	1.7	20.8	6.4	1.6				Sandstone	Litharenite
KRF-54	32.2	40.7		20.2	6.9					Sandstone	Litharenite
KRF-56	43.6	8.8	3	40		4.6				Sandstone	Sublitharenite
KRF-58	22.4	44.9	6	23	1.2	2				Sandstone	Litharenite
KRF-64	21.6	45.1	5.8	22		3.4				Sandstone	Litharenite

Table B2. Point counting data derived from the samples of studied section limestones

LIMESTONES

Sample No.	Quartz	Rock fr.	Feldspar	Cement(sparrite)	Matrix	Bioclast	Ooid	Facies	Classification 1	Classification 2
	%	%	%	%	%	%	%		Dunham (1962)	Folk (1959)
KRF-1				27.2		37.8	34.9	Limestone	Grainstone	Oosparite
KRF-2				28.5	4.3	48.9	18.3	Limestone	Grainstone	Biosparites
KRF-3				17.3		77.8	4.9	Limestone	Grainstone	Biosparite
KRF-4				25.6		46	28.4	Limestone	Grainstone	Biosparite
KRF-5				31	18.5	29.4	21.1	Limestone	Packstone	Biosparite
KRF-6				18.5		3.5	78	Limestone	Grainstone	Oosparite
KRF-7				12.8		9.8	77.4	Limestone	Grainstone	Oosparite
KRF-8				17.2		2.7	80.1	Limestone	Grainstone	Oosparite
KRF-9				18		6.9	75.1	Limestone	Grainstone	Oosparite
KRF-10	5.6	4.1		30.6	0.6	9.6	49.5	Limestone with sand	Grainstone	Oosparite
KRF-11	4.2	5.9		10	2.5	3.8	73.6	Limest with sand	Grainstone	Oosparite
KRF-21				17.4		16.2	66.4	Limestone	Grainstone	Oosparite
KRF-22				19.4		28.1	52.5	Limestone	Grainstone	Oosparite
KRF-23				16.8		12.1	71.1	Limestone	Grainstone	Oosparite
KRF-24				20.3		14.6	64.7	Limestone	Grainstone	Oosparite
KRF-25				27.5	14.8	24.9	32.8	Limestone	Grainstone	Oosparite
KRF-26	3.3			40.7	4.6	30.1	20.9	Limestone	Grainstone	Biosparite
KRF-32	18.8	18.3	2.9	32		28		Sandy limestone	Dolomitic [illegible] limes.	
KRF-60	5.3	18.1	1.6	34.8		37.5	2.7	Sandy limest	Rudstone(gr>2mm)	Biosparite
KRF-61	2.9	3	0.6	32.2		57.3	4	Limestone	Rudstone(gr>2mm)	Biosparite
KRF-62	2.3	6.6	0.5	26.9	5.5	58.2		Limestone	Rudstone(gr>2mm)	Biosparite

Table B3. Point counting data derived from the samples of studied section conglomerates

CONGLOMERATE

Samples No.	Quartz	Rock fr.	Feldspar	Cement(calcite)	Matrix	Opaque	Bioclast	Facies	Classification of matrix	Classification
	%	%	%	%	%	%	%		Pettijohn *et al*., (1987)	Boggs (1992)
KRF-16	7.9	14.1	1.4	24.1	7.9	12.4	32.3	Conglomerate	Polygenic sandy conglomerate	Orthoconglomerate
KRF-18	21	31	2.8	34.1	8.5	2.4		Conglomerate	Litharenite	Orthoconglomerate
KRF-29	25.3	37	3.7	29.4	2.4	2.2		Conglomerate	Litharenite	Orthoconglomerate
KRF-31	16.8	30.2	1.5	48.5	2.8			Conglomerate	Litharenite	Orthoconglomerate

Table B4. Point counting data derived from the samples of studied section mudrocks

MUDROCKS

Sample No.	Quartz	Rock fr.	Feldspar	Matrix (micrite)	Matrix (clay)	Muscovite	Opaque	Facies	Classification 1	Classification 2
	%	%	%	%	%	%	%		Pettijohn (1975)	McKee & Weer (1953)
KRF-17				43.2	56.8			Marl	Marl	
KRF-18A	10	0.4		2	79.4			Mudrock	Mudstone	Fine mudstone
KRF-30	8.8	2.8		27.4	61			Mudrock	Mudstone	Fine mudstone
KRF-36	25.8	15.4	0.7	1.9	50.4	1.6	4.2	Silty mudrock	Mudstone	Coarse mdstn.
KRF-37	20.2	6.8		3	70			Silty mudrock	Mudstone	Coarse mdstn.
KRF-39	3.8	4.4		54	37.8			Silty marl	Marl	
KRF-41	18.6	3.4	0.2		77.8			Silty mudrock	Mudstone	Coarse mdstn.
KRF-45	2.6			26.2	71.2			Mudrock	Mudstone	Very fine mdstn.
KRF-46	17	17			66			Silty mudrock	Mudstone	Fine mudstone
KRF-49	26.6	14.8	2.4	2.2	51.6	2.4		Silty mudrock	Mudrock/marl	Coarse mdstn.
KRF-50	15.8	9.2	2	0.8	72.2			Silty mudrock	Mudstone	Fine mudstone
KRF-51				55.6	44.4			Marl	Marl	
KRF-53	15.4	4.4	0.2	2.6	77.4			Silty mudrock	Mudstone	Fine mudstone
KRF-55				55.6	44.4			Marl	Marl	
KRF-57	12.3			49.9	34.3	3.5		Silty mudrock	Mudstone	Fine mudstone
KRF-63	7.5			28.5	64			Mudrock	Mudstone	Very fine mdstn.

APPENDIX C

CD with Excel file of the Grain size parameters data – Back Cover of Thesis

APPENDIX D

Class	Freq %	Cum freq
0-1	7.5	7.5
1-2	34.5	42
2-3	51.5	93.5
3-4	6.5	100

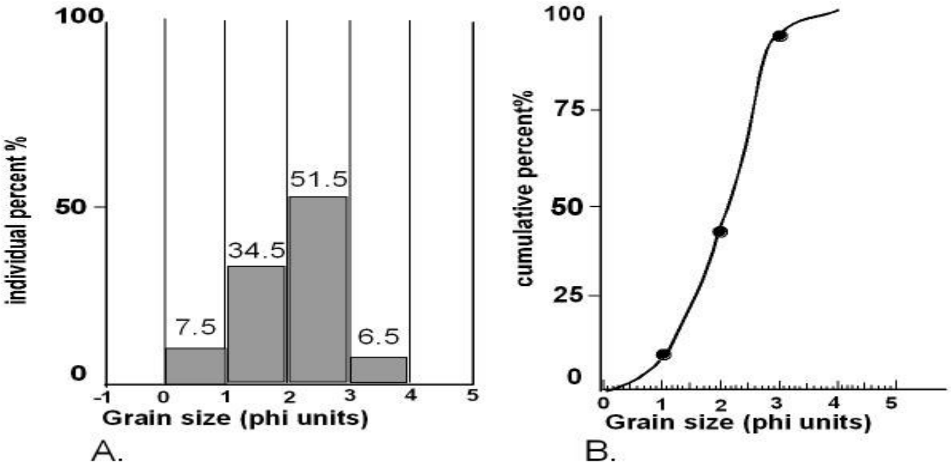

Figure 1D. Graphic presentation of grain size data for a sample 12 (A-histogram, B-cumulative frequency curves plotted with an arithmetic scale).

Class	Freq %	Cum freq
1-2	16.5	16.5
2-3	78.5	95
3-4	5	100

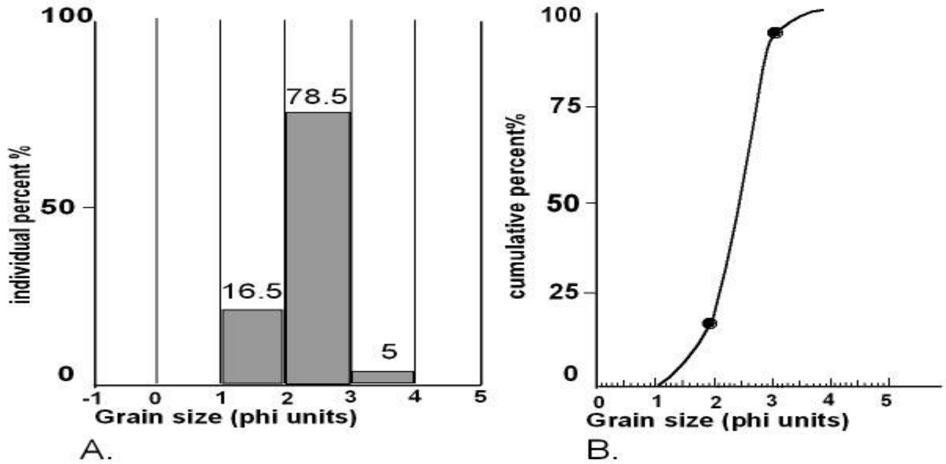

Figure 2D. Graphic presentation of grain size data for a sample 13 (A-histogram, B-cumulative frequency curves plotted with an arithmetic scale).

Class	Freq %	Cum freq
1-2	4	4
2-3	77	81
3-4	19	100

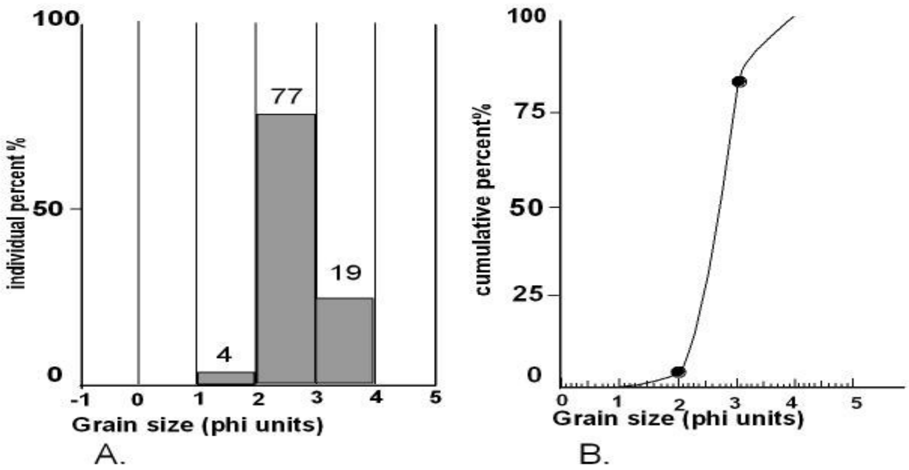

Figure 3D. Graphic presentation of grain size data for a sample 14 (A-histogram, B-cumulative frequency curves plotted with an arithmetic scale).

Class	Freq %	Cum freq
0-1	2.5	2.5
1-2	35.5	38
2-3	62	100

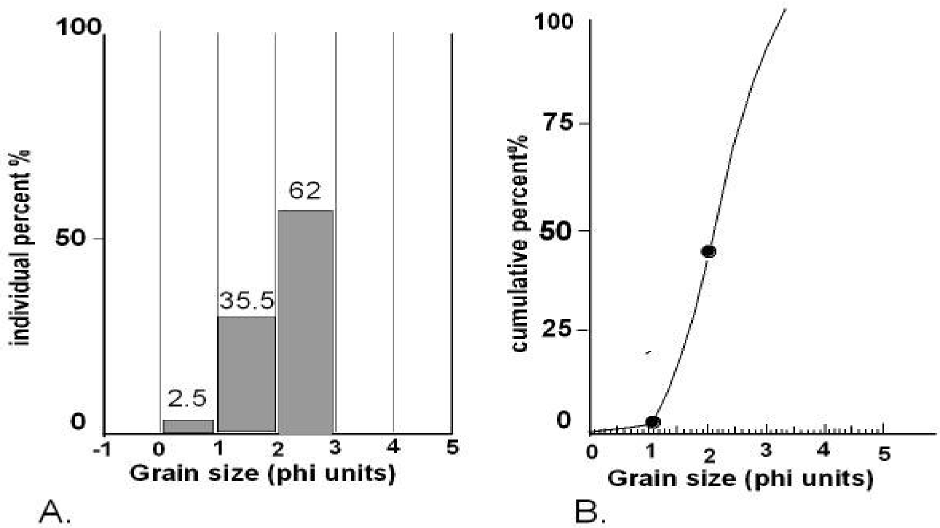

Figure 4D. Graphic presentation of grain size data for a sample 20 (A-histogram, B-cumulative frequency curves plotted with an arithmetic scale).

Class	Freq %	Cum. freq.
0-1	6	6
1-2	82	88
2-3	12	100

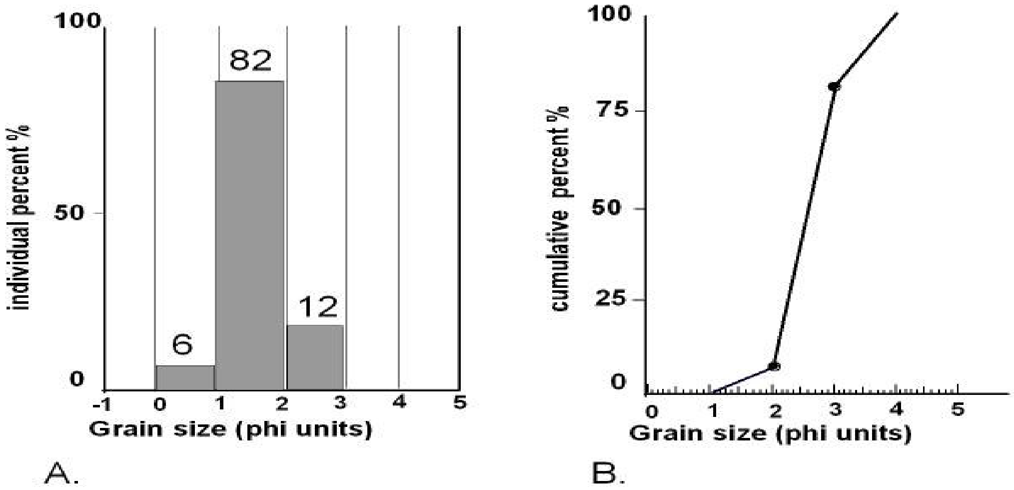

Figure 5D. Graphic presentation of grain size data for a sample 27 (A-histogram, B-cumulative frequency curves plotted with an arithmetic scale).

Class	Freq %	Cum. freq.
0-1	18.5	18.5
1-2	70.5	89
2-3	11	100

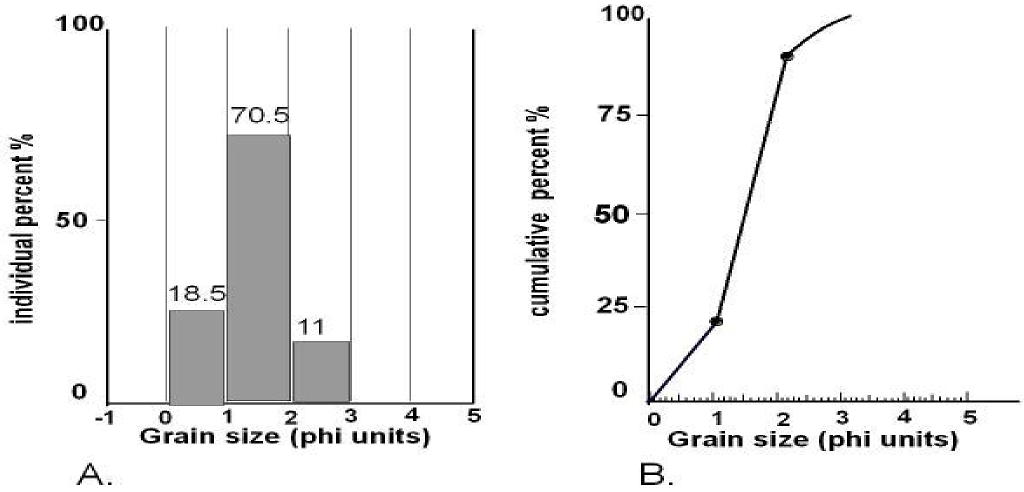

Figure 6D. Graphic presentation of grain size data for a sample 34 (A-histogram, B-cumulative frequency curves plotted with an arithmetic scale).

Class	Freq %	Cum freq
0-1	1	1
1-2	20	21
2-3	59	80
3-4	20	100

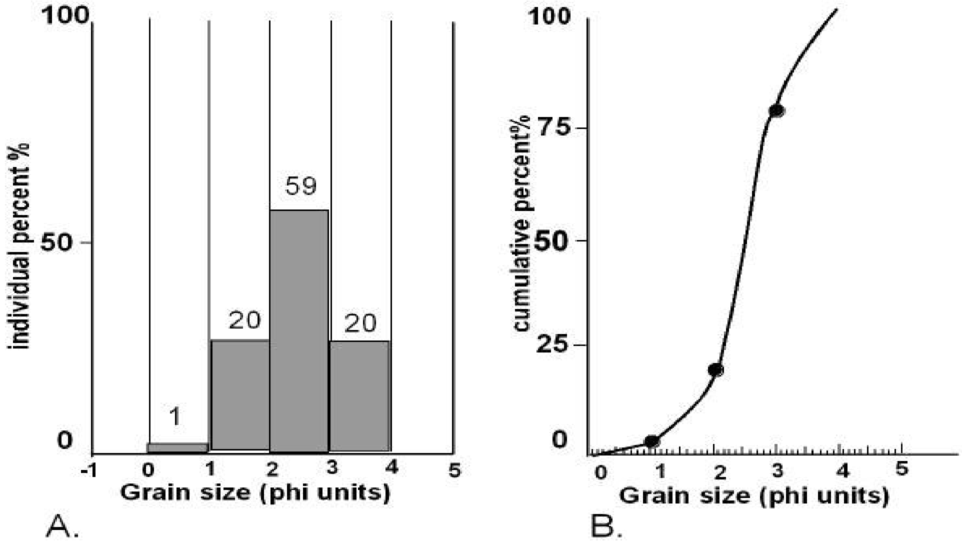

Figure 7D. Graphic presentation of grain size data for a sample 35 (A-histogram, B-cumulative frequency curves plotted with an arithmetic scale).

Class	Freq %	Cum. freq.
1-2	29	29
2-3	66	95
3-4	5	100

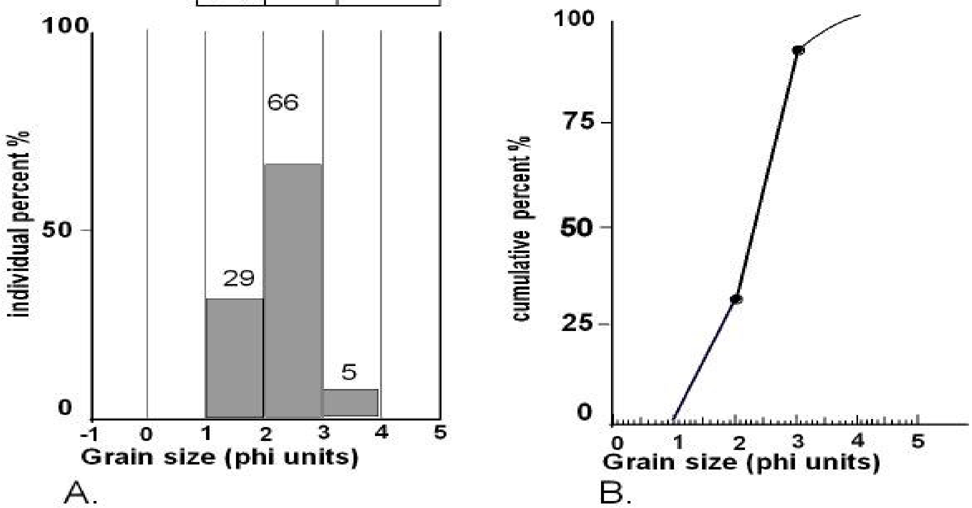

Figure 8D. Graphic presentation of grain size data for a sample 38 (A-histogram, B-cumulative frequency curves plotted with an arithmetic scale).

Class	Freq %	Cum. freq.
(-1)-0	1.5	1.5
0-1	9.5	11
1-2	69.5	80.5
2-3	19.5	100

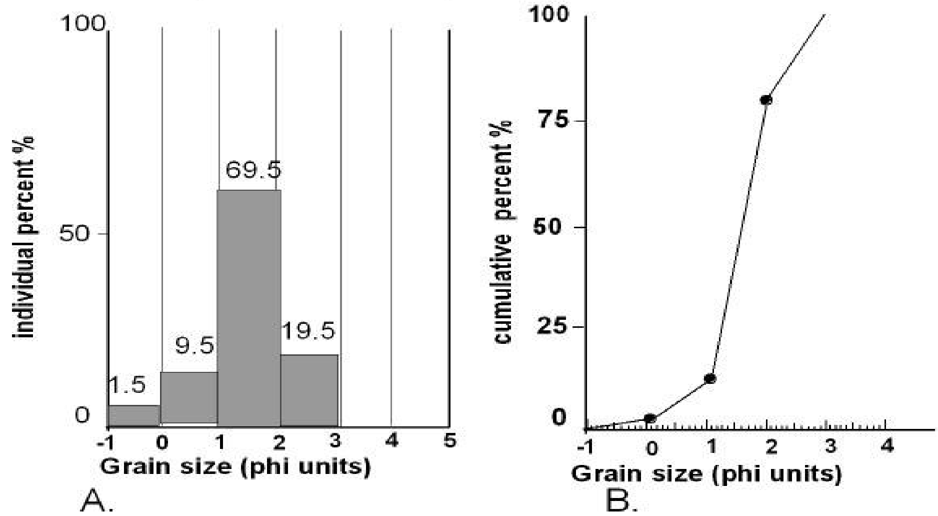

Figure 9D. Graphic presentation of grain size data for a sample 40 (A-histogram, B-cumulative frequency curves plotted with an arithmetic scale).

Class	Freq %	Cum freq
1-2	1	1
2-3	45	46
3-4	54	100

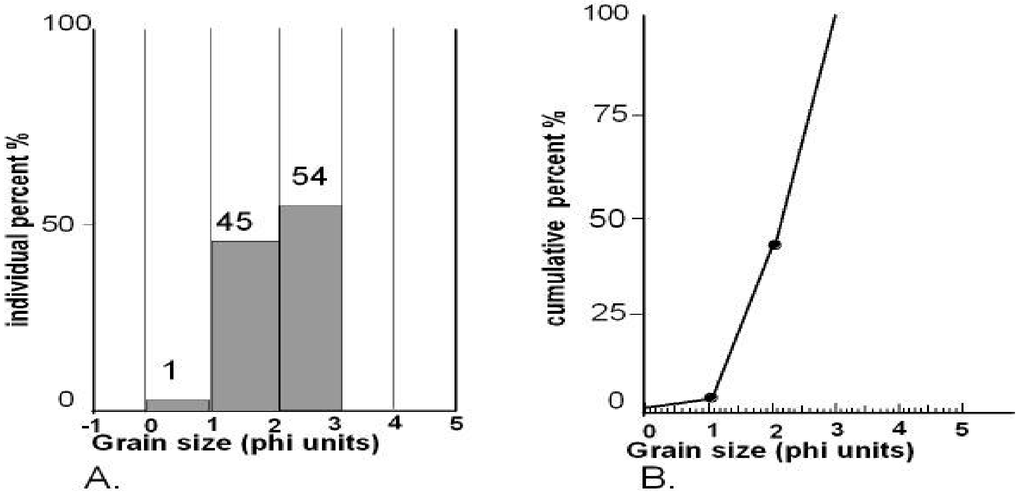

Figure 10D. Graphic presentation of grain size data for a sample 42 (A-histogram, B-cumulative frequency curves plotted with an arithmetic scale).

Class	Freq %	Cum freq
0-1	5	5
1-2	61	66
2-3	34	100

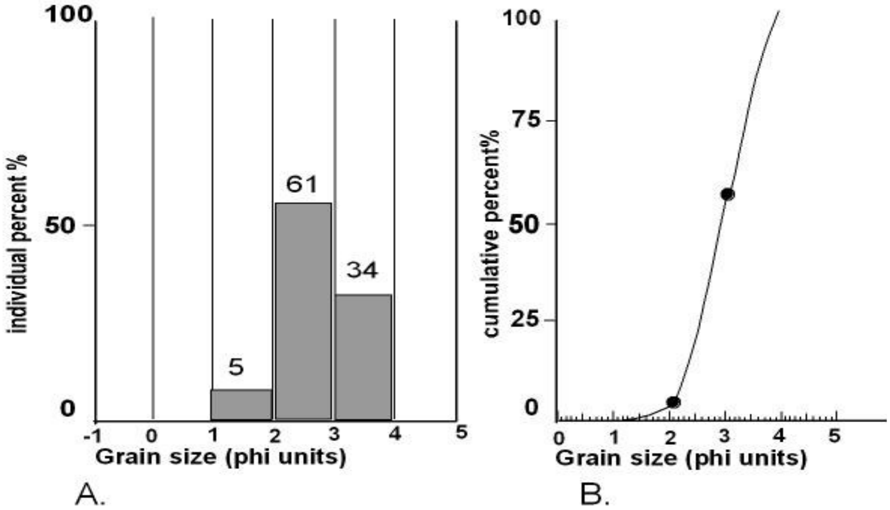

Figure 11D. Graphic presentation of grain size data for a sample 48 (A-histogram, B-cumulative frequency curves plotted with an arithmetic scale).

Class	Freq %	Cum freq
1-2	6.5	6.5
2-3	64	70.5
3-4	29.5	100

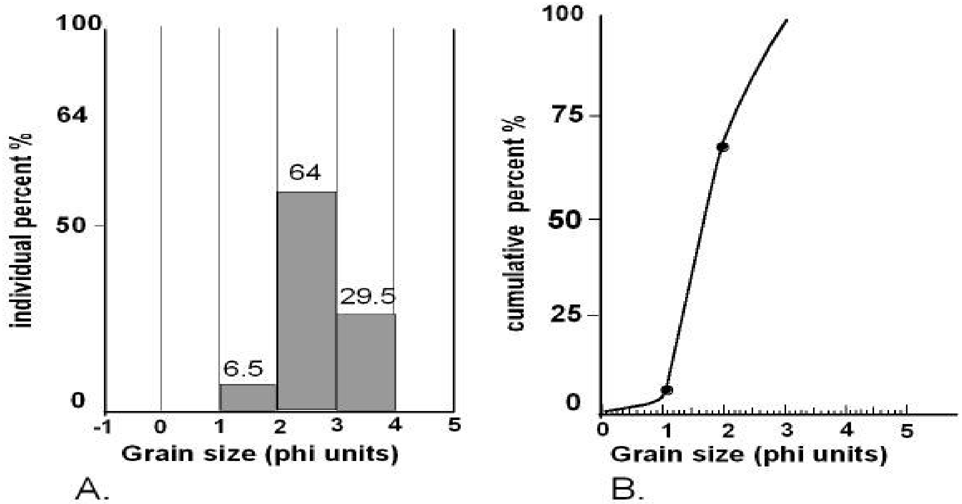

Figure 12D. Graphic presentation of grain size data for a sample 52 (A-histogram, B-cumulative frequency curves plotted with an arithmetic scale).

Class	Freq %	Cum freq
1-2	34	34
2-3	61	95
3-4	5	100

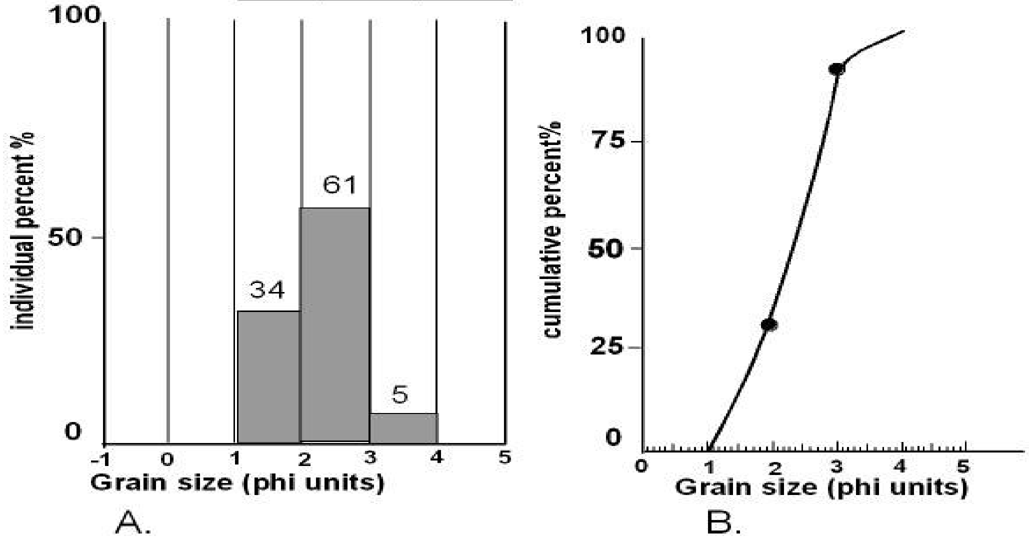

Figure 13D. Graphic presentation of grain size data for a sample 54 (A-histogram, B-cumulative frequency curves plotted with an arithmetic scale).

Class	Freq %	Cum. freq.
1-2	9	9
2-3	85	94
3-4	6	100

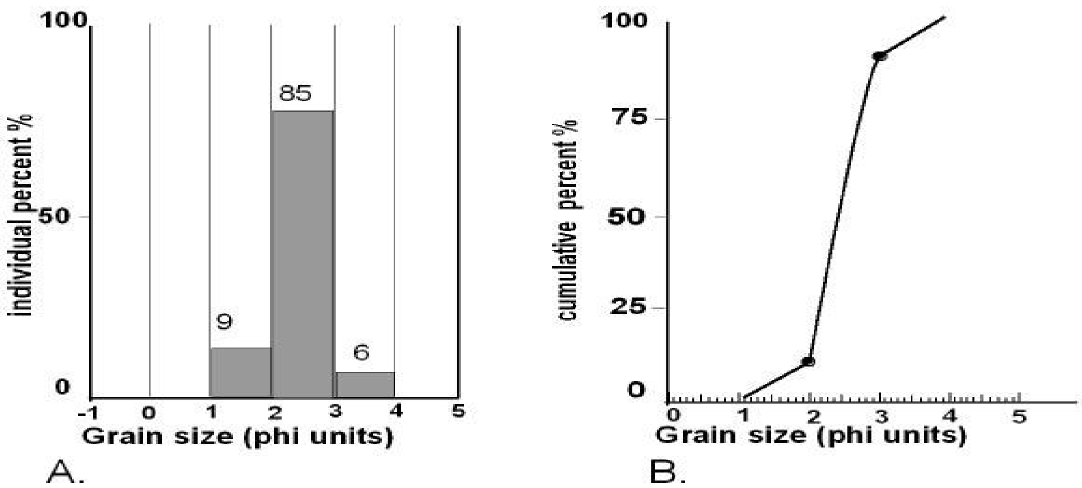

Figure 14D. Graphic presentation of grain size data for a sample 56 (A-histogram, B-cumulative frequency curves plotted with an arithmetic scale).

Class	Freq %	Cum. freq.
0-1	15.5	15.5
1-2	44.5	60
2-3	40	100

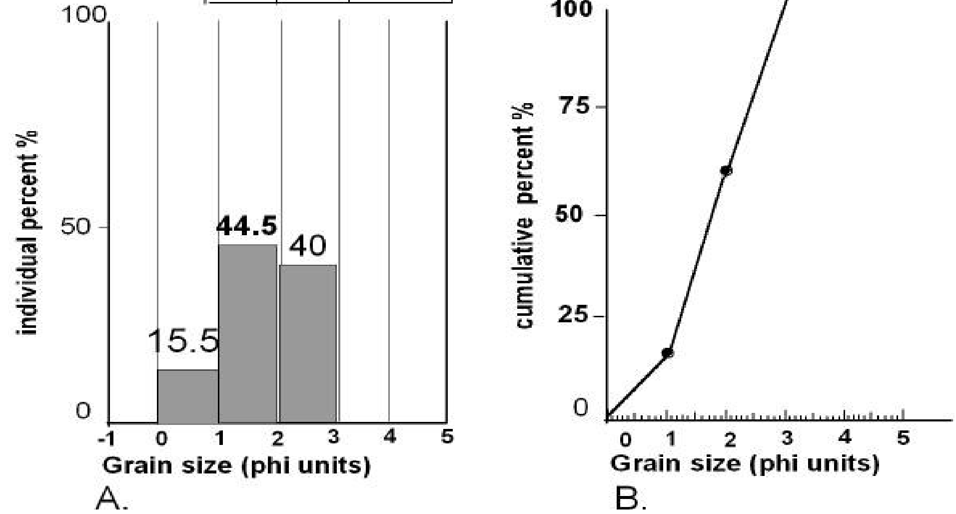

Figure 14D. Graphic presentation of grain size data for a sample 58 (A-histogram, B-cumulative frequency curves plotted with an arithmetic scale).

Class	Freq %	Cum freq
(-1)-0	0.5	0.5
0-1	7.5	8
1-2	55	63
2-3	37	100

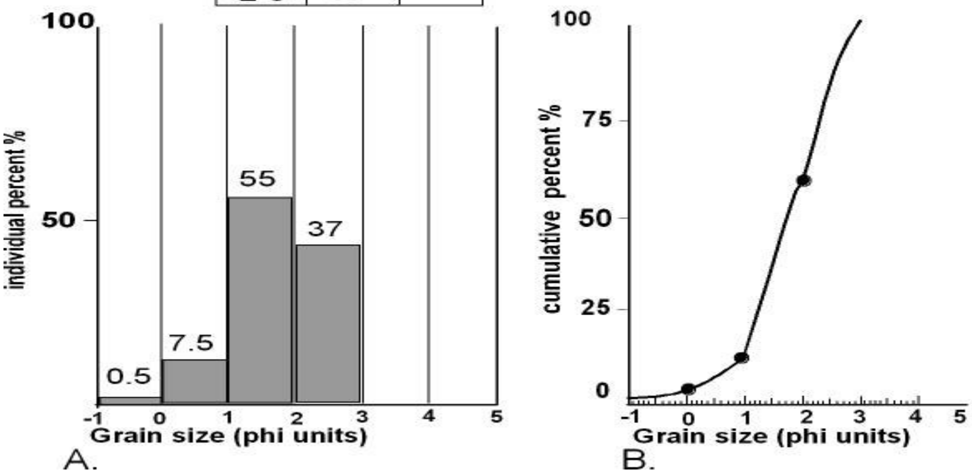

Figure 15D. Graphic presentation of grain size data for a sample 64 (A-histogram, B-cumulative frequency curves plotted with an arithmetic scale).

APPENDIX E

Sample no	Long (cm)	Intermediate (cm)	Short (cm)	SPH	O/P index	I/L	S/I	Shape index
1	5.76	3.52	2.77	0.72	5.18	0.61	0.79	0.62
2	4.23	3.44	1.74	0.59	-4.44	0.81	0.51	0.46
3	3.41	2.74	1.91	0.73	-0.95	0.80	0.70	0.62
4	4.45	3.34	1.98	0.64	-1.14	0.75	0.59	0.51
5	3.35	2.53	1.24	0.57	-3.01	0.76	0.49	0.43
6	4.36	2.73	1.25	0.51	0.84	0.63	0.46	0.36
7	3.45	2.78	1.46	0.61	-3.86	0.81	0.53	0.47
8	3.24	2.23	1.35	0.63	0.83	0.69	0.61	0.50
9	2.5	1.56	0.78	0.54	1.49	0.62	0.50	0.39
10	2.64	2.27	1.25	0.64	-4.94	0.86	0.55	0.51
11	1.85	1.14	1.13	0.85	7.96	0.62	0.99	0.78
12	3.26	2.15	1.49	0.68	2.78	0.66	0.69	0.56
13	2.74	2.14	1.53	0.74	-0.07	0.78	0.71	0.63
14	2.56	2.23	1.69	0.79	-1.83	0.87	0.76	0.71
15	2.04	1.46	0.93	0.66	0.49	0.72	0.64	0.54
16	2.75	2.13	2.24	0.95	8.79	0.77	1.05	0.93
17	3	2.35	1.92	0.81	1.59	0.78	0.82	0.72
18	2.74	2.14	1.53	0.74	-0.07	0.78	0.71	0.63
19	4.84	3.15	1.73	0.58	1.21	0.65	0.55	0.44
20	3.95	3.53	3.41	0.94	3.22	0.89	0.97	0.91
21	3.24	1.55	0.96	0.57	8.14	0.48	0.62	0.43
22	2.64	1.64	0.76	0.51	1.11	0.62	0.46	0.37
23	4.91	3.61	3	0.80	2.96	0.74	0.83	0.71
24	2.93	1.95	1.84	0.84	6.35	0.67	0.94	0.77
25	2.36	1.24	1.15	0.77	8.73	0.53	0.93	0.67
26	4.45	2.96	2.75	0.83	6.09	0.67	0.93	0.76
27	6.63	4.43	3.24	0.71	3.05	0.67	0.73	0.60
28	5.16	3.67	2.95	0.77	3.05	0.71	0.80	0.68
29	3.31	2.62	1.95	0.76	0.12	0.79	0.74	0.66
30	2.64	2.23	1.78	0.81	-0.34	0.84	0.80	0.73
31	2.53	2.23	1.45	0.72	-3.88	0.88	0.65	0.61
32	2.36	1.55	1.28	0.77	4.61	0.66	0.83	0.67
33	2.45	2.16	1.25	0.67	-5.06	0.88	0.58	0.54
34	3.13	2.76	1.96	0.76	-2.93	0.88	0.71	0.67
35	2.91	1.96	1.13	0.61	0.87	0.67	0.58	0.47
36	2	1.67	0.93	0.64	-4.12	0.84	0.56	0.51
37	2.53	1.53	1.46	0.82	7.53	0.60	0.95	0.74
38	2.76	2.34	2.12	0.89	2.03	0.85	0.91	0.83
39	3.34	2.52	1.87	0.75	1.03	0.75	0.74	0.64
40	3.64	2.19	1.35	0.61	3.59	0.60	0.62	0.48
41	2.79	1.73	1.25	0.69	4.20	0.62	0.72	0.57
42	2.53	1.83	1.29	0.71	1.27	0.72	0.70	0.60
43	2.59	2.24	1.33	0.67	-4.33	0.86	0.59	0.55
44	3.54	1.94	1.45	0.67	6.48	0.55	0.75	0.55
45	1.86	1.73	1.54	0.90	-1.13	0.93	0.89	0.86
46	2.24	1.97	1.55	0.82	-1.57	0.88	0.79	0.74
47	2.36	2.14	1.48	0.76	-3.99	0.91	0.69	0.66
48	2.13	1.25	1.14	0.79	7.27	0.59	0.91	0.70
49	2.63	2.23	1.49	0.72	-2.63	0.85	0.67	0.62
50	1.86	1.43	1.14	0.79	1.59	0.77	0.80	0.70

Figure E1. Grain size parameters for conglomeratic Bed-1.

Sample no	Long (cm)	Intermediate (cm)	Short (cm)	SPH	O/P index	I/L	S/I	Shape index
51	1.63	1.14	0.78	0.69	1.60	0.70	0.68	0.57
52	2	1.82	1.06	0.68	-5.82	0.91	0.58	0.56
53	3.34	2.25	1.73	0.74	3.42	0.67	0.77	0.63
54	4.96	4.35	2.44	0.65	-5.24	0.88	0.56	0.53
55	2.46	1.83	1.54	0.81	2.95	0.74	0.84	0.73
56	3.42	1.77	1.34	0.67	7.48	0.52	0.76	0.54
57	3.41	2.68	1.81	0.71	-0.82	0.79	0.68	0.60
58	3.53	2.39	1.72	0.71	2.66	0.68	0.72	0.59
59	3.94	2.43	1.84	0.71	4.69	0.62	0.76	0.59
60	3.52	1.95	1.82	0.78	8.19	0.55	0.93	0.69
61	3.49	2.08	1.85	0.78	6.79	0.60	0.89	0.69
62	1.74	1.35	1.13	0.82	2.15	0.78	0.84	0.74
63	4.63	3.98	3.44	0.86	0.62	0.86	0.86	0.80
64	1.58	1.44	1.23	0.87	-1.28	0.91	0.85	0.82
65	6.43	5.84	4.32	0.79	-3.28	0.91	0.74	0.70
66	2.24	1.54	1.32	0.80	4.43	0.69	0.86	0.71
67	2.13	1.97	1.75	0.90	-0.96	0.92	0.89	0.85
68	3.54	2.78	2.57	0.88	3.91	0.79	0.92	0.82
69	2.38	1.77	1.43	0.79	2.37	0.74	0.81	0.70
70	4.77	2.78	1.12	0.46	1.93	0.58	0.40	0.31
71	4.15	2.96	2.78	0.86	5.50	0.71	0.94	0.79
72	5.74	4.95	3.52	0.76	-2.35	0.86	0.71	0.66
73	5.19	3.79	2.12	0.61	-1.08	0.73	0.56	0.48
74	4.75	2.74	2.57	0.80	7.80	0.58	0.94	0.71
75	5.53	3.94	2.99	0.74	2.33	0.71	0.76	0.64
76	11.24	6.64	5.74	0.76	6.59	0.59	0.86	0.66
77	5.14	2.74	2.13	0.69	7.18	0.53	0.78	0.57
78	3.94	3.17	2.36	0.76	-0.21	0.80	0.74	0.67
79	2.82	2.08	1.85	0.84	4.01	0.74	0.89	0.76
80	5.23	3.35	2.34	0.68	3.36	0.64	0.70	0.56
81	3.13	2.64	2.43	0.89	2.58	0.84	0.92	0.85
82	4.13	2.24	1.73	0.69	6.86	0.54	0.77	0.57
83	2.47	1.97	1.38	0.73	-0.74	0.80	0.70	0.63
84	3.53	2.53	2.19	0.81	3.97	0.72	0.87	0.73
85	3.63	1.85	1.34	0.64	7.51	0.51	0.72	0.52
86	3.43	1.53	1.65	0.80	11.80	0.45	1.08	0.72
87	3.12	2.95	1.14	0.52	-11.33	0.95	0.39	0.38
88	2.43	1.53	1.23	0.74	4.94	0.63	0.80	0.64
89	2.84	1.93	1.53	0.75	3.61	0.68	0.79	0.65
90	2.32	1.73	1.64	0.88	5.20	0.75	0.95	0.82
91	1.92	1.55	0.97	0.68	-2.19	0.81	0.63	0.56
92	2.93	1.25	0.94	0.62	10.73	0.43	0.75	0.49
93	2.77	2.62	1.86	0.78	-4.99	0.95	0.71	0.69
94	3.74	2.32	1.91	0.75	5.40	0.62	0.82	0.65
95	2.34	1.75	1.43	0.79	2.43	0.75	0.82	0.71
96	4.42	2.32	1.45	0.59	6.31	0.52	0.63	0.45
97	3.72	2.65	2.14	0.77	3.08	0.71	0.81	0.68
98	4.12	2.94	2.25	0.75	2.40	0.71	0.77	0.65
99	3.57	2.42	1.88	0.74	3.43	0.68	0.78	0.64
100	3.73	2.15	1.84	0.75	6.81	0.58	0.86	0.65

Figure E1. Continued.

Sample no	Long (cm)	Intermediate (cm)	Short (cm)	SPH	O/P index	I/L	S/I	Shape index
1	5.76	3.52	2.77	0.72	5.18	0.61	0.79	0.62
2	4.23	3.44	1.74	0.59	-4.44	0.81	0.51	0.46
3	3.41	2.74	1.91	0.73	-0.95	0.80	0.70	0.62
4	4.45	3.34	1.98	0.64	-1.14	0.75	0.59	0.51
5	3.35	2.53	1.24	0.57	-3.01	0.76	0.49	0.43
6	4.36	2.73	1.25	0.51	0.84	0.63	0.46	0.36
7	3.45	2.78	1.46	0.61	-3.86	0.81	0.53	0.47
8	3.24	2.23	1.35	0.63	0.83	0.69	0.61	0.50
9	2.5	1.56	0.78	0.54	1.49	0.62	0.50	0.39
10	2.64	2.27	1.25	0.64	-4.94	0.86	0.55	0.51
11	1.85	1.14	1.13	0.85	7.96	0.62	0.99	0.78
12	3.26	2.15	1.49	0.68	2.78	0.66	0.69	0.56
13	2.74	2.14	1.53	0.74	-0.07	0.78	0.71	0.63
14	2.56	2.23	1.69	0.79	-1.83	0.87	0.76	0.71
15	2.04	1.46	0.93	0.66	0.49	0.72	0.64	0.54
16	2.75	2.13	2.24	0.95	8.79	0.77	1.05	0.93
17	3	2.35	1.92	0.81	1.59	0.78	0.82	0.72
18	2.74	2.14	1.53	0.74	-0.07	0.78	0.71	0.63
19	4.84	3.15	1.73	0.58	1.21	0.65	0.55	0.44
20	3.95	3.53	3.41	0.94	3.22	0.89	0.97	0.91
21	3.24	1.55	0.96	0.57	8.14	0.48	0.62	0.43
22	2.64	1.64	0.76	0.51	1.11	0.62	0.46	0.37
23	4.91	3.61	3	0.80	2.96	0.74	0.83	0.71
24	2.93	1.95	1.84	0.84	6.35	0.67	0.94	0.77
25	2.36	1.24	1.15	0.77	8.73	0.53	0.93	0.67
26	4.45	2.96	2.75	0.83	6.09	0.67	0.93	0.76
27	6.63	4.43	3.24	0.71	3.05	0.67	0.73	0.60
28	5.16	3.67	2.95	0.77	3.05	0.71	0.80	0.68
29	3.31	2.62	1.95	0.76	0.12	0.79	0.74	0.66
30	2.64	2.23	1.78	0.81	-0.34	0.84	0.80	0.73
31	2.53	2.23	1.45	0.72	-3.88	0.88	0.65	0.61
32	2.36	1.55	1.28	0.77	4.61	0.66	0.83	0.67
33	2.45	2.16	1.25	0.67	-5.06	0.88	0.58	0.54
34	3.13	2.76	1.96	0.76	-2.93	0.88	0.71	0.67
35	2.91	1.96	1.13	0.61	0.87	0.67	0.58	0.47
36	2	1.67	0.93	0.64	-4.12	0.84	0.56	0.51
37	2.53	1.53	1.46	0.82	7.53	0.60	0.95	0.74
38	2.76	2.34	2.12	0.89	2.03	0.85	0.91	0.83
39	3.34	2.52	1.87	0.75	1.03	0.75	0.74	0.64
40	3.64	2.19	1.35	0.61	3.59	0.60	0.62	0.48
41	2.79	1.73	1.25	0.69	4.20	0.62	0.72	0.57
42	2.53	1.83	1.29	0.71	1.27	0.72	0.70	0.60
43	2.59	2.24	1.33	0.67	-4.33	0.86	0.59	0.55
44	3.54	1.94	1.45	0.67	6.48	0.55	0.75	0.55
45	1.86	1.73	1.54	0.90	-1.13	0.93	0.89	0.86
46	2.24	1.97	1.55	0.82	-1.57	0.88	0.79	0.74
47	2.36	2.14	1.48	0.76	-3.99	0.91	0.69	0.66
48	2.13	1.25	1.14	0.79	7.27	0.59	0.91	0.70
49	2.63	2.23	1.49	0.72	-2.63	0.85	0.67	0.62
50	1.86	1.43	1.14	0.79	1.59	0.77	0.80	0.70

Figure E2. Grain size parameters for conglomeratic Bed-2.

Sample no.	Long (cm)	Intermediate (cm)	Short (cm)	O/P index	SPH	I/L	S/I
51	3.13	2.15	1.74	3.69	0.77	0.62	0.81
52	2.65	1.65	1.54	6.90	0.82	0.42	0.93
53	6.15	2.57	1.25	11.35	0.46	0.69	0.49
54	4.49	3.12	2.14	1.74	0.69	0.66	0.69
55	7.15	4.72	3.25	2.71	0.68	0.53	0.69
56	8.26	4.4	2.64	5.85	0.58	0.57	0.60
57	4.14	2.36	1.15	3.43	0.51	0.88	0.49
58	4.02	3.54	2.81	-1.48	0.82	0.77	0.79
59	12.74	9.76	6.45	-0.52	0.69	0.45	0.66
60	5.01	2.25	1.83	10.07	0.67	0.57	0.81
61	3.75	2.14	1.62	5.92	0.69	0.77	0.76
62	3.85	2.95	1.98	-0.36	0.70	0.60	0.67
63	5.45	3.26	2.45	5.12	0.70	0.64	0.75
64	3.94	2.54	1.57	2.28	0.63	0.51	0.62
65	3.36	1.73	0.94	6.20	0.53	0.66	0.54
66	4.92	3.26	2.72	4.60	0.77	0.79	0.83
67	7.55	5.98	5.27	2.70	0.85	0.72	0.88
68	5.85	4.23	2.14	-1.73	0.57	0.78	0.51
69	4.48	3.51	1.76	-3.65	0.58	0.72	0.50
70	4.54	3.28	2.36	1.50	0.72	0.73	0.72
71	7.48	5.43	2.25	-3.59	0.50	0.65	0.41
72	6.95	4.53	3.18	3.10	0.68	0.50	0.70
73	6.22	3.14	2.73	8.72	0.73	0.91	0.87
74	6.19	5.65	4.25	-3.23	0.80	0.61	0.75
75	6.25	3.83	2.36	3.23	0.62	0.74	0.62
76	7.24	5.36	3.95	1.31	0.74	0.79	0.74
77	6.3	4.99	3.55	-0.42	0.74	0.46	0.71
78	4.24	1.97	1.65	9.67	0.69	0.46	0.84
79	4.25	1.94	1.23	9.15	0.57	0.88	0.63
80	2.55	2.24	0.99	-7.76	0.56	0.54	0.44
81	5.23	2.84	2.55	8.04	0.76	0.78	0.90
82	3.67	2.85	2.13	0.56	0.76	0.68	0.75
83	7.39	5.05	2.13	-1.91	0.50	0.67	0.42
84	3.92	2.64	2.37	5.39	0.82	0.55	0.90
85	2.94	1.63	0.92	4.75	0.56	0.68	0.56
86	6.02	4.12	0.94	-8.07	0.33	0.62	0.23
87	3.46	2.15	1.27	2.67	0.60	0.72	0.59
88	3.84	2.78	2.28	3.02	0.79	0.78	0.82
89	9.12	7.1	5.3	0.50	0.76	0.48	0.75
90	3.95	1.91	1.34	8.30	0.62	0.77	0.70
91	3.15	2.42	2.13	3.19	0.84	0.88	0.88
92	4.84	4.25	3.82	0.99	0.89	0.47	0.90
93	3.13	1.47	0.65	8.16	0.45	0.80	0.44
94	5.62	4.48	2.52	-2.95	0.63	0.70	0.56
95	6.78	4.75	1.93	-2.86	0.49	0.84	0.41
96	6.43	5.42	2.81	-5.06	0.61	0.55	0.52
97	3.34	1.85	1.54	7.11	0.73	0.63	0.83
98	3.39	2.14	1.43	3.27	0.66	0.71	0.67
99	3.92	2.79	2.15	2.52	0.75	0.64	0.77
100	4.24	2.7	2.28	5.31	0.77	0.64	0.84

Figure E2. Continued.

Sample	L	I	S	SPH	O/P index	I/L	S/I	Shape index
1	7.6	5.85	2.26	0.49	-5.79	0.70	0.39	0.34
2	7.53	5.24	2.74	0.58	-0.60	0.68	0.52	0.44
3	4.25	2.87	2.36	0.77	4.14	0.78	0.82	0.68
4	8.01	6.25	4.24	0.71	-0.63	0.64	0.68	0.60
5	4.7	3.01	2.35	0.73	4.38	0.77	0.78	0.62
6	10.84	8.36	3.56	0.52	-4.85	0.72	0.43	0.37
7	4.3	3.09	2.48	0.77	2.86	0.52	0.80	0.68
8	6.27	3.25	2.75	0.72	8.16	0.77	0.85	0.61
9	4	3.08	2.43	0.78	1.42	0.56	0.79	0.69
10	4.8	2.67	2.12	0.71	6.67	0.89	0.79	0.59
11	8.68	7.72	2.23	0.42	-13.67	0.90	0.89	0.27
12	5.18	4.68	2.73	0.67	-5.61	0.60	0.58	0.55
13	4.56	2.73	2.66	0.83	7.94	0.75	0.97	0.75
14	11.23	8.42	5.99	0.72	0.68	0.59	0.71	0.62
15	9.86	5.78	4.54	0.71	5.80	0.77	0.79	0.60
16	9.76	7.48	6.35	0.82	2.59	0.73	0.85	0.74
17	9.73	7.14	2.34	0.43	-6.22	0.71	0.33	0.28
18	6.42	4.58	2.5	0.60	-0.79	0.88	0.55	0.46
19	20	17.5	14	0.82	-1.19	0.63	0.80	0.75
20	8	5.07	3.64	0.69	3.78	0.84	0.72	0.57
21	6.23	5.25	2.89	0.63	-4.45	0.71	0.55	0.51
22	11.56	8.19	4.56	0.60	-0.47	0.93	0.56	0.47
23	5.22	4.85	2.34	0.60	-8.29	0.72	0.48	0.47
24	3.26	2.35	2.16	0.85	4.94	0.97	0.92	0.78
25	4.39	4.25	2.22	0.64	-8.61	0.64	0.52	0.51
26	3.94	2.54	2.53	0.86	7.68	0.61	1.00	0.80
27	3.24	1.98	2.15	0.90	9.89	0.55	1.09	0.85
28	7.99	4.39	2.94	0.63	5.79	0.67	0.67	0.50
29	7.84	5.27	3.95	0.72	3.19	0.64	0.75	0.61
30	6.67	4.25	2.84	0.66	3.10	0.84	0.67	0.53
31	8.12	6.81	5.7	0.84	0.59	0.50	0.84	0.77
32	4.96	2.5	2.43	0.78	9.64	0.73	0.97	0.69
33	20.5	15	13.5	0.84	4.34	0.61	0.90	0.77
34	5.25	3.22	2.54	0.73	5.15	0.67	0.79	0.62
35	4.85	3.25	2.19	0.67	2.25	0.84	0.67	0.55
36	2.54	2.13	1.86	0.86	1.41	0.43	0.87	0.80
37	5.72	2.45	2.11	0.68	11.00	0.68	0.86	0.56
38	4.64	3.14	1.26	0.48	-2.07	0.67	0.40	0.33
39	5.64	3.78	2.32	0.63	1.46	0.62	0.61	0.50
40	3.17	1.95	1.14	0.59	2.81	0.72	0.58	0.46
41	3.83	2.74	1.86	0.69	1.10	0.62	0.68	0.57
42	5.12	3.18	2.55	0.74	5.12	0.76	0.80	0.63
43	4.33	3.28	2.36	0.73	0.61	0.68	0.72	0.63
44	5.7	3.89	1.32	0.43	-3.75	0.87	0.34	0.28
45	2.23	1.93	1.74	0.89	1.44	0.62	0.90	0.84
46	10.28	6.35	2.35	0.44	-0.19	0.85	0.37	0.29
47	3.24	2.74	1.32	0.58	-5.88	0.74	0.48	0.44
48	7.68	5.67	3.55	0.66	-0.29	0.61	0.63	0.54
49	10.85	6.62	5.53	0.75	5.79	0.77	0.84	0.65
50	4.84	3.73	1.32	0.46	-6.77	0.78	0.35	0.31

Figure E3. Grain size parameters for conglomeratic Bed-3.

Sample	L	I	S	SPH	O/P index	I/L	S/I	Shape index
51	7.65	5.98	2.66	0.54	-4.75	0.82	0.44	0.39
52	4.4	3.59	3.14	0.85	2.00	0.67	0.87	0.79
53	4.35	2.93	2.65	0.82	5.50	0.79	0.90	0.74
54	5.5	4.32	2.05	0.56	-4.24	0.97	0.47	0.42
55	7.16	6.93	6.03	0.90	-3.52	0.77	0.87	0.86
56	6.9	5.34	3.92	0.75	0.41	0.85	0.73	0.65
57	6.13	5.22	4.94	0.91	3.28	0.54	0.95	0.87
58	12.8	6.9	5.63	0.71	7.34	0.72	0.82	0.60
59	4.66	3.36	1.32	0.48	-3.91	0.84	0.39	0.33
60	8.06	6.79	5.09	0.78	-1.15	0.91	0.75	0.69
61	4.25	3.85	2.93	0.81	-2.86	0.82	0.76	0.72
62	4.64	3.82	3.46	0.88	2.61	0.88	0.91	0.82
63	6.52	5.71	4.6	0.83	-1.11	0.81	0.81	0.75
64	4.88	3.93	2.76	0.74	-0.92	0.78	0.70	0.63
65	2.29	1.79	1.73	0.90	5.20	0.74	0.97	0.85
66	4.95	3.65	1.8	0.56	-2.40	0.96	0.49	0.42
67	2.83	2.72	1.27	0.59	-9.57	0.61	0.47	0.46
68	4.13	2.53	1.47	0.59	2.85	0.92	0.58	0.45
69	4.13	3.78	2.15	0.67	-6.21	0.75	0.57	0.54
70	4.42	3.33	2.12	0.67	-0.54	0.67	0.64	0.55
71	3.34	2.23	1.29	0.61	1.07	0.79	0.58	0.47
72	4.36	3.44	0.9	0.38	-11.34	0.78	0.26	0.23
73	3.67	2.86	1.75	0.66	-1.64	0.71	0.61	0.54
74	3.18	2.25	1.9	0.80	3.79	0.69	0.84	0.71
75	2.83	1.95	1.26	0.66	1.36	0.61	0.65	0.54
76	2.83	1.73	1.37	0.73	5.23	0.84	0.79	0.62
77	6.03	5.05	3.19	0.69	-2.93	0.85	0.63	0.58
78	2.26	1.91	0.74	0.50	-8.24	0.86	0.39	0.36
79	6.11	5.25	3.09	0.67	-4.26	0.57	0.59	0.55
80	3.22	1.85	1.51	0.73	6.42	0.69	0.82	0.62
81	2.85	1.96	1.78	0.83	5.31	0.77	0.91	0.75
82	5.46	4.21	3.28	0.78	1.22	0.66	0.78	0.68
83	7.89	5.24	3.62	0.68	2.63	0.53	0.69	0.56
84	8.96	4.76	3.79	0.70	7.39	0.90	0.80	0.58
85	4.57	4.1	2.01	0.60	-7.19	0.64	0.49	0.46
86	2.25	1.44	0.95	0.65	2.91	0.56	0.66	0.53
87	3.27	1.82	1.23	0.63	5.60	0.48	0.68	0.50
88	8.69	4.15	4.01	0.76	10.19	0.88	0.97	0.67
89	2.75	2.43	1.89	0.81	-1.86	0.60	0.78	0.73
90	6.8	4.05	2.75	0.65	4.43	0.70	0.68	0.52
91	7.52	5.24	3.42	0.67	1.23	0.57	0.65	0.54
92	4.75	2.69	1.95	0.67	5.74	0.68	0.72	0.55
93	3.38	2.3	1.82	0.75	3.57	0.80	0.79	0.65
94	4.66	3.72	2.61	0.73	-0.74	0.70	0.70	0.63
95	1.84	1.29	1.12	0.81	4.34	0.76	0.87	0.73
96	2.64	2.01	1.42	0.72	0.30	0.79	0.71	0.62
97	2.15	1.69	1.46	0.84	2.45	0.79	0.86	0.77
98	3.88	3.06	2.7	0.85	2.80	0.59	0.88	0.78
99	3.84	2.25	1.87	0.74	6.31	0.64	0.83	0.64
100	4.78	3.05	2.44	0.74	4.69		0.80	0.64

Figure E3. Continued.